# TO INVESTIGATE THERMAL CONDUCTIVITY AND VISCOSITY OF $Al_2O_3$/ R-11 NANOREFRIGERANT

*A Thesis Submitted on partial fulfillment of requirement for the award of the degree of*

## Master of Engineering

**IN**

## THERMAL


***Submitted By***

**Gurprinder Singh Dhindsa**

**Roll No. 801183006**

***Under guidance of***

**Mr. Kundan Lal, Asst. Prof.**

**Department of Mechanical Engineering,**

**Thapar University, Patiala**



**DEPARTMENT OF MECHANICAL ENGINEERING**

**THAPAR UNIVERSITY**

**PATIALA-147004, INDIA**



**JULY 2013**

# DECLARATION

I hereby declare that thesis entitled, **"To investigate thermal conductivity and viscosity of $Al_2O_3$/R-11 nanorefrigerant"** is an authentic record of my study carried out as requirements for the award of degree of **M.E. (Thermal Engineering)** at **Thapar University**, under the guidance of **Mr. Kundan Lal**, Assistant Professor, **Department of Mechanical Engineering**, Thapar University, Patiala. The matter embodied in this thesis has not been submitted in part or full to any other university or institute for the award of any degree.

**(Gurprinder Singh Dhindsa)**

This is to certify that above declaration made by the student concerned is correct to the best of my knowledge and belief.

**Mr. Kundan Lal**

Asst. Professor, MED

TU, Patiala-147004

Countersigned by:

**Dr. Ajay Batish**

Professor & Head

Department of Mechanical Engineering

Thapar University

Patiala-147004

**Dr. S.K. Mohapatra**

Senior Professor, MED

Dean of Academic Affairs

Thapar University

Patiala-147004

# ABSTRACT

Nanorefrigerant is one kind of nanofluids that seems to be possessing better heat transfer performance over traditional refrigerants. Thermal conductivity & viscosity are important thermophysical properties of the refrigeration which affects its performance. Experimental investigations are done on thermal conductivity and viscosity of $Al_2O_3$/R-11 nanorefrigerant at different weight concentrations and temperature with varying size and shape of nanoparticles. $Al_2O_3$ (20 nm-spherical, 40 nm-spherical and 40 nm-elongated) nanoparticles are mixed with the refrigerant R-11 at varying concentration (0.02-0.10 wt. %) using ultrasonic vibration. The objective of this study is to investigate the dependence of thermal conductivity and viscosity of $Al_2O_3$–R11 nanorefrigerant on temperature (4-16°C) at different weight concentrations, shape (spherical & elongated) and size (20 nm & 40 nm). As use of nanorefrigerant is in the initial stage, it has been observed in literature that there are significant discrepancies in the reported data about nanorefrigerant thermal conductivity and viscosity. A detailed literature review is coined about the unique features of nanofluids, such as their preparation, viscosity and thermal conductivity. Experimental studies are discussed in terms of the effects of various parameters such as particle volume fraction, particle size and temperature on the thermal conductivity and viscosity of nanofluids/nanorefrigerants. Based on the experimental analysis it is observed that thermal conductivity and viscosity augmented significantly with the increase of weight concentrations. Thermal conductivity increase around 42% at 0.10 wt. % (4°C) of 40 nm elongated $Al_2O_3$ nanoparticles and viscosity up to 31%. A nonlinear relationship is observed of thermal conductivity and viscosity with increment of particle weight concentrations for 40 nm (elongated) nanoparticles. The absolute thermal conductivity and viscosity of nanorefrigerant decrease with temperature (4-16°C) in both the base fluids (R-11) and the nanorefrigerant ($Al_2O_3$/R-11). But the relative viscosity remains almost invariant within variation of 1-2% with increase in temperature. $Al_2O_3$ nanoparticles of size 20 nm have more thermal conductivity & viscosity than 40 nm nanoparticles within measured temperature range (4-16°C). Also, the thermal conductivity & viscosity enhance-

ment of nanorefrigerant with elongated shaped $Al_2O_3$ nanoparticles (40 nm) is more than spherical shaped (40 nm) $Al_2O_3$ nanoparticles within measured temperature range (4-16°C). Therefore, low weight concentration (up to 0.08 wt.%) of 20 nm (spherical) size nanoparticles is suggested to improve the performance of a refrigeration system in the temperature range from 4-16°C.

# AKNOWLEDGEMENT

I would like to express my sincere gratitude to Mr. Kundan Lal, Assistant Professor, Department of Mechanical Engineering, Thapar University, Patiala, for introducing the present topic and for their inspiring guidance, constructive criticism and valuable suggestion during thesis work. I have experienced an excellent academic study under their supervision and their invaluable recommendations and support helped me to plan my further academic studies in the best way.

**(Gurprinder Singh Dhindsa)**

# TABLE OF CONTENTS

ABSTRACT ....……i

ACKNOWLEDGMENT …….……..……...…….iii

TABLE OF CONTENTS ……iv

LIST OF TABLES ……...……..viii

LIST OF FIGURES ……..……..ix

NOMENCLATURE ……..……..……xiv

LIST OF PUBLICATIONS ……xvi

**CHAPTERS** **PAGE NO.**

1 NANOFLUIDS/ NANOREFRIGERANTS ..……..…(1-8)

1.1 Introduction ……..1

1.1.1 Particle material and base fluid …….……...3

1.1.2 Particle size ….……4

1.1.3 Particle shape ……4

1.2 Preparation methods ……..……4

1.2.1 Preparation of nanoparticles …….……..4

1.2.2 Preparation of nanofluids ..……..……..4

1.2.2.1 One step method ……...5

1.2.2.2 Two step method ……..……..5

1.3 Applications of nanofluids ……..……6

1.3.1 Heat transportation ……7

1.3.2 Electronics cooling ……7

1.3.3 Military applications ……7

1.3.4 Medical applications ……8

2 LITERATURE SURVEY …… (9-37)

2.1 Thermal conductivity ……9

2.1.1 Thermal conductivity of nanorefrigerant .....9
2.1.2 Effects of various parameters on thermal conductivity of nanofluids.....11
2.1.2.1 Particle volume fraction .....11
2.1.2.2 Particle material .....12
2.1.2.3 Base fluid .....13
2.1.2.4 Particle size .....14
2.1.2.5 Particle shape .....15
2.1.2.6 Temperature .....16
2.1.2.7 Clustering .....17
2.1.2.8 pH Value .....18
2.1.3 Measurement techniques for thermal conductivity .....18
2.1.3.1 Transient hot wire method .....19
2.1.3.2 Transient plane source method .....20
2.1.3.3 Cylindrical cell method .....21
2.1.3.4 Thermal comparator method .....21
2.1.4 Theoretical models of thermal conductivity .....22
2.1.4.1 Classical models .....22
2.1.4.2 Model based on Brownian motion .....23
2.1.4.3 Models based on clustering .....24
2.1.4.4 Models based on liquid layering .....25
2.2 Viscosity .....26
2.2.1 Viscosity of nanorefrigerant .....26
2.2.2 Effect of various parameters on viscosity .....27
2.2.2.1 Temperature .....27
2.2.2.2 Volume fraction .....28
2.2.2.3 Shear rate .....28
2.2.2.4 Dispersion method .....28
2.2.3 Viscosity measurement methods .....29
2.2.3.1 Capillary Viscometer .....29

2.2.3.2 Rotational Viscometer ……29
2.2.4 Theoretical models of viscosity ……30
2.3 Experimental investigations of refrigeration system ……31
2.4 Characterization Techniques ……32
2.4.1 X-Ray Diffraction (XRD) ……32
2.4.2 Transmission Electron Microscopy (TEM) ……34
2.4.3 Dynamic Light Scattering ……36
2.5 Summary of literature about nanorefrigerants ……37
3 RESEARCH GAPS AND OBJECTIVES ……(38-39)
3.1 Research gaps ……38
3.2 Research objectives ……39
4 INSTRUMENTS USED FOR EXPERIMENTAL WORK ……(40-48)
4.1 Ultrasonic Sonicator ……40
4.2 KD2 Pro thermal properties analyzer ……41
4.2.1 Preventing forced convection ……43
4.2.2 Preventing free convection ……43
4.2.3 Liquid sample temperature control ……45
4.3 Viscometer/ Rheometer ……46
4.3.1 Setup ……46
4.3.2 Setting the gap ……48
5 METHODOLOGY ……(49-57)
5.1 Materials used for preparing nanorefrigerant ……49
5.2 Characterization of nanorefrigerant ……50
5.3 Preparation of nanorefrigerant ……54
5.4 Measurement of thermal conductivity ……55
5.5 Measurement of viscosity ……56
6 RESULTS AND DISCUSSION ……(58-89)
6.1 Introduction ……58
6.2 Thermal conductivity of $Al_2O_3$/R-11 nanorefrigerant ……58

6.2.1 Effect of weight concentration on thermal conductivity ……58

6.2.2 Effect of temperature on thermal conductivity ……61

6.2.3 Effect of size of $Al_2O_3$ nanoparticles on thermal conductivity ……64

6.2.4 Effect of shape of $Al_2O_3$ nanoparticles on thermal conductivity ……68

6.2.5 Comparison of experimental data of thermal conductivity with theoretical models ……72

6.3 Viscosity of $Al_2O_3$/R-11 nanorefrigerant ……75

6.3.1 Effect of weight concentration on viscosity ……75

6.3.2 Effect of temperature on viscosity ……77

6.3.3 Effect of size of $Al_2O_3$ nanoparticles on viscosity ……81

6.3.4 Effect of shape of $Al_2O_3$ nanoparticles on viscosity ……84

6.3.5 Comparison of experimental data of viscosity with theoretical models ……88

7 CONCLUSION AND FUTURE SCOPE ……(90-95)

7.1 Thermal conductivity of $Al_2O_3$ /R-11 nanorefrigerant ……90

7.2 Viscosity of $Al_2O_3$/R-11 nanorefrigerant ……92

7.3 Suggestions for future work ……94

REFERENCES ……96

BIBLIOGRAPHY ……102

# LIST OF TABLES


| Table No. | Table Caption | Page No. |
|---|---|---|
| **Table 1.1** | Refrigerant properties …….…… | 2 |
| **Table 2.1** | $\beta$ values for different nanoparticles to be used in Eq.2.5 …….…… | 24 |
| **Table 2.2** | Nanofluid viscosity models proposed by several authors …..…… | 30 |
| **Table 2.3** | List of literature about nanorefrigerants …… | 37 |
| **Table 4.1** | Specifications of Ultrasonic Sonicator …… | 41 |
| **Table 4.2** | KD2 Pro needle specifications …… | 42 |
| **Table 5.1** | Properties of R-11 refrigerant …… | 49 |
| **Table 5.2** | Properties of $Al_2O_3$ nanoparticles …… | 50 |

# LIST OF FIGURES


| Figure No. | Figure Caption | Page No. |
|---|---|---|
| **Figure 1.1** | Thermal Conductivity of materials | 1 |
| **Figure 1.2** | Common base fluids and nanoparticles for synthesizing nanofluid | 3 |
| **Figure 2.1** | Schematic of transient hot-wire experimental setup | 20 |
| **Figure 4.1** | Ultra Sonicator | 40 |
| **Figure 4.2** | KD2 Pro thermal properties analyzer | 42 |
| **Figure 4.3** | Components of Viscometer | 46 |
| **Figure 4.4** | Spindle attachment of viscometer | 47 |
| **Figure 4.5** | Cup attachment of viscometer | 47 |
| **Figure 4.6** | Micrometer adjustment of viscometer | 48 |
| **Figure 5.1** | R-11 Refrigerant cylinder | 49 |
| **Figure 5.2** | R-11 Refrigerant sample in a beaker | 49 |
| **Figure 5.3** | X-Ray Diffraction (XRD) of 20 nm $Al_2O_3$ nanoparticles | 51 |
| **Figure 5.3** | TEM photograph of 20 nm $Al_2O_3$ nanoparticles | 51 |
| **Figure 5.5** | Size distributions of 20 nm $Al_2O_3$ nanoparticles | 51 |
| **Figure 5.6** | X-Ray Diffraction (XRD) of 40 nm (spherical) $Al_2O_3$ nanoparticles | 52 |
| **Figure 5.7** | X-Ray Diffraction (XRD) of 40 nm $Al_2O_3$ (elongated) nanoparticles | 52 |
| **Figure 5.8** | TEM photograph of 40 nm (spherical) $Al_2O_3$ nanoparticles | 53 |
| **Figure 5.9** | TEM photograph of 40 nm (elongated) $Al_2O_3$ nanoparticles | 53 |

| | | |
|---|---|---|
| **Figure 5.10** | Sonication of $Al_2O_3$/R-11 nanorefrigerant | 54 |
| **Figure 5.11** | $Al_2O_3$/R-11 nanorefrigerant after sonication | 55 |
| **Figure 5.12** | Measurement of thermal conductivity using KD2 Pro | 56 |
| **Figure 5.13** | Measurement of viscosity by Brookfield Rheometer (LV DV-IIICP) | 57 |
| **Figure 6.1** | Thermal conductivity v/s weight concentration % of 20 nm (spherical) $Al_2O_3$ nanoparticles at different temperatures | 58 |
| **Figure 6.2** | Thermal conductivity v/s weight concentration % of 40 nm (spherical) $Al_2O_3$ nanoparticles at different temperatures | 59 |
| **Figure 6.3** | Thermal conductivity v/s weight concentration % of 40 nm (elongated) $Al_2O_3$ nanoparticles at different temperatures | 59 |
| **Figure 6.4** | Thermal conductivity ratio v/s weight concentration % of 20 nm (spherical), 40 nm (spherical & elongated) $Al_2O_3$ nanoparticles | 60 |
| **Figure 6.5** | Thermal conductivity v/s temperature at different weight concentrations % of 20 nm (spherical) $Al_2O_3$ nanoparticles | 61 |
| **Figure 6.6** | Thermal conductivity v/s temperature at different weight concentrations % of 40 nm (spherical) $Al_2O_3$ nanoparticles | 62 |
| **Figure 6.7** | Thermal conductivity v/s temperature at different weight concentrations % of 40 nm (elongated) $Al_2O_3$ nanoparticles | 62 |
| **Figure 6.8** | Thermal conductivity ratio v/s temperature at different weight concentrations % of 20 nm (spherical) $Al_2O_3$ nanoparticles | 63 |
| **Figure 6.9** | Thermal conductivity ratio v/s temperature at different weight concentrations % of 40 nm (spherical) $Al_2O_3$ nanoparticles | 63 |
| **Figure 6.10** | Thermal conductivity ratio v/s temperature at different weight concentrations % of 40 nm (elongated) $Al_2O_3$ nanoparticles | 64 |
| **Figure 6.11** | Thermal conductivity v/s temperature for different size of $Al_2O_3$ nanoparticles at 0.02 wt. % concentration | 65 |

| | | |
|---|---|---|
| **Figure 6.12** | Thermal conductivity v/s temperature for different size of $Al_2O_3$ nanoparticles at 0.04 wt. % concentration | 65 |
| **Figure 6.13** | Thermal conductivity v/s temperature for different size of $Al_2O_3$ nanoparticles at 0.06 wt. % concentration | 66 |
| **Figure 6.14** | Thermal conductivity v/s temperature for different size of $Al_2O_3$ nanoparticles at 0.08 wt. % concentration | 66 |
| **Figure 6.15** | Thermal conductivity v/s temperature for different size of $Al_2O_3$ nanoparticles at 0.10 wt. % concentration | 67 |
| **Figure 6.16** | Thermal conductivity ratio v/s wt. concentration % for different size of $Al_2O_3$ nanoparticles | 67 |
| **Figure 6.17** | Thermal conductivity v/s temperature for different shape of $Al_2O_3$ nanoparticles at 0.02 wt. % concentration | 68 |
| **Figure 6.18** | Thermal conductivity v/s temperature for different shape of $Al_2O_3$ nanoparticles at 0.04 wt. % concentration | 69 |
| **Figure 6.19** | Thermal conductivity v/s temperature for different shape of $Al_2O_3$ nanoparticles at 0.06 wt. % concentration | 69 |
| **Figure 6.20** | Thermal conductivity v/s temperature for different shape of $Al_2O_3$ nanoparticles at 0.08 wt. % concentration | 70 |
| **Figure 6.21** | Thermal conductivity v/s temperature for different shape of $Al_2O_3$ nanoparticles at 0.10 wt.% concentration | 70 |
| **Figure 6.22** | Thermal conductivity ratio v/s wt. concentration % for different shape of $Al_2O_3$ nanoparticles | 71 |
| **Figure 6.23** | Measured thermal conductivities of $Al_2O_3$ /R-11 nanorefrigerant v/s effective thermal conductivities calculated from theories for spherical nanoparticles | 72 |
| **Figure 6.24** | Measured thermal conductivities of $Al_2O_3$ /R-11 nanorefrigerant v/s effective thermal conductivities calculated from theories for elongated nanoparticles | 73 |
| **Figure 6.25** | Viscosity v/s weight concentration % at different temperatures for 20 nm (spherical) $Al_2O_3$ nanoparticles | 75 |

**Figure 6.26** Viscosity v/s weight concentration % at different temperatures for 40 nm (spherical) $Al_2O_3$ nanoparticles 75

**Figure 6.27** Viscosity v/s weight concentration % at different temperatures for 40 nm (elongated) $Al_2O_3$ nanoparticles 76

**Figure 6.28** Relative viscosity v/s wt. concentration % for 20 nm (spherical) & 40 nm (spherical & elongated) $Al_2O_3$ nanoparticles 76

**Figure 6.29** Viscosity v/s temperature at different weight concentrations % for 20 nm (spherical) $Al_2O_3$ nanoparticles 77

**Figure 6.30** Viscosity v/s temperature at different weight concentrations % for 40 nm (spherical) $Al_2O_3$ nanoparticles 78

**Figure 6.31** Viscosity v/s temperature at different weight concentrations % for 40 nm (elongated) $Al_2O_3$ nanoparticles 78

**Figure 6.32** Relative viscosity v/s temperature at different wt. concentrations for 20 nm (spherical) $Al_2O_3$ nanoparticles 79

**Figure 6.33** Relative viscosity v/s temperature at different wt. concentrations for 40 nm (spherical) $Al_2O_3$ nanoparticles 79

**Figure 6.34** Relative viscosity v/s temperature at different wt. concentrations for 40 nm (elongated) $Al_2O_3$ nanoparticles 80

**Figure 6.35** Viscosity v/s temperature for different size of $Al_2O_3$ nanoparticles at 0.02 wt. % concentration 81

**Figure 6.36** Viscosity v/s temperature for different size of $Al_2O_3$ nanoparticles at 0.04 wt. % concentration 81

**Figure 6.37** Viscosity v/s temperature for different size of $Al_2O_3$ nanoparticles at 0.06 wt. % concentration 82

**Figure 6.38** Viscosity v/s temperature for different size of $Al_2O_3$ nanoparticles at 0.08 wt. % concentration 82

**Figure 6.39** Viscosity v/s temperature for different size of $Al_2O_3$ nanoparticles at 0.10 wt. % concentration 83

**Figure 6.40** Relative viscosity v/s wt. concentration % for different size of $Al_2O_3$ nanoparticles 83

**Figure 6.41** Viscosity v/s temperature for different shape of $Al_2O_3$ nanoparticles at 0.02 wt. % concentration 84

**Figure 6.42** Viscosity v/s temperature for different shape of $Al_2O_3$ nanoparticles at 0.04 wt. % concentration 85

**Figure 6.43** Viscosity v/s temperature for different shape of $Al_2O_3$ nanoparticles at 0.06 wt. % concentration 85

**Figure 6.44** Viscosity v/s temperature for different shape of $Al_2O_3$ nanoparticles at 0.06 wt. % concentration 86

**Figure 6.45** Viscosity v/s temperature for different shape of $Al_2O_3$ nanoparticles at 0.08 wt. % concentration 86

**Figure 6.46** Relative viscosity v/s wt. concentration % for different shape of $Al_2O_3$ nanoparticles 87

**Figure 6.47** Measured relative viscosity of $Al_2O_3$ /R-11 nanorefrigerant v/s relative viscosity calculated from theories for nanoparticles 88

# NOMENCLATURE

| | |
|---|---|
| $C_p$ | Specific heat capacity, J/kgK |
| $K$ | Thermal conductivity, W/mK |
| $r$ | Radius, m |
| $d$ | Interspacial distance, m |
| $t$ | Nanolayer thickness, m |
| $v$ | Velocity of sound |
| $n$ | Order of diffraction |
| $m$ | Mass, Kg |
| $T$ | Temperature, K |
| $R$ | Gas constant, J/K/mol |
| $ODP$ | Ozone depletion potential |
| $GWP$ | Glowal warming potential |
| $cP$ | Centi poise |

**Greek letters**

| | |
|---|---|
| $\alpha$ | Thermal diffusivity, $m^2/s$ |
| $\mu$ | Dynamic viscosity, Pa.s |
| $\rho$ | Density, $kg/m^3$ |
| $\phi$ | Particle volume fraction |
| $\Psi$ | Sphericity |
| $\varphi$ | Weight concentration |
| $\lambda$ | Wavelength of radiations, nm |
| $\theta$ | Angle |
| $\upsilon$ | Refractive index |
| $\epsilon$ | Mean distance of separation |

**Subscripts**

| | |
|---|---|
| *cl* | Cluster |
| *f* | Base fluid |
| *l* | Liquid Nanolayer |
| *nf* | Nanofluid |
| *p* | Nanoparticle |
| *r* | Refrigerant |

# LIST OF PUBLICATIONS

## International Conferences

Dhindsa, GS & Kundan, L 2013 ‘Experimental investigation of the viscous behavior of $Al_2O_3$ based nanorefrigerant’, *ICMIE 2013* by IRD India, Chandigarh.

## International Journals

Dhindsa, GS & Kundan, L 2013 ‘Experimental investigation of the viscous behavior of $Al_2O_3$ based nanorefrigerant’ *International Journal on Theoretical and Applied Research in Mechanical Engineering*, vol.2, no. 3, pp.143-147.

# CHAPTER-1

# NANOFLUIDS/NANOREFRIGERANTS

## 1.1 Introduction

With the recent improvements in nanotechnology, the preparation of particles with sizes on the order of nanometers (nanoparticles) can be achieved with relative ease. The idea of suspending these nanoparticles in a base liquid for improving its thermal performance has been proposed recently. Such suspension of nanoparticles in a base fluid is called a nanofluid. Due to their small size, nanoparticles fluidize easily inside the base fluid, so clogging of channels and erosion in channel walls are no longer a problem. Hence, it is possible to use nanofluids in microchannels.

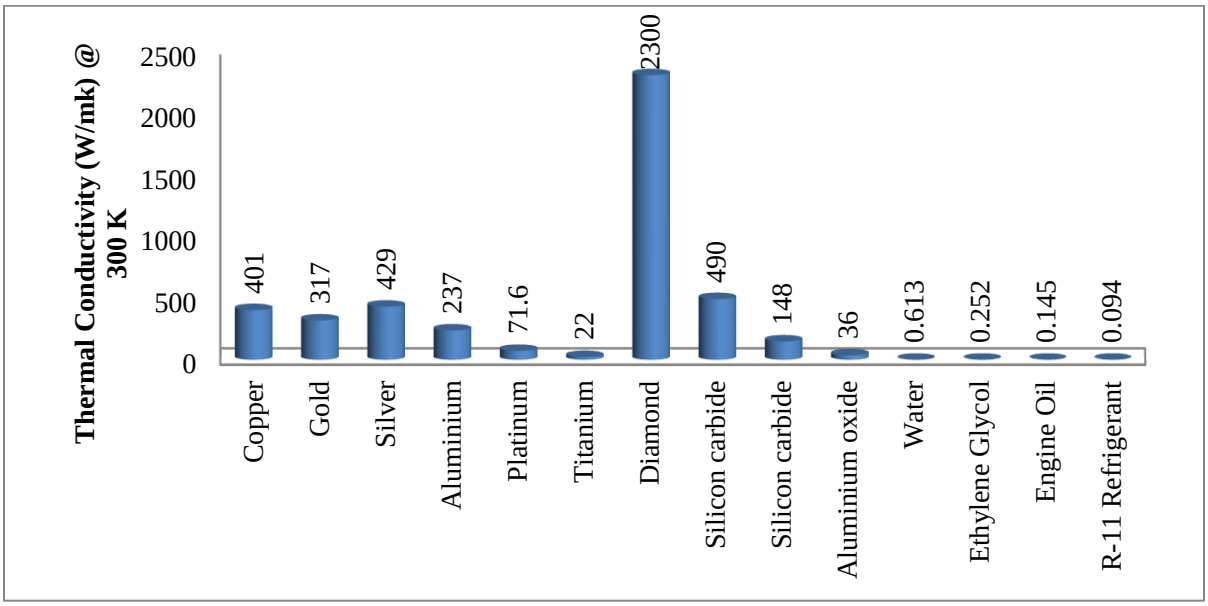


**Figure 1.1** Thermal Conductivity of materials (Frank P. Incropera, 2009)

However, conventional heat transfer fluids such as water, oil and ethylene glycol have an inherently poor thermal performance due to their low thermal conductivities. Figure 1.1 shows the solid metals such as silver, copper, iron and non-metallic materials, such as $Al_2O_3$, SiC, CuO and carbon tubes that possess higher thermal conductivity than the conventional heat transfer fluids. The nanorefrigerant is one kind of nanofluid and its host fluid is

refrigerant. Refrigerant have poor heat transfer properties like other conventional thermo fluids. The thermal and physical properties of various refrigerants are shown below in Table 1.1.

**Table 1.1** Refrigerant properties (ASHRAE, 2001)

| Ref. No. | Chemical Formula | Normal Boiling point ( °C) | Critical point | | Viscosity (cP) @4.44C liq. | Thermal Conductivity w/mK @ 4.44°C liq. | ODP | GWP |
|---|---|---|---|---|---|---|---|---|
| | | | Temp. (°C) | Press. (bar) | | | | |
| R-11 | $CCl_3F$ | 23.70 | 198 | 44.0 | 0.539 | 0.094 | 1 | 3800 |
| R-123 | $CHCl2CF_3$ | 27.82 | 184 | 36.6 | 0.534 | 0.082 | 0.02 | 90 |
| R-718 | $H_2O$ | 100.00 | 374 | 220.0 | 1.545 | 0.569 | 0 | < 1 |
| R-12 | $CCl_2F_2$ | -29.75 | 1<br>12 | 41.3 | 0.237 | 0.074 | 1 | 8100 |
| R-22 | $CHClF_2$ | -40.81 | 96 | 49.9 | 0.208 | 0.093 | 0.055 | 1500 |
| R-134a | $CF_3CH_2F$ | -26.07 | 101 | 40.6 | 0.256 | 0.090 | 0 | 1300 |
| R-717 | $NH_3$ | -33.33 | 132 | 113.3 | 0.162 | 0.545 | 0 | 0 |
| R-744 | $CO_2$ | -78.33 | 31 | 73.7 | 0.222 | 0.104 | 0 | 1 |

Maxwell (1873) initiated a novel concept of dispersing solid particles in base fluids to break the fundamental limit of heat transfer fluids having low thermal conductivities. Most of these earlier studies on this concept used millimeter or micrometer solid particles, which led to major problems such as rapid settling of the solid spherical particles in the fluids, clogging in micro channels and surface abrasion and the high pressure drop caused by these particles limited their practical applications. When it comes to the stability of the suspension, it was observed that sedimentation of particles can be prevented by utilizing proper dispersants fluids and the heat transfer performance of such fluids can be significantly improved. This is due to the following:

i. The suspended nanoparticles in fluid increase the surface area and heat capacity.

ii. The suspended nanoparticles in fluid increase the effective thermal conductivity of fluid.

iii. The interaction and collision among particles, fluid and the surface of flow passage are intensified.

iv. By suspending nano sized particles in cooling or heating.

v. The dispersion of nanoparticles flattens the transverse temperature gradient of the fluid in its flow passage.

vi. The pumping power is low as compare to that of pure fluids to achieve equivalent heat transfer enhancements.

vii. The particle clogging is reduced as compared to conventional slurries.

### 1.1.1 Particle material and base fluid

Many different particle materials are used for nanofluid preparation. Ag, Cu, Au, Fe $Al_2O_3$, $TiO_2$, CuO and SiC nanoparticles are frequently used in nanofluid research. Carbon nanotubes are also utilized due to their extremely high thermal conductivity in the longitudinal (axial) direction.

Base fluids mostly used in the preparation of nanofluids are the common working fluids of heat transfer applications; such as, water, ethylene glycol and engine oil as shown in Figure 1.2. In order to improve the stability of nanoparticles inside the base fluid, some additives are added to the mixture in small amounts.

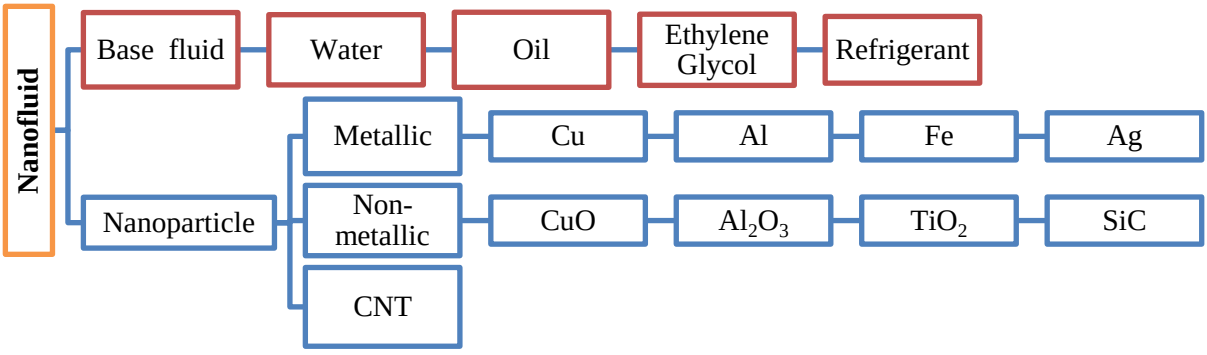


**Figure 1.2** Common base fluids and nanoparticles for synthesizing nanofluid

### 1.1.2 Particle size

Nanoparticles used in nanofluid preparation usually have diameters below 100 nm. Particles as small as 10 nm are also been used in nanofluid research. When particles are not spherical but rod or tube-shaped, the diameter is still below 100 nm, but the length of the particles may be on the order of micrometers. It should also be noted that due to the clustering phenomenon, particles may form clusters with sizes on the order of micrometers and it has a remarkable impact on the thermo physical properties of any nanofluid.

### 1.1.3 Particle shape

Spherical particles have been used extensively in preparation of nanofluids. However, rod-shaped, tube- shaped and disk-shaped nanoparticles can also be used.

## 1.2 Preparation methods

### 1.2.1 Preparation of nanoparticles

Preparation of nanoparticles is done mainly by two ways, namely, physical synthesis and chemical synthesis. The common preparation techniques of nanofluids are as follows.
**Physical Synthesis**: Mechanical grinding and inert-gas-condensation technique.
**Chemical Synthesis**: Chemical precipitation, micro- emulsions, chemical vapor deposition, pray pyrolysis, thermal spraying.

### 1.2.2 Preparation of nanofluids

There are mainly two methods of nanofluid preperation, namely, one-step technique and two-step technique. One-step technique combines the preparation of nanoparticles and dispersion of nanoparticles in the base fluid into a single step. There are some variations of one- step technique. In one of the common methods, named direct evaporation one-step method, the production of nanofluid is done by the solidification of the

nanoparticles, which are initially in gas phase inside the base fluid. The dispersion characteristics of nanofluids produced with one-step techniques are better than those produced with two-step technique. The main drawback of one-step techniques is that they are not proper for mass preparation.

In the two-step technique, the first step is the preparation of nanoparticles and the second step is the dispersion of the nanoparticles in a base fluid. Two-step technique is advantageous when mass preparation of nanofluids is considered, because nanoparticles can be produced in large quantities by utilizing the technique of inert gas condensation. The main disadvantage of the two-step technique is that the nanoparticles form clusters during the preparation of the nanofluid which prevents the proper dispersion of nanoparticles inside the base fluid.

#### 1.2.2.1 One-step method

There are following steps in the process of the direct evaporation - condensation method:

a. A cylinder containing a heat transfer fluid is rotated so that a thin film of the fluid is constantly transported over the top of the chamber.
b. A piece of the metallic material as the source of the nanoparticle is evaporated by heating on a crucible.
c. The evaporated particles contact the fluid overhead and condense as a nanofluid.
d. The fluid is cooled at the base of chamber to prevent any of its unwanted evaporation.

There are following guidelines for the synthesis of nanofluids.

i. Dispersability of nanoparticles
ii. Stability of nanoparticles
iii. Chemical compatibility of nanoparticles
iv. Thermal stability of nanofluids

#### 1.2.2.2 Two-step method

The preparation of nanofluids begins by direct mixing of the base fluid with the nanomaterials. In the first step, nanomaterials are synthesized and obtained as powders,

which are then introduced to the base fluid in a second step. Nanoparticles can be produced from several processes which can be categorized into one of five general synthetic methods. These five methods are:

i. Transition metal salt reduction
ii. Thermal decomposition and photochemical methods
iii. Legend reduction and displacement from organometallics
iv. Metal vapor synthesis
v. Electrochemical synthesis

Transition-metal nanoclusters are only kinetically stable because the formation of the bulk metal is its thermodynamic minimum. Therefore, nanoclusters that are freely dissolved in solution must be stabilized in a way that prevents the nanoclusters from coalescing, because such agglomeration would eventually lead to the formation of the thermodynamically favoured bulk metal.

The two-step process is commonly used for the synthesis of metal, metal oxides and carbon nanotube-based nanofluids. Single-wall carbon nanotubes (SWCNTs) and multi-walled carbon nanotubes (MWCNTs) are cylindrical allotropes of carbon. SWCNTs consist of a single cylinder of graphene, while MWCNTs contain multiple graphene cylinders nesting within each other.

## 1.3 Applications of nanofluids

Experimentally and theoretically nanofluids have been shown to possess improved heat transport properties and higher energy efficiency in a variety of thermal exchange systems for different industrial applications, such as heat transportation, electronic cooling, military, nuclear energy etc. The research on nanofluid could lead to a major impact in developing next generation coolants for numerous engineering and medical applications. The applications are stated and briefly discussed below.

### 1.3.1 Heat transportation

The mixture of ethylene glycol and water is almost a universally used vehicle coolant due to its lowered freezing point as well as its elevated boiling point. The thermal conductivity of ethylene glycol is relatively low as compare to water, while the engine oils are much worse heat transfer fluids than ethylene glycol in heat transport performance. The inclusion of nanoparticles and nanotubes to these coolants and lubricants to form nanofluids can increase their thermal conductivity and give the potential to improve the heat exchange rates and fuel efficiency. The above improvements can be used to reduce the size of the cooling systems or remove the heat from the vehicle engine exhaust in the same cooling system.

Refrigerant are widely used in refrigeration and air conditioning equipment in industries, offices and domestic and commercial buildings. Huge amount of energy is used by this equipment. Nanorefrigerant has potential to enhance heat transfer rate thus making heat exchanger of air conditioning and refrigeration equipment compact. This consequently will reduce energy consumption in these sectors along with reduction in emissions, global warming potential and greenhouse-gas effects.

### 1.3.2 Electronics cooling

The power dissipation of IC (Integrated Circuits) and microelectronic components has dramatically increased due to their size reduction. Better cooling fluids and thermal management with improved thermal transport properties are needed for safe operation. Nanofluids have been considered as working fluids in heat pipes for electronic cooling application.

### 1.3.3 Military applications

Military hardware both mechanical and electrical devices dissipates a large amount of heat and consequently requires high heat flux cooling fluids having sufficient cooling capacity. Nanofluids have the capability to provide the required cooling capacity in such applications, including high power laser and submarines.

### 1.3.4 Medical applications

Nanofluids are now being developed for medical applications, including cancer therapy. Iron based nanoparticles can be used as delivery vehicle for drugs or radiation without damaging the neighboring healthy tissues by guiding the particles up the blood stream to the tumor locations with magnets. Nanofluids can be used to produce higher temperatures around tumors to kill cancerous cells without affecting the nearby healthy cells. Nanofluids could also be used for safer surgery by cooling around the surgical region, thereby enhancing the patient's health and reducing the risk of organ damage.

Nanofluids are expensive due to the difficulty in manufacturing. The development of new synthesis methods is necessary to make nanofluids more affordable before they will see wide-spread practical and commercial applications.

# CHAPTER-2

# LITERATURE SURVEY

## 2.1 Thermal conductivity

In the last decade, a significant amount of experimental and theoretical research has been done to investigate the thermo physical behavior of nanofluids. In these studies, it was observed that a high thermal conductivity enhancement can be obtained with nanofluids, when small amount of nanoparticles are added in the base fluids. Most of the experimental work showed that the thermal conductivity enhancement obtained by using nanoparticle suspensions is relatively higher than that obtained by using conventional suspensions with particles which are millimeter or micrometer-sized. The nanorefrigerant is one kind of nanofluid and its host fluid is refrigerant. Refrigerant have poor heat transfer properties like other conventional thermo fluids. Various researchers have proposed theoretical models to explain and predict those anomalous thermal conductivity ratios, defined as thermal conductivity of the nanofluid ($k_{nf}$) divided by the thermal conductivity of the base fluid ($k_f$) (Turgut et al., 2009). But still the debates are going on to confirm this anomalous behavior of thermal conductivity.

### 2.1.1 Thermal conductivity of nanorefrigerant

Jwo et al. (2008) conducted studies on thermal conductivity of lubricant of R-134a refrigeration system. The objectives of the study were to discuss the dependence of thermal conductivity of $Al_2O_3$ nanorefrigerants on the temperature (20-40°C) under different weight fractions (1.0, 1.5, 2.0 wt.%). The results showed that the thermal conductivity was enhanced by 2.0%, 4.6%, and 2.5% when the nanoparticles of $Al_2O_3$ of 1.0, 1.5, and 2.0 wt.% were added at 40°C. It was found that optimal enhancement of the thermal conductivity was at 1.5 wt.%. The enhancement of thermal conductivity did not grow with the increase of weight ratios and it was different from the general nanofluids with lubricant as the basic solvent. Besides, thermal conductivity was increased from 1.5 to 4.6% when the sample temperature

was varied from 20℃ to 40℃ at 1.5 wt.%, and the trend of growth rates of the thermal conductivity was proportional to the temperature. From the results, it can be found that temperature has greater effects than weight fraction on the increase of thermal conductivities. Thus, it is better for nanorefrigerants of $Al_2O_3$ to be applied in the high temperature field than in the low temperature field.

Jiang et al. (2009) measured thermal conductivity of carbon nanotube nanorefrigerants and build a model for predicting the thermal conductivities of CNT nanorefrigerants. The effects of CNT diameters and CNT aspect ratios on nanorefrigerant's thermal conductivity were reflected in the experiments, and R-113 was used as the host refrigerant for the convenience of the experiments. The experimental results predicted that the thermal conductivity of CNT nanorefrigerants is much higher than those of CNT–water nanofluids or spherical-nanoparticle R-113 nanorefrigerants. Experiments also showed that the smaller the diameter of CNT or larger the aspect ratio of CNT, larger the thermal conductivity enhancement of CNT nanorefrigerant is. The existing models for predicting thermal conductivity of CNT nanofluids, including Hamilton- Crosser model, Xue model and Yu-Choi model were verified by the experimental data of CNT nanorefrigerants. The study predicted that Yu & Choi model has the mean deviation of 15.1% and it is more accurate than the other two models. And a modified Yu-Choi model was presented by improving the empirical constant of Yu & Choi model, and the mean deviation of the modified Yu-Choi model from the experimental results was 5.5%.

Mahbubul et al. (2013) investigated the thermal conductivity of $Al_2O_3$ nanoparticles suspended in R-134a. Suitable models from existing studies have been used to determine the thermal conductivity of the nanorefrigerants for the nanoparticle concentrations of 1 to 5 vol.%. It was found that the thermal conductivity of $Al_2O_3$/R-134a nanorefrigerant increased with the augmentation of particle concentration and temperature, but decreased with particle size intensification. Therefore, optimal particle volume fraction is important to be considered in producing nanorefrigerants that can enhance the performance of refrigeration systems.

The effect of particle size on the thermal conductivity of nanorefrigerant was investigated by using the modified model. Instead of using nanoparticles with constant particle size of 30 nm, the particle radius was assumed to be about 5 to 25 nm. The thermal conductivity of $Al_2O_3$/R-134a nanorefrigerant decreased with increasing particle size of

$Al_2O_3$ due to nanolayer or interfacial layer consideration. The interfacial layers around the nanoparticles are enhancement mechanisms that increase the thermal conductivity of nanorefrigerant as the augmentation effects of interfacial layer's increases by increasing the specific surface area of nanoparticles.

Effects of temperature on the thermal conductivity of nanorefrigerant have been investigated by changing the temperatures from 300 to 325 K. The thermal conductivity enhancement was about 43% at a temperature of 325 K with 5 vol. % of nanoparticle concentration. For temperature of 300 K and particle concentration of 1 vol. %, the obtained result shows lowest thermal conductivity increase of only about 4%. The results showed that the thermal conductivity of nanorefrigerant is proportional to temperature and the thermal conductivity enhancement can be considered low with temperature increment of 5 K for low concentration of nanoparticles. The high nanorefrigerant temperature intensifies the Brownian motion of nanoparticles and reduces the viscosity of nanorefrigerant. With the intensified Brownian motion, the contribution of micro convection in heat transport also could be increased. It was shown that the thermal conductivity of nanorefrigerant can be enhanced by increasing the temperature.

### 2.1.2 Effects of various parameters on thermal conductivity of nanofluids

Experimental studies show that thermal conductivity of nanofluids depends on many factors such as particle volume fraction, particle size, particle material, base fluid material, particle shape and temperature. Types and amount of additives and the acidity of the nanofluid were also shown to be effective in the thermal conductivity enhancement. In the following sections, experimental studies about the thermal conductivity of nanofluids are summarized. In each section, a specific parameter which effect thermal conductivity of nanofluid is discussed.

#### 2.1.2.1 Particle volume fraction

There are many studies in the literature which discuss the effect of volumetric concentration of the nanoparticles on the thermal conductivity of nanofluids.

Particle volume fraction is a parameter which is investigated extensively in the study of nanofluids and results are normally found in agreement qualitatively. Most of the researchers have reported increase in thermal conductivity with increasing particle volume fraction and the relation found is usually linear (Özerinç et al., 2010). However, there are also some studies which indicate nonlinear behavior. An example is the study made by Murshed et al. (2005).They measured the thermal conductivity of $TiO_2$/deionized water nanofluid at room temperature by using transient hot-wire method. The volume fraction of nanoparticles was varied between 0.5 and 5%. A nonlinear relationship was observed between thermal conductivity ratio and particle volume fraction, especially at very low volume fractions. The authors observed that the nonlinear behavior might be due to the cetyltrimethyl ammonium bromide surfactant, application of sonication for a long time or hydrophobic surface forces involved.

Choi et al. (2001) investigated the thermal conductivity of nanofluids prepared by dispersing multiwalled carbon nanotubes (MWCNT) in oil. They also found a nonlinear relation between thermal conductivity ratio and particle volume fraction. According to the authors, a nonlinear relation is an indication of interactions between particles. It was predicted that despite the fact that particle volume fraction is very small nanotubes interact with each other due to the very high particle concentration ($10^{11}$ particles/$cm^2$).

#### 2.1.2.2 Particle material

Most of the studies show that particle material is an important parameter that affects the thermal conductivity of nanofluids. It might be thought that the difference in the thermal conductivities of particle materials is the main reason of this effect. However, studies shows that particle type may affect the thermal conductivity of nanofluids in other ways.

Lee et al. (1999) considered the thermal conductivity of nanofluids with $Al_2O_3$ and CuO nanoparticles and they found that nanofluids with CuO nanoparticles showed better enhancement when compared to the nanofluids prepared using $Al_2O_3$ nanoparticles. It should be noted that $Al_2O_3$, as a material, has higher thermal conductivity than CuO. Therefore, thermal conductivity of particle material may not be the

dominant parameter that determines the thermal conductivity of the nanofluid. According to the authors, the main factor is the fact that $Al_2O_3$ nanoparticles formed relatively larger clusters when compared to CuO nanoparticles. It might be an explanation if the main mechanism of thermal conductivity enhancement is accepted to be the Brownian motion of nanoparticles, the effect of Brownian motion diminishes with increasing particle size.

Choi et al. (2001) studied the thermal conductivity enhancement of oil based nanofluids containing MWCNT with a mean diameter of around 25 nm and length around 50 μm. The base fluid used was synthetic poly oil. Measurements were conducted at room temperature and 160% enhancement (a thermal conductivity ratio of 2.6) was observed for 1 vol.% MWCNT/oil nanofluid. The author noted that such an anomalous enhancement might be due to the liquid nanolayers forming around the nanotubes. On the other hand, the fact is that heat transported ballistically inside the nanotubes improves the conduction of heat in the tubes and the effect of this factor is not dominant according to the authors. It should also be noted that the shape of nanotubes might also be effective in the anomalous enhancement values. The length of the nanotubes is on the order of micrometers and this enables rapid heat conduction across relatively large distances, that is not possible for spherical nanoparticles as long as there is no clustering.

#### 2.1.2.3 Base fluid

According to the conventional models for thermal conductivity such as the Maxwell model, as the base fluid thermal conductivity of a mixture decreases, the thermal conductivity ratio (thermal conductivity of nanofluid ($k_{nf}$) divided by the thermal conductivity of base fluid ($k_f$) increases. When it comes to nanofluids, the situation is more complicated due to the fact that the viscosity of the base fluid affects the Brownian motion of nanoparticles and that in turn affects the thermal conductivity of the nanofluid (Xuan et al., 2003). Moreover, Lee et al. (2007) examined the effect of electric double layer forming around nanoparticles on the thermal conductivity of nanofluids and showed that the thermal conductivity and thickness of the layer depends on base fluid. It is

tough to determine the quantitative effects of these factors completely. So, systematic experiments are required that will show the effect of base fluid on the thermal conductivity of nanofluids.

Chopkar et al. (2008) also analyzed the effect of base fluid by comparing water and ethylene glycol. $Al_2Cu$ and $Ag_2Al$ nanoparticles were used in the study and it was found that water-based nanofluids showed a higher thermal conductivity ratio. It should be noted that more than 100% enhancement was obtained for the 2.0 vol.% $Ag_2Al$(30 nm)/water nanofluid. Base fluid effect was also investigated with MWCNT nanofluids. Ethylene glycol and synthetic engine oil were used as base fluids in the experiments conducted by Liu et al. (2005). Thermal conductivity of nanofluids were measured by a transient hot-wire method. 1 vol. % MWCNT/ethylene glycol nanofluid showed 12.4% thermal conductivity enhancement, whereas for 2 vol.% MWCNT/synthetic engine oil nanofluid, enhancement was 30%. It was observed that higher enhancements were achieved with synthetic engine oil as the base fluid.

#### 2.1.2.4 Particle size

Particle size is another important parameter on which thermal conductivity of nanofluids depends and with the advancement in nanotechnology, it is possible to produce nanoparticles of various sizes, generally ranging between 5 and 100 nm.

Eastman et al. (2001) studied Cu nanoparticles with ethylene glycol as the base fluid. By using a one-step production method, suspension with Cu nanoparticles smaller than 10 nm was obtained. Thioglycolic acid less than 1 vol.% was added to some of the samples for stabilizing purposes and those samples showed much better enhancement when compared to samples without thioglycolic acid. A 40% increase in thermal conductivity was observed at a particle volume fraction of 0.3% (with thioglycolic acid). To make a comparison, it should be noted that in the study of Lee et al. (2002), the researchers obtained 20% enhancement with 4 vol.% CuO (23.6 nm)/ethylene glycol nanofluid. As a result of the tremendous enhancements obtained, Eastman et al. (2001) concluded that the size of the nanoparticles is an important factor that affects the thermal conductivity enhancement, which contradict the predictions of conventional models such

as Hamilton and Crosser model (1962), which does not take the effect of particle size on thermal conductivity into account.

Chopkar et al. (2008) investigated the effect of particle size on the thermal conductivity of water- and ethylene glycol-based nanofluids with $Al_2Cu$ and $Ag_2Al$ nanoparticles. Nanoparticles with sizes varying between 30 and 120 nm were used in the study. For all noted nanofluids, it was observed that thermal conductivity enhancement increases with decreasing particle size.

The general trend in the experimental data is that the thermal conductivity of nanofluids increases with decreasing particle size. This trend is theoretically supported by two mechanisms of thermal conductivity enhancement; Brownian motion of nanoparticles and liquid layering around nanoparticles (Özerinç et al., 2010)

#### 2.1.2.5 Particle shape

There are mainly two particle shapes used in nanofluid research; spherical particles and cylindrical particles. Cylindrical particles usually have a large length-to-dia. ratio. The thermal conductivity of SiC/distilled water and SiC/ethylene glycol nanofluids were investigated by Xie et al. (2002). Two types of nanoparticles were used for the preparation of nanofluids; spherical particles with 26 nm average diameter and cylindrical particles with 600 nm average diameter. It was found that 4.2 vol.% water-based nanofluid with spherical particles had a thermal conductivity enhancement of 15.8%, whereas 4 vol.% nanofluid with cylindrical particles had a thermal conductivity enhancement of 22.9%. The authors compared the results with the Hamilton and Crosser model (1962). It was noted that Hamilton and Crosser model was successful in predicting the enhancement in cylindrical particles, whereas it underestimated the values associated with nanofluids with spherical particles.

In addition to these experimental results, the fact that nanofluids with carbon nanotubes (which are cylindrical in shape) generally show greater thermal conductivity enhancement than nanofluids with spherical particles should be considered. As a result, one can conclude that cylindrical nanoparticles provide higher thermal conductivity enhancement than spherical nanoparticles. One of the possible reasons of this is the rapid

heat transport along relatively larger distances in cylindrical particles since cylindrical particles usually have lengths on the order of micrometers (Özerinç et al., 2010). However, it should be noted that nanofluids with cylindrical particles usually have much larger viscosities than those with spherical nanoparticles. As a result, the associated increase in pumping power is large and this reduces the feasibility of usage of nanofluids with cylindrical particles.

### 2.1.2.6. Temperature

In conventional suspensions of solid particles (with sizes on the order of millimeters or micrometers) in liquids, thermal conductivity of the mixture depends on temperature only due to the dependence of thermal conductivity of base liquid and solid particles on temperature (Özerinç et al., 2010). However, in case of nanofluids, the change of temperature affects the Brownian motion of nanoparticles nanofluids were varied between 0.2 & 3 vol.%. It was observed that thermal conductivity ratio does not vary with temperature significantly. This observation is contradictory with the afore-mentioned studies. The results can be considered as an indication of the importance of the usage of surfactants in nanofluids, because no surfactant was used in the study. Temperature dependence of thermal conductivity of nanofluids was also investigated for the case of nanofluids with carbon nanotubes.

Ding et al. (2006) measured the thermal conductivity of MWCNT/water nanofluid and ultrasonic vibration was applied to the samples. First Gum Arabic was added to the samples in order to obtain better dispersion and to adjust the pH value and then the nanofluid was homogenized with a high shear homogenizer. Transient hot-wire method was applied for thermal conductivity measurements. There is no information was given about the size of MWCNT but from the provided scanning electron microscopy images, a very rough estimation of nanotube diameter could be made as 40 nm. Measurements were made at three different temperatures; 20, 25, and 30°C. Particle weight fraction was varied between 0.1 and 1%. It was found that thermal conductivity ratio increases with both particle volume fraction and temperature. However, at 20 and 25°C, increase of thermal conductivity ratio with particle volume fraction stopped after 0.5 wt%. On the other

hand, at 30°C, thermal conductivity ratio continued to increase after 0.5 wt%. A maximum enhancement of 80% was achieved at 30°C for 1 wt% of MWCNT/water nanofluid. At 20°C, the associated enhancement decreased to 10%. Thermal conductivity research of nanofluids in terms of temperature dependence is not limited to the aforementioned studies.

The relationship for the k in terms of fundamental properties of the liquid is $k=2Rv€^{-2}$, where R is the gas constant, 'v' is the velocity of sound in the liquid and € is the mean distance of separation of the centers of the molecules (Bridgman et al., 1923).The conductivity of water is three to four times as high as that of the ordinary organic liquids because of its low compressibility and the fact that the centers of the molecules in water are closer together than in the ordinary liquid. The above formula gives the right sign for the temperature coefficient of conductivity at atmospheric pressure, both for ordinary liquids and water.

For the ordinary liquid, both 'v' and $€^{-2}$ decreases with rising temperature, so that thermal conductivity is expected to decrease with rising temperature, as it actually does, whereas for water increases with rising temperature (both the isothermal compressibility and the thermal expansion of water vary abnormally with temperature) at a rate more than that is sufficient to compensate for the decrease of €, so that on the whole the conductivity should increase. This explains the different trend in temperature dependence observed between aqueous and nonaqueous nanofluids. These results suggest that the k of the nanofluids simply track the thermal conductivity of the base fluid.

#### 2.1.2.7 Clustering

Clustering is the formation of larger particles through aggregation of nanoparticles. Clustering effect is always present in nanofluids and it is an effective parameter in the evaluation of thermal conductivity of nanofluids.

Hong et al. (2006) investigated this effect for Fe (10 nm)/ethylene glycol nanofluids. The thermal conductivity of nanofluids were determined as a function of the duration of the application of the ultrasonic vibration, which was varied between 0 min, that is, no vibration applied, and 70 min. It was seen that thermal conductivity ratio increased with

increasing vibration time and the rate of this increase became smaller for longer vibration time. The variation of thermal conductivity of nanofluid with time after the application of vibration was investigated and it was found that thermal conductivity decreased as time progressed. Also, the variation of average size of clusters was determined as a function of time after the application of vibration and it was noted that cluster size increases with time. As a result of these observations, it was concluded that the size of the clusters formed by the nanoparticles had a major influence on the thermal conductivity.

#### 2.1.2.8 pH Value

The number of studies regarding the pH value of nanofluids is limited when compared to the studies regarding the other parameters. Xie et al. (2002) measured the thermal conductivity of nanofluids, which are prepared by dispersing $Al_2O_3$ nanoparticles into water, pump oil and ethylene glycol. They reported significant decrease in thermal conductivity ratio with increasing pH values. It was also observed that the rate of change of thermal conductivity with particle volume fraction was dependent on pH value.

Thermal conductivity enhancement of 5 vol.% $Al_2O_3$/water nanofluid was 23% when pH is equal to 2.0 and it became 19% when pH is equal to 11.5. The authors compared the dependence of thermal conductivity on pH to the fact that as the difference between the isoelectric point of $Al_2O_3$ nanoparticles and pH value of the solution increases, mobility of nanoparticles increases, which improve the micro-convection effect.

### 2.1.3 Measurement techniques for thermal conductivity

Nanofluids attracted a vast attention due to increment in thermal conductivity compared to basefluid. Measuring these thermophysical properties have been a challenge for a long time since different methods and techniques give different results. Thus, the method which is going to be used would be significant to lower the measurement error and uncertainty as much as possible. In this section, major thermal conductivity measurement methods from different literatures have been described briefly, and following are methods which are

going to be investigated (Paul et al., 2010).

a) Transient hot-wire techniques
b) Transient Plane Source (TPS) method
c) Cylindrical cell method
d) Thermal comparator method

Generally, Fourier's law for conduction heat transfer can be utilized to measure thermal conductivity of a material. Temperature difference can cause heat transfer through materials which is known as conduction heat transfer. In Case of liquids, avoiding convection should be regarded during measurements and since fluids does not have definite shape, size and cross sectional area, it would be more difficult to calculate thermal conductivity. Thus, measurement should take place in a very short time. Even the situation is worse in case of nanofluids, whereas suspended nanoparticles may cause a major problem (Paul et al., 2010).

#### 2.1.3.1 Transient hot-wire (THW) method

This can be known as the most regular and the oldest method of measuring thermal conductivity. Comparing other methods, it can be known as a very fast measurement method and conceptual design of the apparatus is simple as well. It has been used to measure thermal conductivity of powders at the beginning. However, it has been improved by many researchers. Inasmuch as the potential of method to lower possibility of natural convection, it is applied to measure thermal conductivity of fluids (Paul et al., 2010).

Transient hot-wire experimental setup is composed of Whetstone bridge circuit, DC power supply, stabilizer, switch, A/D converter and a computer (Figure 2.1). In this method, a platinum wire is used for both heating and measuring temperature. Constant power is supplied to the wire causing temperature increment of that (Paul et al., 2010).

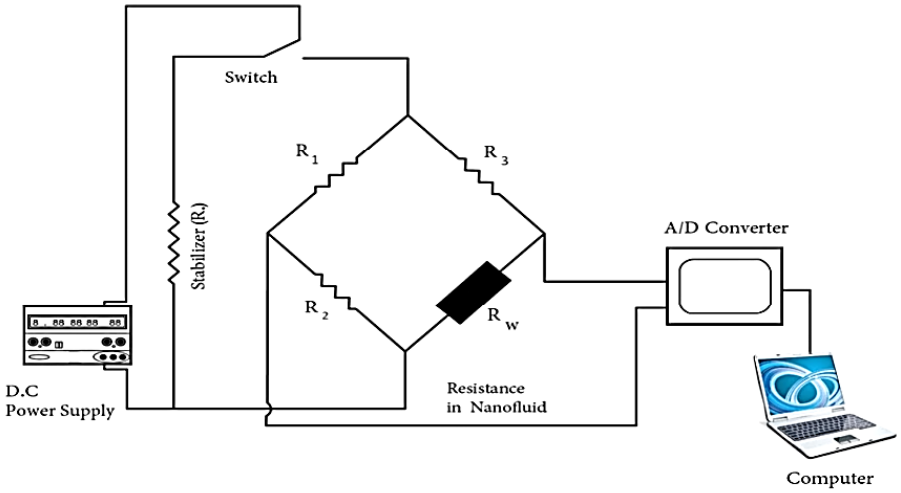


**Figure 2.1** Schematic of transient hot-wire experimental setup (Paul et al., 2010)

Consequently, wire would heat up the temperature of material which can be solid, liquid or nanofluid. Afterwards, thermal conductivity of the sample can be calculated concerning heat flux, temperature difference, and some geometric parameters based on Fourier's law.

#### 2.1.3.2 Transient Plane Source (TPS) method

To compute thermal conductivity, transient plane source (TPS) theory is utilized by thermal constant analyzer. TPS sensor plays similar role as what probe or wire does in THW method; which means it acts as heating source together with temperature sensor. Main components of experimental setup for transient plane source method are thermal bath with thermometer, TPS sensor, sample holder, thermal constants analyzer and computer. For calculating thermal conductivity of solids, probe of the analyzer is sandwiched between two sections of the material while for liquids it is immersed into the sample. The sample holder would be kept inside thermal bath with constant temperature and small amount of power will be supplied in short time to the sensor. Analyzer can calculate thermal conductivity later on (Paul et al., 2010).

#### 2.1.3.3 Cylindrical cell method

It might be known as one of the most common steady-state methods used for measuring thermal conductivity of fluids (Paul et al., 2010).The instrument applying cylindrical cell method is composed of two coaxial cylinders which can be named as inner and outer cylinders. Inside the inner cylinder (made of copper), heater is placed while inside the outer cylinder (made of galvanize) where there is a gap between outer and inner cylinder, fluid sample would be kept. Two thermocouples are utilized to measure temperature difference after applying power and heat transform caused by heater. Using Fourier's law in coaxial cylinders, thermal conductivity of sample in the gap could be computed.

#### 2.1.3.4 Thermal comparator method

Through the years, idea was developed by some researches until Paul et al. developed the idea inherently to measure thermal conductivity of nanofluids (Paul et al., 2010). Mainly, new device is composed of a copper probe, sample holder, DC voltmeter, voltage stabilizer and a heater. It is interested to note that unlike some other mentioned methods, in this technique probe is required to have only a point contact with the sample.

Thermocouple is placed between the sample and the probe which is supposed to have constant temperature by heater. Direct relationship should exist between thermal conductivity and observed differential emf after sensing temperature by thermocouple. It occurs when probe would be kept in point contact with the sample and thermo-emf is generated in circuit to cover the probe assembly and nanofluid. Considering different voltages in the circuit as well as boundary conditions and proper equations, thermal conductivity can be calculated. Paul et al. (2010) reported it as a reliable method when they tested some samples such as water and ethylene glycol.

### 2.1.4 Theoretical models of thermal conductivity

#### 2.1.4.1 Classical models

More than a century ago, Maxwell derived an equation for calculating the effective thermal conductivity of solid-liquid mixtures consisting of spherical particles (Maxwell, 1873):

$$k_{n_f} = \frac{k_p + 2k_f + 2(k_p - k_f)\phi}{k_p + 2k_f - (k_P - k_f)\phi}\, k_f, \tag{2.1}$$

where $k_{n_f}$, $k_p$, and $k_f$ are the thermal conductivity of the nanofluid, nanoparticles and base fluid, respectively. $\phi$ is the volume fraction of particles in the mixture. As seen from the expression, the effect of the size and shape of the particles was not included in the analysis. It should be noted that the interaction between the particles was also neglected in the derivation.

Hamilton and Crosser (1962) extended the Maxwell model in order to take the effect of the shape of the solid particles into account, in addition to the thermal conductivities of solid and liquid phases and particle volume fraction. The model is as follows:

$$k_{n_f} = \frac{k_p + (n-1)k_f + (n-1)(k_p - k_f)\phi}{k_p + (n-1)k_f - (k_P - k_f)\phi}\, k_f, \tag{2.2}$$

where n is the empirical shape factor and it is defined as:

$$n = \frac{3}{\Psi} \tag{2.3}$$

where $\Psi$ is the sphericity. Sphericity is the ratio of the surface area of a sphere with a volume equal to that of the particle to the surface area of the particle. Therefore, n = 3 for a sphere and in that case the Hamilton and Crosser model becomes identical to the Maxwell model.

Both Maxwell and Hamilton and Crosser models were originally derived for relatively larger solid particles that have diameters on the order of millimeters or micrometers. Therefore, it is questionable whether these models are able to predict the effective thermal

conductivity of nanofluids. Nevertheless, these models are utilized frequently due to their simplicity in the study of nanofluids to have a comparison between theoretical and experimental findings (Özerinç et al., 2010).

Recently, many theoretical studies were made and several mechanisms were proposed in order to explain the anomalous thermal conductivity enhancement obtained with nanofluids. In the following sections, proposed mechanisms of thermal conductivity enhancement in nanofluids are discussed and thermal conductivity models based on those mechanisms are summarized.

#### 2.1.4.2 Model based on Brownian motion

Brownian motion is the random motion of particles suspended in a fluid. When nanofluids are considered, this random motion transports energy directly by nanoparticles. In addition, a micro-convection effect, which is due to the fluid mixing around nanoparticles is also proposed to be important. There are many studies in the literature regarding the effect of Brownian motion on the thermal conductivity of nanofluids.

Koo and Kleinstreuer (2004) considered the thermal conductivity of nanofluids to be composed of two parts:

$$k_{n_f} = k_{static} + k_{Brownian} \tag{2.4}$$

Where, $k_{static}$ represents the thermal conductivity enhancement due to the higher thermal conductivity of the nanoparticles and $k_{Brownian}$ takes the effect of Brownian motion into account. For the static part, the classical Maxwell model was proposed.

For $k_{Brownian}$, Brownian motion of particles was considered together with the effect of fluid particles moving with nanoparticles around them. As a result, the following expression was proposed:

$$k_{Brownian} \equiv 5 \times 10^4 \beta \phi \rho_f C_{P,f} \sqrt{\frac{k_B T}{\rho_p d_p}} f, \tag{2.5}$$

Where, $\rho_p$ and $\rho_f$ are the density of nanoparticles and base fluid, respectively, and T the temperature in K. $C_{P,f}$ is specific heat capacity of base fluid. In the analysis, the interactions between nanoparticles and fluid volumes moving around them were not considered and an additional term, $\beta$ was introduced in order to take that effect into account. Koo and Kleinstreuer indicated that this term becomes more effective with increasing volume fraction. Another parameter, f, was introduced to the model in order to increase the temperature dependency of the model. Both f and $\beta$ were determined by utilizing available experimental data:

$$f = (-134.63 + 1722.3\phi) + (0.4705 - 6.04\phi)T, \quad (2.6)$$

which is obtained by using the results of the study of Das et al. (2010) for CuO nanofluids. For other nanofluids, f can be taken as 1 due to lack of experimental data. Associated values are listed in Table 2.1. It is difficult to determine theoretical expressions for f and due to the complexities involved and this can be considered as a drawback of the model (Özerinç et al., 2010).

**Table 2.1** $\beta$ values for different nanoparticles to be used in Eq.2.5 (Koo et al., 2004)

| **Types of particles** | $\beta$ | **Remarks** |
|---|---|---|
| **Au-citrate, Ag-citrate and CuO** | $0.0137(100\,\phi)^{-0.8229}$ | $\phi < 1\%$ |
| **Cuo** | $0.0011(100\,\phi)^{-0.7272}$ | $\phi > 1\%$ |
| **$Al_2O_3$** | $0.0017(100\,\phi)^{-0.0841}$ | $\phi > 1\%$ |

### 2.1.4.3 Models based on clustering

Xuan et al. (2003) studied the thermal conductivity of nanofluids by considering Brownian motion and clustering of nanoparticles. An equation was proposed to predict the thermal conductivity of nanofluids:

$$k_{n_f} = \frac{k_p + 2k_f + 2(k_p - k_f)\phi}{k_p + 2k_f - (k_P - k_f)\phi}\, k_f + k_f \phi \rho_p C_{p,p} \sqrt{\frac{k_B T}{3\pi r_{cl} \mu_f}} \quad (2.7)$$

Here, $r_{cl}$ is the apparent radius of the nanoparticle clusters, which should be determined by experiment. T is temperature in K. $\mu_f$ is the dynamic viscosity of the base fluid and it can be calculated from the study of Li and Xuan (2000). The first term on the right-hand side of Eq. (2.7) is the Maxwell model (1873) for thermal conductivity of suspensions of solid particles in fluids. The second term on the right-hand side of Eq. (2.7) adds the effect of the random motion of the nanoparticles into account.

#### 2.1.4.4 Models based on liquid layering

Yu and Choi (2003) presented a model for the determination of the effective thermal conductivity of nanofluids by modifying the Maxwell model (1873). In the modification, the effect of the liquid nanolayers formed around nanoparticles was taken into account. The nanoparticle and the layer around it were considered as a single particle and the thermal conductivity of this particle was determined by using effective medium theory (Li et al., 2002).The result was substituted into the Maxwell model and the following expression was obtained.

$$\mathrm{k_{n_f}} = \frac{\mathrm{k_{pe}} + 2\mathrm{k_f} + 2(\mathrm{k_{pe}} - \mathrm{k_f})(1+\beta)^3\phi}{\mathrm{k_p} + 2\mathrm{k_f} - (\mathrm{k_{Pe}} - \mathrm{k_f})(1+\beta)^3\phi}\, \mathrm{k_f} \quad (2.8)$$

where $k_{pe}$ is the thermal conductivity of the equivalent nanoparticle;

$$\mathrm{k_{pe}} = \frac{[2(1-\gamma) + (1+\beta)^3(1+2\gamma)]\gamma}{(1+\beta)^3(1+2\gamma) - (1-\gamma)}\, \mathrm{k_{p,}} \quad (2.9)$$

$$\gamma = \frac{\mathrm{k_l}}{\mathrm{k_p}}, \quad (2.10)$$

where, $k_l$ is thermal conductivity of the nanolayer. β is defined as:

$$\beta = \frac{t}{r_p}, \tag{2.11}$$

where, t is nanolayer thickness and $r_p$ the nanoparticle radius.

## 2.2 Viscosity

### 2.2.1 Viscosity of nanorefrigerant

Mahbubul *et al.* (2013) found that the viscosity of nanorefrigerant also increases with the augmentation of nanoparticles concentrations and the viscosity enhancement due to same particle concentration is differed for different types of refrigerants.Investigating the relative viscosity of nanorefrigerant by using different models shows that it is proportional to the particle volume fraction. The result from the study has an almost similar indication to other models. However, a slope constructed by using Einstein's model is parted away from others as the particle concentration increase since this model is valid only for particle concentration less than 2 % volume. To overcome this limitation, Krieger and Dougherty (K–D) model have been included to determine the viscosity of nanorefrigerant at higher particle concentrations up to 5 % volume in the study. Even though K–D, Batchelor and Ward models used different consideration in proposing their equations; (for example Batchelor considered the Brownian motion of rigid and spherical particles), the results from different models are similar. The reason for this is that their theoretical works on particle suspensions were developed based on Einstein's model, which introduced that the viscosity of nanofluids was strongly influenced by particle concentration.

Mahbubul et al. 2012 investigated that the volumetric and temperature effects over viscosity of R123-$TiO_2$ nanorefrigerants have been studied for 5 to 20°C temperature and up to 2% volume. The effect of pressure drop with the increase of viscosity has also been investigated. Based on the analysis it was found that viscosity of nanorefrigerant increased accordingly with the increase of nanoparticle volume concentrations and decreases with the increment of temperature. Also, the pressure drop augmented significantly with the intensification of volume concentrations and vapor quality. So, low volume concentrations of nanorefrigerant are suggested for better performance of a refrigeration system.

### 2.2.2 Effect of various parameters on viscosity

In the past decades the investigation of nanofluids viscosities was not considered as same as thermal properties. Yet, viscosity of nanofluid is one of the most critical parameter in nanofluids, which should be considered by researches and need to be investigated thoroughly. In order to design a proper cooling system, it is expected that nanofluids as cooling media have almost considerable increment in thermal conductivity. On the other hand, almost less increment or constant viscosity is expected which means higher ratio of thermal conductivity and viscosity. There are different crucial parameters influencing the viscosity that are investigated by researches. These factors consist of temperature, volume concentration, particle size, morphology, time sonication, shear rate, etc. (Li et al., 2009).

Given papers reviewed, it is tried to list different factors which can influence the viscosity.

a. Temperature
b. Volume fraction
c. Shear rate
d. Dispersion method, stabilizers and Clustering

#### 2.2.2.1 Temperature

Temperature is discussed in literature as one of most important parameters affecting the viscosity. Prasher et al. (2009) have shown that the relative viscosity of nanofluids is not a strong function of temperature while Li et al. (2002) have proven a decrement of apparent viscosity by increasing the temperature for CuO. L. Chen et al. (2008) investigated the multi walled carbon nano tubes (MWCNTs) in distilled water. They showed there is almost no change in viscosity of nanofluid with increase of temperature up to 55°C. Surprisingly, sudden increment of viscosity happened in range of 55 to 70°C. On the other hand, Lee et al. (2011) measured SiC and observed that the viscosity of SiC decreases by temperature.

#### 2.2.2.2 Volume fraction

Volume concentration of nanofluids is another important characteristic of these coolant media which directly influences the viscosity of nanofluids, on the other hand, it affects the thermal properties. There have been many researches to see the effect of wt.% of nanoparticles on viscosity. The result almost shows the higher wt.% is, the more viscosity nanofluid. Concerning the Prasher et al. (2006) experiments, the volume concentration can highly affects the viscosity of nanofluids.

Lee et al. (2011) investigating on volume concentration found that the viscosity increases by versus volume fraction. L.Chen et al. (2008) found the increment of volume concentration is led to higher viscosity for MWCNTs (they measured volume fractions of 0.002, 0.004, 0.006, 0.008 and 0.010). Das et al. (2003) measured $Al_2O_3$ and found that viscosity is higher for nanofluids with stronger particle concentration. Besides, they believed that there is a firm dependency of volume concentration and nonNewtonian behavior of nanofluids.

#### 2.2.2.3 Shear rate

Shear rate is another parameter which can affect the viscosity in non-Newtonian nanofluids. Ding et al. (2006) worked by CNTs found shear thinning phenomenon in nanofluids. It means nanofluids can sometimes show more appropriate fluid flow performance because of shear thinning which happens at higher shear rates. Shear viscosity of nanofluids, which can be especially altered in non-Newtonian nanofluids, tested by Chen et al. (2007) using titania ethylene glycol based. They showed Newtonian behavior and proved that shear viscosity depends on both Temperature and particle's concentration.

#### 2.2.2.4 Dispersion method

Wang et al. (1999) made a dispersion method and its contribution to viscosity. They analyzed three different methods of dispersion and measured dianoized water-based $Al_2O_3$ with 5 vol.% and particle size of 28 nm. They reported 86% increment in viscosity for this

nanofluid. The dispersion method that they used was a mechanical blending technique (method 1). Besides, coating particles with polymers (method 2) and ltration (method 3) were applied for dispersion of nanoparticles. 40 % increment is showed for ethylene glycol based $Al_2O_3$ at a volumetric loading of 3.5 volume % by them. In general their results demonstrate a dependency of viscosity on dispersion method and first method contributes to viscosity increment compared to two other ones. Moreover, other parameters such as pH and Sonication time can affect the viscosity of nanofluids.

### 2.2.3 Viscosity Measurement Methods

The following instruments which are generally used in viscosity measurement have been discussed.

#### 2.2.3.1. Capillary Viscometer

This method is introduced as the best method for fluid viscosity measurement. Capillary viscometers are basically used for Newtonian, incompressible and wall adherence liquids. The principle of capillary viscometers is the time at which a standard volume of fluid passes through a length of capillary tube. The pre-condition assumed for this measurement is having a laminar, incompressible and stationary fluid. Moreover, since flow influence at the entry and exit of capillary is negligible, the viscosity of fluids is considered to be pressure independent.

Li et al. (2002) measured the viscosity of water-based CuO by a capillary viscometer. In this study, they mentioned that the capillary tube diameter probably influences the apparent viscosity for higher volume concentrations and lower temperature, where the viscosity is higher.

#### 2.2.3.2 Rotational viscometer

This is a kind of viscometer in which the principal of operation is to drive a spindle (which is immersed in the test fluid) through a calibrated spring. Torque on cylinder rotating in the

sample is applied to calculate the viscosity. The viscous resistant of the sample against the cylinder is measured by a spring deflection and spring deflection is measured with a rotary transducer. This genre of viscometers are consisting of two concentric cylinders namely a bob (spindle) and a crucible (cylinder).

The measurement range of a rotary cylinder viscometers (in cP/mPs) is determined by the spindle rotational speed, size and shape of the rotary spindle, container in which spindle is rotating in, and the full-scale torque of the calibrated spring and so forth. (Brooks et al., 2005)

### 2.2.4 Theoretical models of viscosity

This section deals with the development of nanofluids viscosity model as shown in Table 2.2.

**Table 2.2:** Nanofluid viscosity models proposed by several authors (Kumar et al., 2012)

| Model Name | Effective Viscosity models | Remarks |
|---|---|---|
| Einstein (1906) | $\frac{\mu_{nf}}{\mu_f} = 1 + 2.5\ \emptyset$ | Valid for spherical particles of low particle volume fraction $\emptyset$ |
| Vand (1948) | $\frac{\mu_{nf}}{\mu_f} = 1 + 2.5\ \emptyset + 7.349\emptyset^{\,2} + \cdots$ | Valid for spherical nanoparticles |
| White (2005) | $ln\frac{\mu_{nf}}{\mu_f} = \mathrm{a} + \mathrm{b}\left(\frac{T_o}{T}\right) + \mathrm{c}\left(\frac{T_o}{T}\right)^2$ | Temperature dependent viscosity of $Al_2O_3$ |
| Nguyen et al. (2007) | $\frac{\mu_{nf}}{\mu_f} = 2.1275 - 0.0215\mathrm{T} + 0.00027\mathrm{T}^{\,2}$ | Temperature dependent nanofluids viscosity model and valid for 1% to 4% |
| Batchelor (1977) | $\frac{\mu_{nf}}{\mu_f} = 1 + 2.5\ \emptyset + 6.5\ \emptyset^{\,2} + \cdots$ | Considered the effect of Brownian motion. |
| Brinkman (1952) | $\frac{\mu_{nf}}{\mu_f} = \frac{1}{(1-\emptyset)^{2.5}}$ | Formulated by two corrections of Einstein's model |

## 2.3 Experimental investigations of vapour compression refrigeration system

Nanoparticles can be used in refrigeration systems because of its remarkable potential to improve thermophysical and heat transfer performance of refrigeration systems. In a vapour compression refrigeration system the nanoparticles can be added to the lubricant (compressor oil). When the refrigerant is circulated through the compressor it carries traces of lubricant and nanoparticles mixture (nanolubricants) so that the other parts of the system will have nanolubricant refrigerant mixture.

Recently, some investigators have conducted studies on vapour compression refrigeration systems, to study the effect of nanoparticle in the refrigerant/lubricant on its performance. Bi et al. (2007) conducted experimental studies on a domestic refrigerator using nanorefrigerants. In their studies R134a was used as refrigerant, and a mixture of mineral oil $TiO_2$ was used as the lubricant. They observed that the refrigeration system with the nanorefrigerant worked normally and efficiently and the energy consumption reduces by 21.2%. When compared with R134a/POE oil system. Later, Bi et al. (2008) found that there is remarkable reduction in the power consumption and significant improvement in freezing capacity. They pointed out the improvement in the system performance is due to better thermo physical properties of mineral oil and the presence of nanoparticles in the refrigerant.

Jwo et al. (2009) conducted studies on a refrigeration system replacing R-134a refrigerant and polyester lubricant with a hydrocarbon refrigerant and mineral lubricant. The mineral lubricant included added $Al_2O_3$ nanoparticles to improve the lubrication and heat-transfer performance. Their studies show that the 60% R-134a and 0.1 wt.% $Al_2O_3$ nanoparticles were optimal. Under these conditions, the power consumption was reduced by about 2.4%, and the coefficient of performance was increased by 4.4%. Henderson et al. (2010) conducted an experimental analysis on the flow boiling heat transfer of R134a based nanorefrigerants in a horizontal tube. They observed excellent dispersion of CuO nanoparticle with R134a and POE oil and the heat transfer coefficient increases more than 100% over baseline R134a/POE oil results.

Bobbo et al. (2010) conducted a study on the influence of dispersion of single wall carbon nanohorns (SWCNH) and $TiO_2$ on the tribological properties of POE oil together with

the effects on the solubility of R134a at different temperatures. They represented that the tribological behaviour of the base lubricant can be either improved or worsen by adding nanoparticles. On the other hand the nanoparticle dispersion did not affect significantly the solubility.Bi et al. (2011) conducted an experimental study on the performance of a domestic refrigerator using $TiO_2$-R600a nanorefrigerant as working fluid. They showed that the $TiO_2$-R600a system worked normally and efficiently in the refrigerator and an energy saving of 9.6%. They too cited that the freezing velocity of nano refrigerating system was more than that with pure R600a system.

## 2.4 Characterization Techniques

### 2.4.1 X-Ray Diffraction

The X-ray Diffraction (XRD) is used as a primary tool to characterize the crystal structure and crystallite size of nanoparticles. It exploits the wave nature of electromagnetic radiation. The phenomenon of diffraction occurs whenever wave motion of an electromagnetic wave encounter a set of regularly spaced scattering objects, provided that the wavelength of electromagnetic is in the same order of distance between the scattering centers. Since the wavelength of X-rays (0.1 to 1 Å) is equal to the interatomic distance in crystals, X-ray diffraction can be observed when X- rays interact with crystalline materials (Kittel et al., 2004). If many atoms are scattering the X-rays together, scattered waves from all the atoms can interfere. If the scattered X-rays are in phase, they interfere constructively resulting diffracted beams in specific directions. These directions are governed by the wavelength ($\lambda$) of incident X-rays and the nature of crystalline sample. Bragg's law, formulated by W. L. Bragg in 1913, relates the wavelength of the X-rays to the spacing of the atomic planes ($d_{hkl}$) as $n\lambda = 2d_{hkl} \sin\theta$ , where $\theta$ is the angle of incident X-rays and 'n' is the order of diffraction. Bragg's law is very important in indexing X-ray diffraction pattern and for determining crystal structure of materials.

The three basic components of an X-ray diffractometer are the X-ray source, specimen and the X-ray detector, all lie on the circumference of a circle, which is known as the focusing circle. The angle between the plane of the specimen and the X-ray source is $\theta$, the

Bragg angle. The angle between the projection of the X-ray source and the detector is 2θ. For this reason the X-ray diffraction patterns produced with this geometry are often known as θ-2θ scans. In the θ-2θ geometry, the X-ray source is fixed and the detector moves through a range of angles. A 2θ range from 30° to 140° is an example of a typical scan. X-rays are generated by directing an electron beam of high voltage on a metal target anode inside an evacuated X-ray tube. Copper is the most frequently used target and the typical operating conditions are 40 kV and 30 mA. The unwanted $k_\beta$ radiation is removed using a monochromator. On the X-ray source side, a line source of X -rays passes through a series of slits called sollar slits which consist of a series of closely spaced parallel metal plates that define and collimate the incident beam. In a typical X- ray diffraction experiments, a thin layer of crystalline powder is spread onto a planar substrate, which is a non-diffracting material such as a glass microscope slide and exposed to the X-rays. The quantity of powder used for each experiments is quite small, usually a few milligrams. After the beam has been diffracted by the specimen, it passes through another set of slits. The antiscatter slit reduces the background radiation, improving the peak to background ratio, making sure that the detector can receive X-rays only from the specimen area. The beam converges on passing the receiving slit, which defines the width of the beam admitted to the detector. An increase in slit width increases the maximum intensity of the reflections in the diffraction pattern. Three main types of X–ray detectors used in X-ray diffractometer are proportional, scintillation and solid state detectors.

Ideally, the specimen should contain numerous small, equiaxed and randomly oriented grains. In a powder or a polycrystalline material in general, the grains are often randomly oriented, and some grains will always be oriented in a favorable direction with respect to the X- ray beam, to allow the diffraction occur from a specific set of lattice planes. Each set of lattice planes in the crystal having spacing $d_{hkl(1)}$ , $d_{hkl(2)}$ , $d_{hkl(3)}$ ,…, will diffract at different angles $\theta_1,\theta_2,\theta_3,\ldots$, where θ increases as '$d_{hkl}$'decreases in such a way to satisfy Bragg's law. The intensity of the diffracted beam at each of these different angles is detected, and forms the X-ray diffraction pattern. The intensity is proportional to the number of X-ray photons of a particular energy that has been counted by the detector for each angle of 2θ.

### 2.4.2 Transmission Electron Microscopy

One of the most powerful tools for determining particle size and morphology is Transmission Electron Microscopy (TEM) (Williams et al. 1996). This technique gives particle size, crystallite size and can provide details of size distribution. In many cases aggregates of smaller particles can be discerned. TEM enables one to see things as small as the order of a few angstroms. If the nanoparticles consist of more than one phase and the phases provide enough contrast, then the individual phases may also be visible. The possibility for high magnifications has made TEM a valuable tool in medical, biological and materials research. The TEM operates on the same basic principles as the light microscope but uses electrons as source instead of light. Theoretically, the maximum resolution can obtain with a light microscope has been limited by the wavelength of light used to probe the sample. The image resolution in TEM, in terms of the classic Rayleigh criterion for visible light microscopy, which states that the smallest distance that can be resolved is approximately given by $\delta = 0.61\ \lambda/\upsilon\sin(\theta)$, where $\lambda$ is the wavelength of the radiation, $\upsilon$ is the refractive index of the viewing medium and the semi-angle of collection of the magnifying lens. For green light ($\lambda$ =400 nm) with oil immersion ($\upsilon \sim 1.7$) and $\sin(\theta) \sim 1$, estimated resolution of an optical microscope is 150 nm. TEM uses electrons as light source, which has much lower wavelength compared to light, thus making the resolution ten thousand times better than a light microscope. For a 200 kV electrons ($\lambda \sim 0.0025$nm), with vacuum ($\upsilon \sim 1$ since no medium in electron lenses) and $\sin\theta \sim \theta \sim 0.1$ radians, resolution is ~ 0.02 nm for an electron microscope.

When electrons are accelerated up to high energy levels (few hundred keV) and focused on a material, they can scatter or backscatter elastically/inelastically or produce many interactions, source of different signals such as X-rays, Auger electrons or light. The scattering processes experienced by electrons during their passage through the specimen, determines the type of information obtained. Elastic scattering involves no energy loss and gives rise to diffraction patterns. Inelastic interactions between primary electrons with grain boundaries, dislocations, defects, density variations, etc. can cause complex absorption and scattering effects, leading to a spatial variation in the intensity of the transmitted electrons. In a typical experiment, a stream of electrons is formed by an electron source and

accelerated (~100–400 kV) towards a thin specimen in vacuum. The beam is confined and focused by apertures and magnetic lenses. Electron beam-specimen interaction generates elastic and inelastic events. The objective lens forms a diffraction pattern in the back focal plane and a magnified image of the sample in image plane.

A number of intermediate lenses are used to project either the image or the diffraction pattern onto a fluorescent screen or film. The electron gun uses $LaB_6$ thermionic emission source or a field emission source. The vacuum system is one of the main components in TEM, without which proper functioning of TEM is not possible. Because of strong interactions of electron with matter, gas particles must be absent in the column. Sample is placed on a specimen stage which serves as a platform for in situ observations during annealing, electric field or mechanical stress induced structural analysis of nanostructures. Instead of glass lenses focusing the light in the light microscope, the TEM uses electromagnetic lenses to focus the electrons into a very thin beam. The electromagnetic lenses are used to (de)focus the electron beam, change magnification, focus image or diffraction pattern and to switch between image and diffraction modes.

In electromagnetic lenses, a strong magnetic field is generated by passing a current through a set of windings. This field acts as a convex lens, bringing off axis rays back to focus. The image is rotated to a degree that depends on the strength of the lens. Focal length can be changed by changing the strength of the current. The double condenser system or illumination system consists of two or more lenses and an aperture. The first condenser lens create a demagnified image of the gun crossover and control the minimum spot size in the rest of the condenser system. The second condenser lens affects the convergence of the beam at the specimen and the diameter of the illuminated area of a specimen. The condenser aperture controls the fraction of the beam which is allowed to hit the specimen and helps to control the intensity of illumination.

The objective lens forms an inverted initial image, which is magnified. A diffraction pattern is formed in the back focal plane of objective lens. The objective aperture placed in the back focal plane of the image. Its function is to select those electrons which contribute to the image and affect the appearance of the image and improve the contrast of the final image. The first intermediate lens magnifies the initial image that is formed by the objective lens. The lens can be focused on initial image formed by the objective lens or diffraction pattern

formed in the back focal plane of the objective lens. This determines whether the viewing screen of the microscope shows a diffraction pattern or an image.

### 2.4.3 Dynamic Light Scattering

Dynamic Light Scattering (DLS), also known as photon correlation spectroscopy is an important supplementary technique for determining the sizes of particles in solution, particularly when the size distribution is narrow and approximately log normal (Schartl, 2007). The DLS technique is sensitive to total particle size and yields information which is weighted by the square of the particle volume, although the results are generally converted to volume or number weighting.

When a laser beam is shined through a liquid with suspended particles, the beam scatters off those particles in all directions, which results in a scattering-angle-dependent intensity pattern. When particles are experiencing the Brownian motion and the intensity pattern fluctuates randomly. When the particles are very small compared to the wavelength of the light, the intensity of the scattered light is uniform in all directions (Rayleigh scattering); for larger particles (above approximately 250 nm diameter), the intensity is angle dependent (Mie scattering). If the light is coherent and monochromatic, a time-dependent fluctuation in the scattered intensity is observed. Measuring the intensity fluctuations at a given scattering angle can yield a great deal of information about the particles that are scattered by laser beam, including the hydrodynamic radius of suspended particles. The hydrodynamic radius of a particle is the effective radius of an irregularly shaped particle that is used when describing the manner in which particles in suspension diffuse through the suspending medium. The hydrodynamic radius for a hard sphere, equals the radius of the sphere.

The randomness of the fluctuation intensity of scattered light allows us to use random statistical methods to analyze that scattering pattern. The most important one is called correlation. If the intensity at a given scattering angle is recorded over a small sample time, the fluctuations of the intensity arising from Brownian motion can be expected to be small. If two such recordings are made from the same scattering angle simultaneously, then two samples can be compared with one another through cross-correlation, which is a measure of

how quickly the scattered light intensity changes with time.

## 2.5 Summary of literature about nanorefrigerants

The following table shows the invesigations done on various nanorefrigerants.

**Table 2.3** List of literature about nanorefrigerants

| Investigator | Nanofluid | Investigation |
|---|---|---|
| Bi et al. (2007) | R134a-$TiO_2$ | 21.2% less energy consumption |
| Jwo et al. (2009) | R134a-$Al_2O_3$ | Power reduced by 2.4% and COP increased by 4.4% |
| Bobbo et al. (2010) | R600a- $TiO_2$ | Nano particle dispersion did not affect solubility of lubricant in refrigerant |
| Henderson et al. (2010) | R134a- CuO | Heat transfer coefficient increased |
| Bi et al. (2011) | R600a- $TiO_2$ | Energy saving of 9.6% |
| Jwo et al. (2008) | R134a- $Al2O_3$ | Thermal conductivity increased by 4.6 % at temperature 40 ℃ and 1.5% wt. conc. |
| Jiang et al. (2009) | CNT-nanorefrigerant | Built a model of thermal conductivities of CNT nanorefrigerant. |
| Mahbubul et al. (2013) | R134a- $Al_2O_3$ | Thermal conductivity increase with decreasing particle size and increasing temperature. Viscosity is proportional to volume fraction. |
| Mahbubul et al. (2012) | R123- $TiO_2$ | Viscosity increase with increase of volume concentration and decrease by increasing temperature. |

# CHAPTER-3

# RESEARCH GAPS AND OBJECTIVES

## 3.1 Research gaps

Reported literature shows a significant discrepancy in thermal conductivity and viscosity data of nanorefrigerant. For the practical application of nanorefrigerant in refrigeration devices, these discrepancies should be eliminated by systematically investigating the effects of some parameters on thermal conductivity and viscosity of a nanorefrigerant. In the literature, the research about the effects of various parameters on thermal conductivity and viscosity is very limited and further research is required for the effects of these parameters.

When it comes to the theoretical studies about the thermal conductivity and viscosity of nanorefrigerant, it is seen that the relative significance of the proposed enhancement mechanisms of thermal conductivity and viscosity are not known. Development of new theoretical models that combine the effects of numerous enhancement mechanisms and comparison of these models' predictions with systematically obtained experimental data will provide insight to the theoretical explanation of anomalous thermal conductivity and viscosity enhancement with nanorefrigerant.

While studying the literature it has been found that mainly work is done with high pressure refrigerants such as R134a. At atmospheric conditions it is difficult to maintain high pressure refrigerant into liquid form to prepare nanorefrigerant. So that researchers have investigated the performance by dispersing nanoparticles in lubricants of the refrigerant system and found that performance of refrigerant's thermo physical properties is improved. From the list of various available refrigerants, R-11 is a low pressure refrigerant which is commonly used in chiller refrigerant systems. But it is found unsuitable for future use due to its high ozone depletion potential (ODP). So, it is replaced by R-123 which has better properties than R-11 and is environmental friendly. But R-11 has similar themophysical properties as R123 refrigerant. For experimental investigation we have chosen R-11 in place of R123 because it was available in Thapar University RAC lab. Also, R-11 is low pressure refrigerant which can be kept at liquid state under normal atmospheric conditions.

The material of nanoparticles is chosen as $Al_2O_3$ because of following reasons:

a. It is chemically more stable than their metallic counterparts.
b. Its nanoparticles are produced in large industrial scale.
c. Its cost is less for commercialization of nanorefrigerants.

## 3.2 Research Objectives

Thermal conductivity and viscosity plays an important role to predict the behavior of nanorefrigerant in the refrigerant system. So, objective of research is

i. To investigate the effect of weight concentration of $Al_2O_3$ nanoparticles on thermal conductivity and viscosity of $Al_2O_3$/ R-11 nanorefrigerant.
ii. To investigate the effect of size (20 & 40 nm) of $Al_2O_3$ nanoparticles on thermal conductivity and viscosity of $Al_2O_3$/ R-11 nanorefrigerant.
iii. To investigate the effect of shape (spherical and elongated) of $Al_2O_3$ nanoparticles on thermal conductivity of $Al_2O_3$/ R-11 nanorefrigerant.
iv. To investigate the effect of temperature (4-16°C) on thermal conductivity of $Al_2O_3$/ R-11 nanorefrigerant.

# CHAPTER-4

# INSTRUMENTS USED FOR EXPERIMENTAL WORK

## 4.1 Ultrasonic Sonicator

Sonication is commonly used in nanotechnology for evenly dispersing nanoparticles in liquids. Sonication is the process of converting an electrical signal into a physical vibration that can be directed toward a substance. The sonication probe transmits the vibration to the solution which is to be sonicated. This probe is a carefully constructed tip that moves in time with vibration and transmitting it into the solution. The probe moves up and down at very high speed, the amplitude can be controlled by the operator and is chosen based on the qualities of the solution being sonicated.

The rapid movement of the probe creates an effect called cavitation. Cavitation takes place when the vibrations create a series of microscopic bubbles in the solution, the pockets of space between the molecules that form and then collapse again under the weight of the solution, sending out small shockwaves into the surrounding substance. Thousands of these bubbles forming and collapsing constantly create powerful waves of vibration that cycle into the solution and break apart the cells. During the experiment, Oscar sonicator was used as shown in Fig 4.1 below.

**Figure 4.1** Ultra sonicator

**Table 4.1** Specifications of Ultrasonic Sonicator

| | |
|---|---|
| Model | Processor SONOPROS PR-250 MP |
| Ultrasonic power | 250 watts |
| Processing capacity | Upto 250 ml |
| Frequency | 20+ 3KHZ |
| Horn | 1) Titanium horn 6mm<br>2) Titanium horn 12mm |
| Converter | PZT sandwich type OUC 116 |
| Generator | Solid state, LOT type |
| Generator cabinet | MS powder coated |
| Stand base and pillar | SS 304 |
| Power input | 230V 50Hz, 3Amp |
| Converter | PZT sandwich type |
| Power variac | 0-230V, 3Amp |
| Application | Particle dispersion |

## 4.2 KD2 Pro thermal properties analyzer

The KD2 Pro uses the transient heated needle to measure thermal properties of solid and fluid. With this technique, a pulse of heat is applied to a needle and the temperature response with time is monitored at the heated needle or at an adjacent needle both during and after the pulse of heat. The nature of the temperature response is a result of the thermal properties of the material. While measuring thermal properties it is required to measure only the heat transfer resulting from conduction. In low viscous fluids, heat transfer by convection can be much greater than heat transfer by conduction. So, accurate measurement of thermal properties of fluids requires that convective heat exchange be negligible.

Convective heat exchange in fluids can be broken down into two categories: forced and free convection. Forced convection takes place when the fluid is agitated or mixed by mechanical forces. Free convection may takes place when a body of higher or lower temperature is inserted into a fluid. The temperature difference between the body and

fluid create density gradients in the fluid which cause the fluid to mix. Particular steps can be taken to minimize both forced and free convective heat exchange.

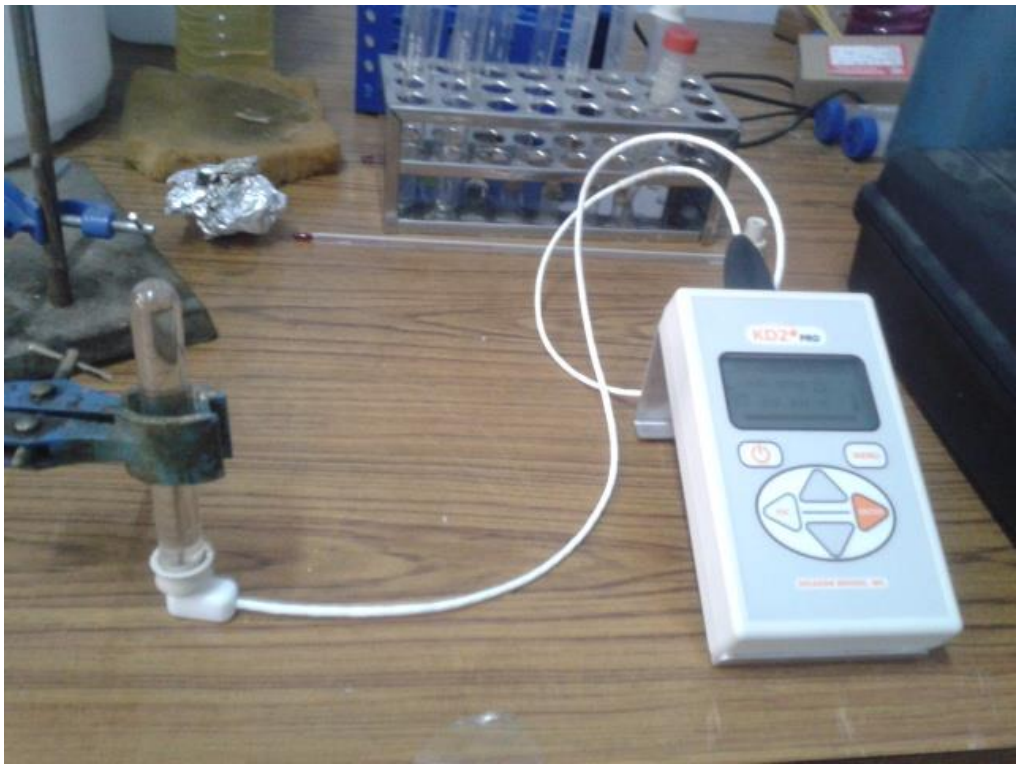

**Figure 4.2** KD2 Pro thermal properties analyzer

The needle used to measure thermal conductivity having following specification which suits our requirement:

**Table 4.2** KD2 Pro needle specifications

| **60 mm (small) single-needle (KS-1)** | |
|---|---|
| Size | 1.3 mm diameter x 60 mm long |
| Range of thermal conductivity | 0.02 to 2.00 W/(m· K) |
| Range of thermal resistivity | 50 to 5000 °C·cm/W |
| Accuracy (Conductivity) | ± 5% from 0.2 - 2 W/(m· K)<br>±0.01 W/(m· K) from 0.02 - 0.2 W/(m· K) |

### 4.2.1 Preventing forced convection

To eliminate forced convection, the fluid sample and the sensor must be absolutely still during the measurement. Even small (minute) vibrations in the sample are often enough to compromise the thermal properties measurement. Some common sources of vibrations observed in the laboratory that must be avoided include:

i. Vibration occurs from Heating, Ventilating, and Air Conditioning (HVAC) systems
ii. Vibration occurs from computer fans that are near the measurement apparatus
iii. Vibration occurs from people moving around the lab
iv. Vibration occurs from other laboratory equipment

If sources of vibration cannot be eliminated in the laboratory, it may be necessary to make the measurement on an optical table or other vibration isolation device to prevent errors from forced convection. Another common strategy is to configure the KD2 Pro in auto mode and make measurements overnight after turning off the HVAC system and any other lab equipment that might cause vibrations.

### 4.2.2 Preventing free convection

Steps should also be taken to eliminate free convection. The heat transfer by free convection is described by

$$g_H = \frac{0.54\ \hat{\rho}\ D_H\left(\frac{g\ d^3 \Delta T}{T\ \nu\ D_H}\right)}{d} \tag{4.1}$$

where $g_H$ is the heat conductance (mol $m^{-2}s^{-1}$), $\hat{\rho}$ is the molar density of the fluid (mol/$m^3$), $D_H$ is the thermal diffusivity of the fluid ($m^2/s$), g is gravitational acceleration ($m/s^2$), d is the characteristic dimension of the object placed in the fluid (m), $\Delta T$ is the temperature difference between the bulk fluid and the object inserted into it, T is temperature (K), and $\upsilon$ is the kinematic viscosity of the fluid ($m^2/s$).

Examining eq. 4.1, we see that the heat conductance is inversely related to the characteristic dimension (d) of the probe inserted into the fluid. The characteristic dimension of an object is a function of the shape of the object and the direction of fluid flow over that object. For this discussion, the needle probe can be accurately described as a cylinder. For a cylinder with its axis parallel to the fluid flow, the characteristic dimension is its length. For a cylinder with its axis perpendicular to the fluid flow, the characteristic dimension is diameter of cylinder. When considering a heated probe inserted into a cooler fluid, the fluid flow near the probe from free convection will be upward, as the warmer and less dense material near the probe is forced upwards by forces of gravity working on the surrounding, denser material. So, if a heated needle is inserted into a fluid horizontally, the fluid flow around the needle will be perpendicular to the axis of the needle and the characteristic dimension will then be the diameter of the needle (1.27 mm for the KS-1 or 1.8 mm for the TR-1). If the needle is inserted into a fluid vertically, the flow will be parallel to the axis of the needle and the characteristic dimension is the length of the needle (60 mm for the KS-1 or 100 mm for the TR-1). By keeping in mind that the heat conducted by free convection is inversely proportional to the characteristic dimension, inserting the needle into the fluid vertically will reduce convective heat transfer and result in more accurate measurement of thermal conductivity.

Again from eq. 4.1, we discover that the heat conductance by free convection is proportional to the temperature difference between the fluid and the object inserted into it. Hence, free convection can be decreased by limiting the heating of the needle. The KD2 Pro KS-1 (60 mm single needle) sensor is specifically designed for use in fluids and provides a very small heat pulse that can measure thermal conductivity of most fluids without causing free convection. When using the KS-1 sensor in low viscosity fluids (such as water or aqueous solutions), the read time should be set to the minimum allowed 1 minute duration to further minimize the temperature difference between the fluid and the needle

Further examination of eq. 4.1 shows us that the heat conductance is inversely proportional to the kinematic viscosity of the fluid. Hence, thermal conductivity measurements in more viscous (thicker) fluids are less affected by free convection. More viscous fluids such as castor oil ($1.0 \times 10^{-3}$ $m^2/s$ @ 20 °C) and glycerol ($7.4 \times 10^{-4}$ $m^2/s$ @ 20 °C) are unaffected by free convection during the thermal conductivity

measurement and are easy to measure with the KS-1 needle without further precautions. However, in low viscosity fluids such as water (8.9 X $10^{-7}$ $m^2/s$ @ 20°C) free convection is difficult to prevent. With careful experiment technique, it is possible to measure the thermal conductivity of water and aqueous solutions with the KS-1 sensor, but fluids with viscosities less than that of water cannot be measured accurately. The viscosities of fluids are inversely proportional to the fluid temperature. With careful experiment technique, researchers are able to measure the thermal conductivity of aqueous solutions up to about 50 °C with the KS-1 sensor.

### 4.2.3 Liquid sample temperature control

Often it is desirable to control the temperature of the liquid sample above or below ambient temperature during thermal properties measurement. It is important that the heating or cooling the sample doesn't cause forced or free convection as mentioned above. There are several things that should be avoided when measuring thermal properties of heated or cooled samples.

a) Do not heat the sample from the bottom (e.g. on a hot plate). The temperature gradient from the heating will cause free convection.
b) Do not make measurements in a conventional refrigerator or freezer. Conventional cooling devices have very large cyclical temperature cycles which can cause excessive sample temperature drift and poor measurements. Vibrations from the compressor also cause forced convection in the sample.
c) Do not measure the thermal properties of the sample while it is in circulating water bath. The vibrations from the water bath pump and from the circulating water will cause forced convection in the sample.

According to several researchers who used the KD2 Pro with liquid samples, the best method for controlling temperature of liquid samples is as follows.

1. Heat or cool the sample (with sensor inserted) in a water bath.
2. Once the sample temperature has equilibrated to the desired water bath temperature, turn the water bath off.
3. Allow enough time for the water bath to become absolutely still and then take readings.

## 4.3 Viscometer/ Rheometer

The Brookfield DV-III (LV DV-IIICP) Ultra Programmable Rheometer measures fluid parameters of Shear Stress and Viscosity at given Shear Rates. The principle of operation of the DV-III Ultra is to drive a spindle (which is immersed in the test fluid) through a calibrated spring. The viscous drag of the fluid against the spindle is measured by the spring deflection. The spring deflection is measured with a rotary transducer. The viscosity measurement range of the DV-III Ultra (cP) is determined by the rotational speed of the spindle, the size and shape of the spindle, the container the spindle is rotating in and the full scale torque of the calibrated spring.

### 4.3.1 Setup

1. The Viscometer is to be securely mounted on the laboratory stand, leveled and zeroed with no cone or cup attached and 0% torque is displayed.
2. Figure 4.3 shows a typical water bath setup. Connect the sample cup inlet/outlet ports to the water bath inlet and outlet and set the bath to the desired test temperature. Allow sufficient time for the bath to reach the test temperature.

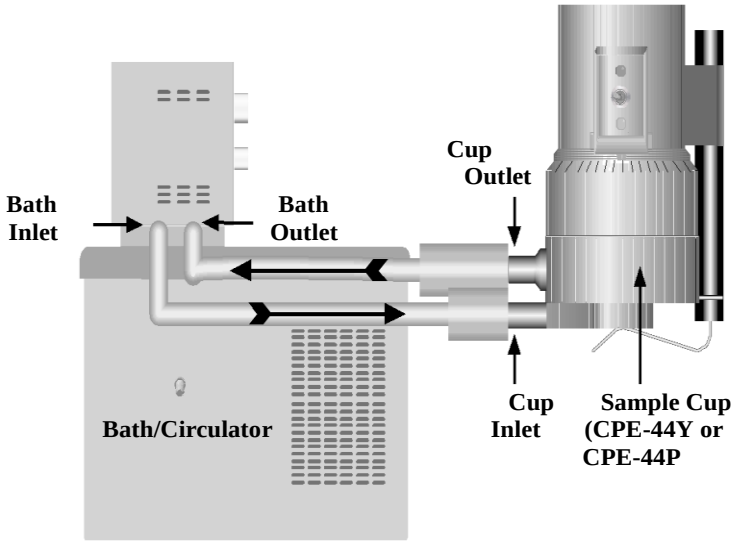


**Figure 4.3** Components of Viscometer

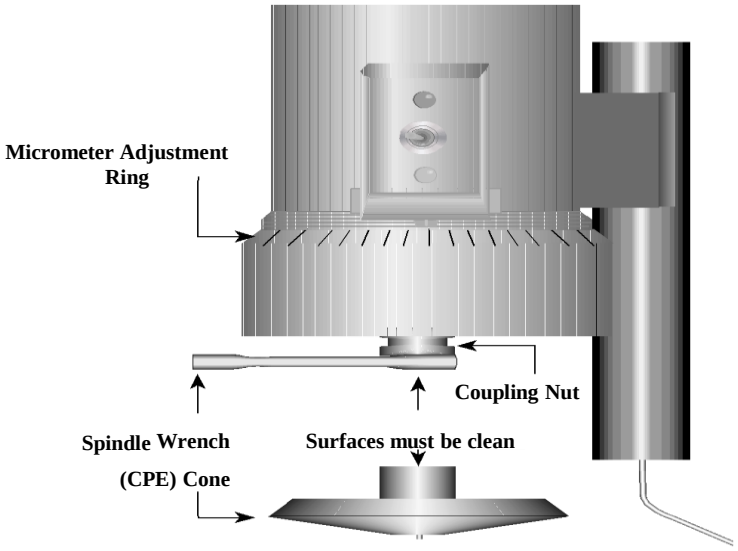


**Figure 4.4** Spindle attachment of viscometer

3. With the motor off, thread the cone spindle by using the spindle wrench to secure the viscometer coupling nut (see Figure 4.4); gently push up on the coupling nut and hold this securely with the wrench. Thread the cone spindle by hand.
4. Attach the cup, taking care not to hit the cone with the cup (Figure 4.5).

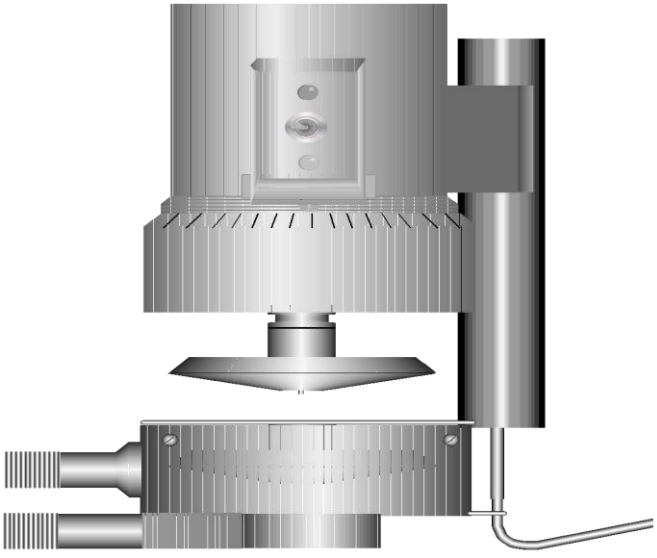

**Figure 4.5** Cup attachment of viscometer

### 4.3.2 Setting the gap

1. Move the toggle switch to the right; this will turn on (enable) the Gap Setting Feature. The Pilot (red) light will be illuminated.
2. If the contact light (yellow) is illuminated, turn the micrometer adjustment ring clockwise (as you look down on the instrument) until the light is just breaking contact, i.e., flickering (see Figure 4.6).

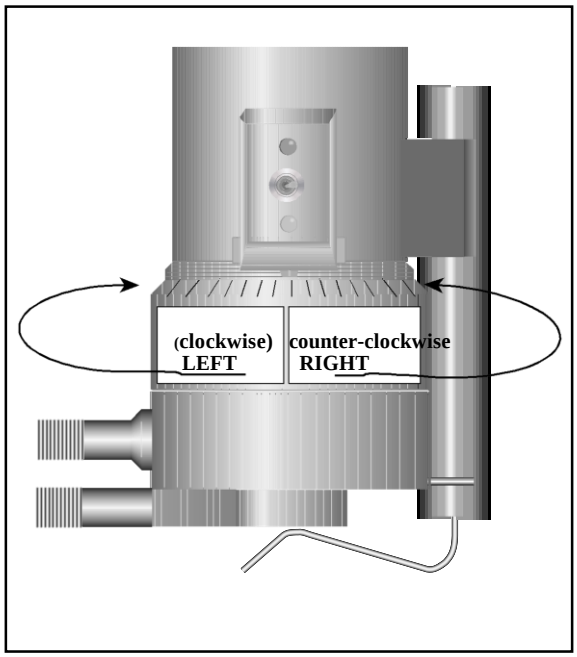


**Figure 4.6** Micrometer adjustment of viscometer

3. If the yellow contact light is not illuminated, slowly turn the micrometer adjustment ring in small increments (one or two scale divisions) counter-clockwise. Continue moving the micrometer adjustment ring slowly counter-clockwise until the contact light (yellow) turns on. Back off (rotate clockwise) until the light is just breaking contact, i.e., flickering.
4. Adjust the sliding reference marker, right or left, to the closest full scale division mark.
5. Turn the micrometer adjustment ring one scale division to the left to meet the line on the sliding reference marker. The yellow contact light should go off.
6. You have established the gap space needed for measurement. Now turn the toggle switch off (left); the red pilot light should go off.
7. Carefully remove the sample cup.

# CHAPTER-5

# METHODOLGY

The thermal conductivity and viscosity of $Al_2O_3$/ R-11 nanorefrigerant is measured under varying conditions of temperature, weight concentration, size and shape of $Al_2O_3$ nano-particles. The step by step methodology is given below:

## 5.1 Materials used for preparing nanorefrigerant

a) **Refrigerant R-11:** It is taken from Refrigeration and Air Conditioning Lab of Thapar University, Patiala. It was stored in liquid state in the cylinder and sample in a beaker as shown in Figure 5.1 & 5.2. The refrigerant R-11 used as base fluid and it has similar thermo physical properties as R-123. Table 5.1 shows the properties of the R-11 refrigerant at atmospheric pressure.

**Table 5.1** Properties of R-11 refrigerant

| Property | Unit | Value |
|---|---|---|
| Chemical formula | | $CCl_3F$ |
| Normal boiling point | $^oC$ | 23.7 |
| Liquid Viscosity | cP | 0.539 |
| Thermal conductivity | W/mC | 0.094 |
| Critical temperature | $^oC$ | 198 |
| Critical pressure | bar | 44 |


**Figure 5.1** R-11 Refrigerant cylinder

**Figure 5.2** R-11 Refrigerant sample in a beaker

**b) $Al_2O_3$ Nanoparticles:** The nanoparticles of alumina ($Al_2O_3$ -20 nm (spherical shape) were purchased from Nanoshel Intelligent materials Pvt. Ltd**.** Derabassi, Punjab. Alumina ($Al_2O_3$ - 40 nm (spherical & elongated shape) nanoparticles were purchased from Reinste Nano Ventures lab, Noida. The properties of these $Al_2O_3$ nanoparticles are shown in Table 5.2.

**Table 5.2** Properties of $Al_2O_3$ nanoparticles

| **Property** | **Unit** | **Value** | **Value** | **Value** |
|---|---|---|---|---|
| Purity | % | 99.99 | 99.9 | 99.8 |
| Avg. particle dia. | nm | 20 | 40 | 40 |
| Density | $g/cm^3$ | 3.8 | 3.8 | 3.8 |
| Shape | | Spherical | Spherical | Elongated |

## 5.2 Characterization of nanorefrigerant

The XRD (X- Ray Diffraction) photograph of 20 nm (spherical) nanoparticles is provided by Nanoshel Intelligent materials Pvt. Ltd**.** Derabassi, Punjab, which confirmed that the material is $Al_2O_3$ as shown in Figure 5.3. The TEM (Transmission Electron Microscopy) photograph shows the average size of nano-particles is 20 nm as shown in Figure 5.4. The size distribution of 20 nm nanoparticles is shown by data provided by company in Figure 5.5. The XRD & TEM report of 40 nm (spherical & elongated) nanoparticles is done in NIPER testing lab, Mohali, Punjab. Figure 5.6 & 5.7 shows the photograph of XRD of 40 nm (spherical) & 40 nm (elongated) respectively. The TEM photograph of XRD of 40 nm (spherical) & 40 nm (elongated) of $Al_2O_3$ nanoparticles is shown in Figure 5.8 & 5.9 respectively.

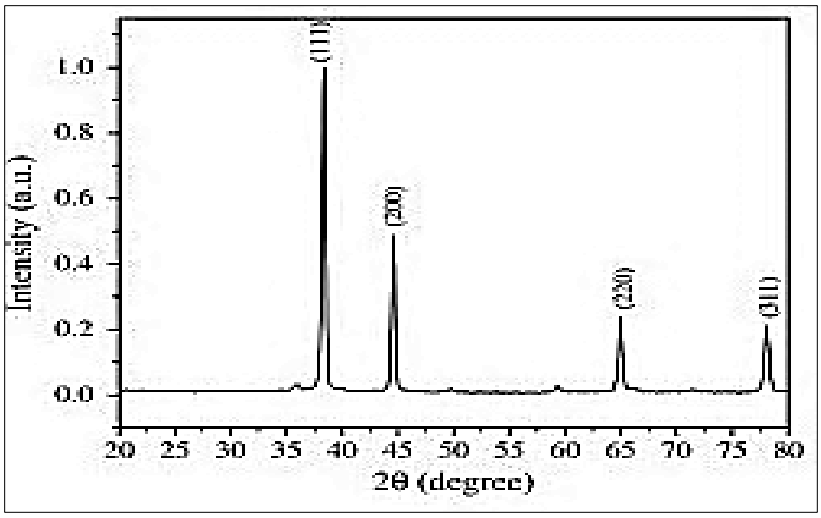


**Figure 5.3** X-Ray Diffraction (XRD) of 20 nm $Al_2O_3$ nanoparticles

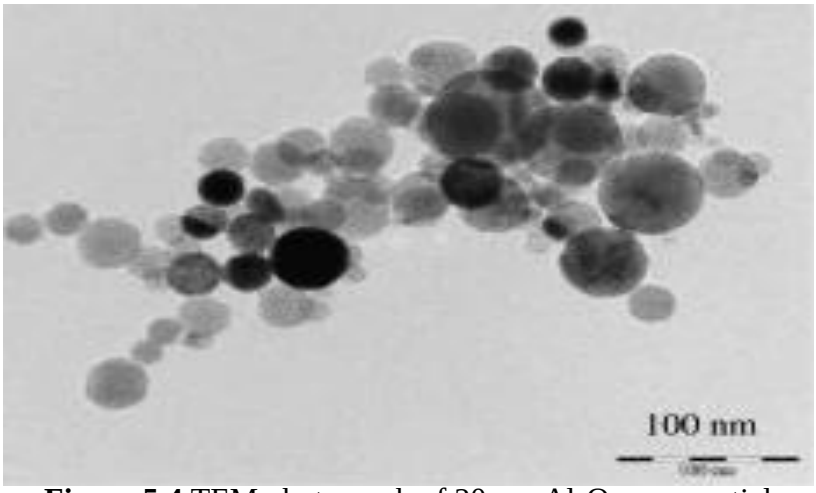


**Figure 5.4** TEM photograph of 20 nm $Al_2O_3$ nanoparticles

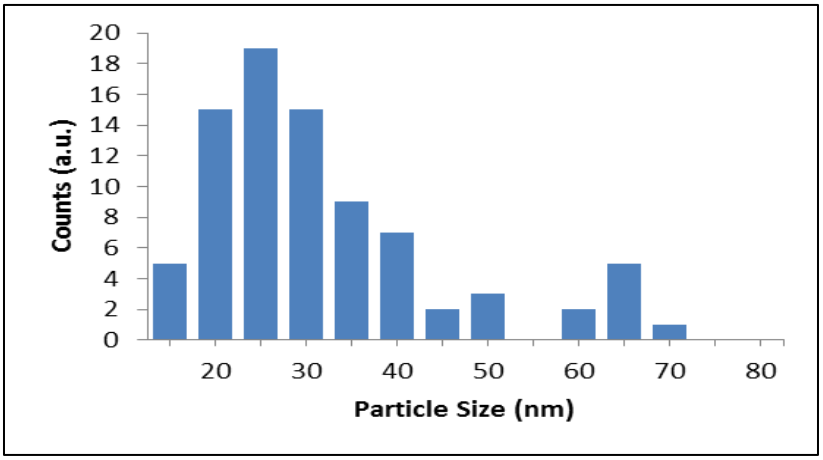


**Figure 5.5** Size distributions of 20 nm $Al_2O_3$ nanoparticles

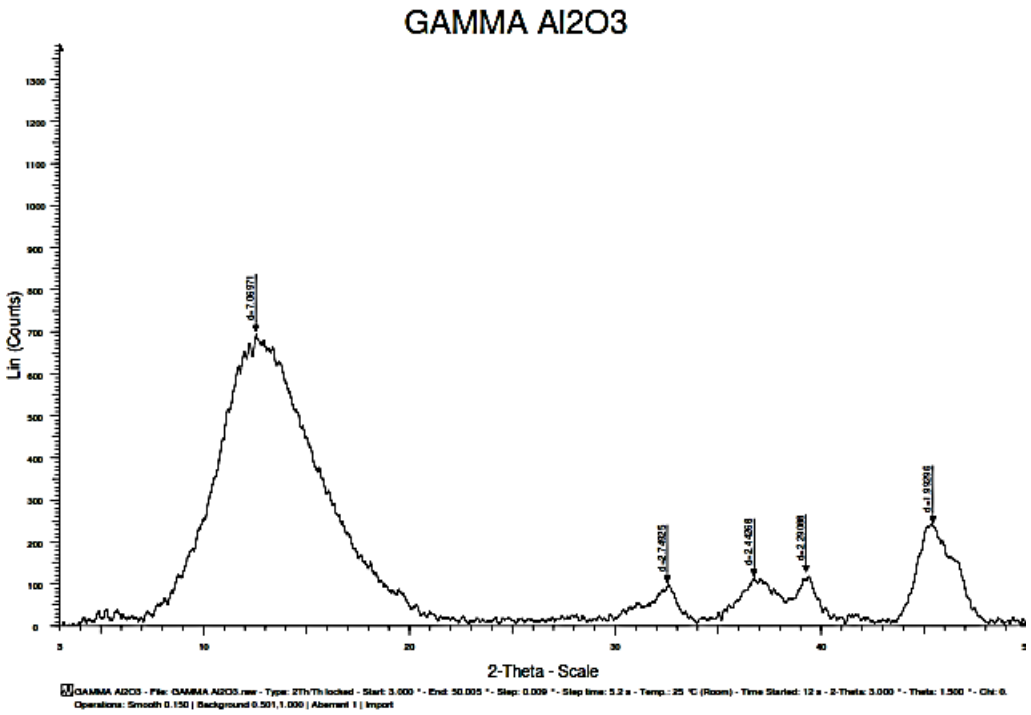


**Figure 5.6** X-Ray Diffraction (XRD) of 40 nm (spherical) $Al_2O_3$ nanoparticles

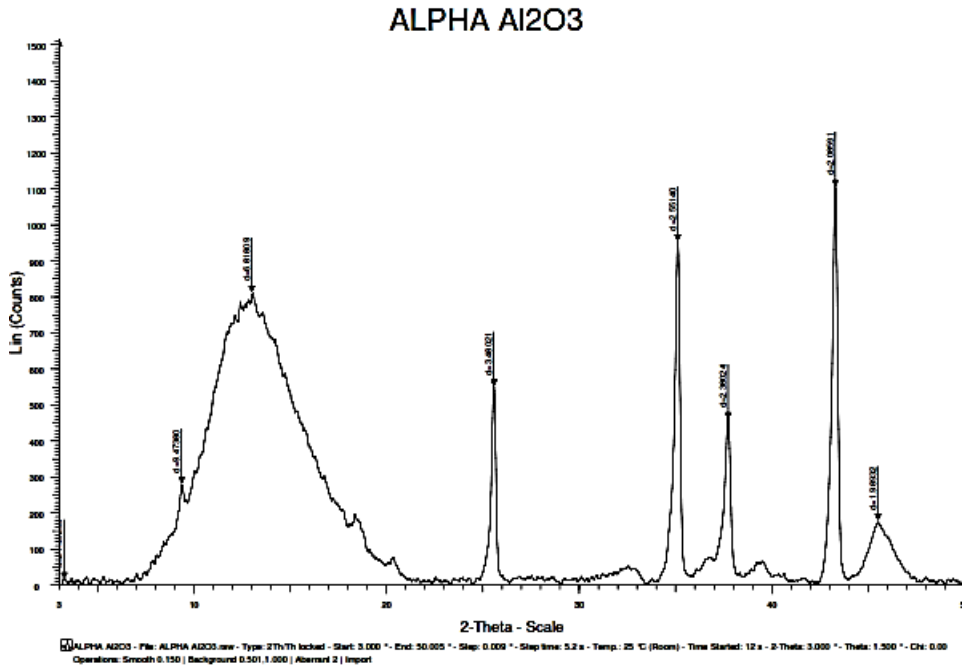


**Figure 5.7** X-Ray Diffraction (XRD) of 40 nm $Al_2O_3$ (elongated) nanoparticles

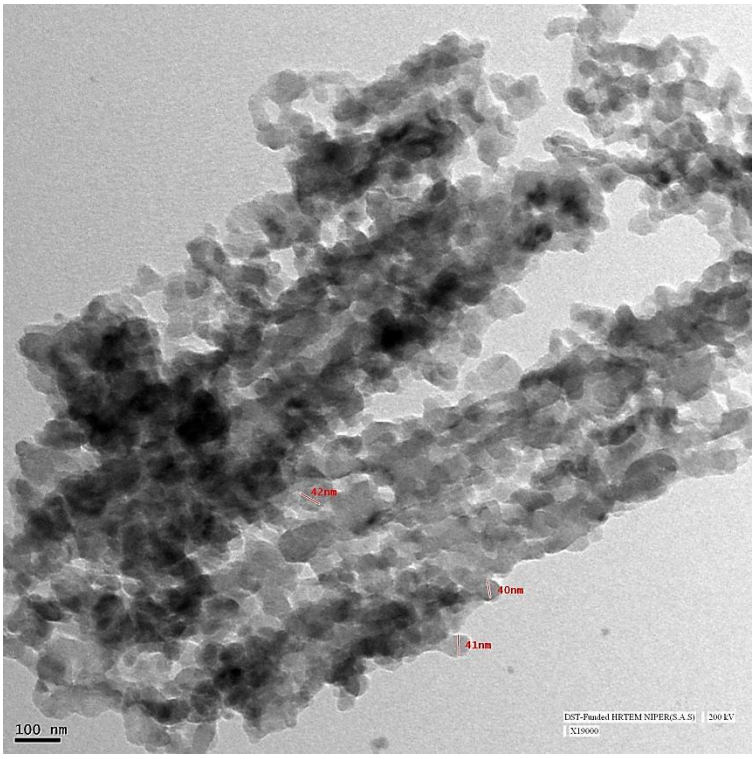


**Figure 5.8** TEM photograph of 40 nm (spherical) $Al_2O_3$ nanoparticles

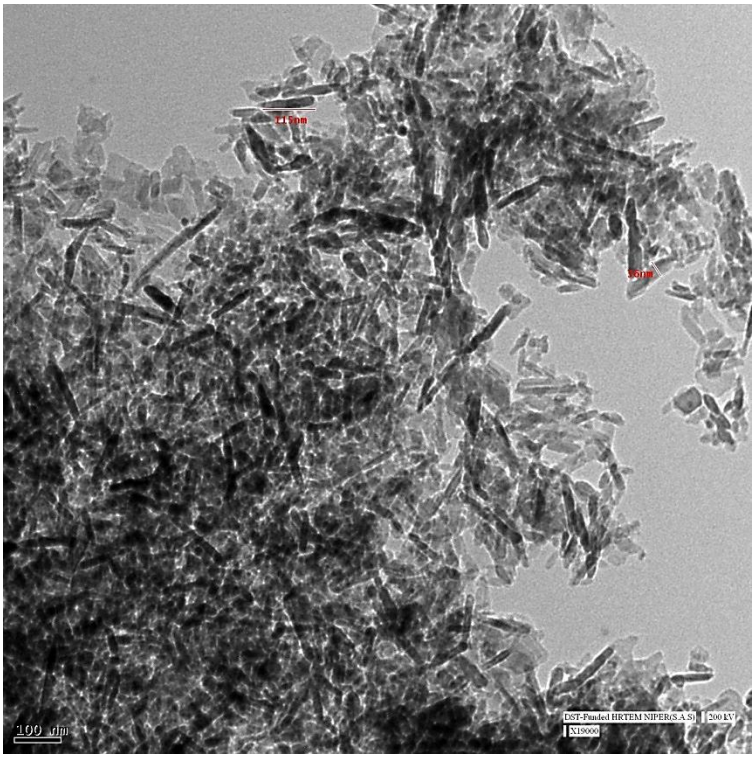


**Figure 5.9** TEM photograph of 40 nm (elongated) $Al_2O_3$ nanoparticles

## 5.3 Preparation of nanorefrigerant

The preparation is done with two step technique. $Al_2O_3$ particles are to be dispersed in liquid R-11 after weighing in required proportion. The weight of $Al_2O_3$ particles is measured by electronic weighing pan. The equation used to calculate the weight concentration of nanorefrigerant is as follows:

$$\varphi = \frac{m_n}{m_n + [\rho_r\,(\mathrm{T}).\ \mathrm{v}]} \tag{5.1}$$

where, φ is the nanoparticle weight concentration; $m_n$ and $m_r$ are the masses of the nanoparticle and refrigerant respectively; v is the volume of refrigerant; and $\rho_r$ (T) is liquid phase density of the refrigerant at temperature T. The weight concentrations of nanoparticles are (0.02%, 0.04%, 0.06%, 0.08% and 0.10%) prepared at 20 °C for all sizes nanoparticles.

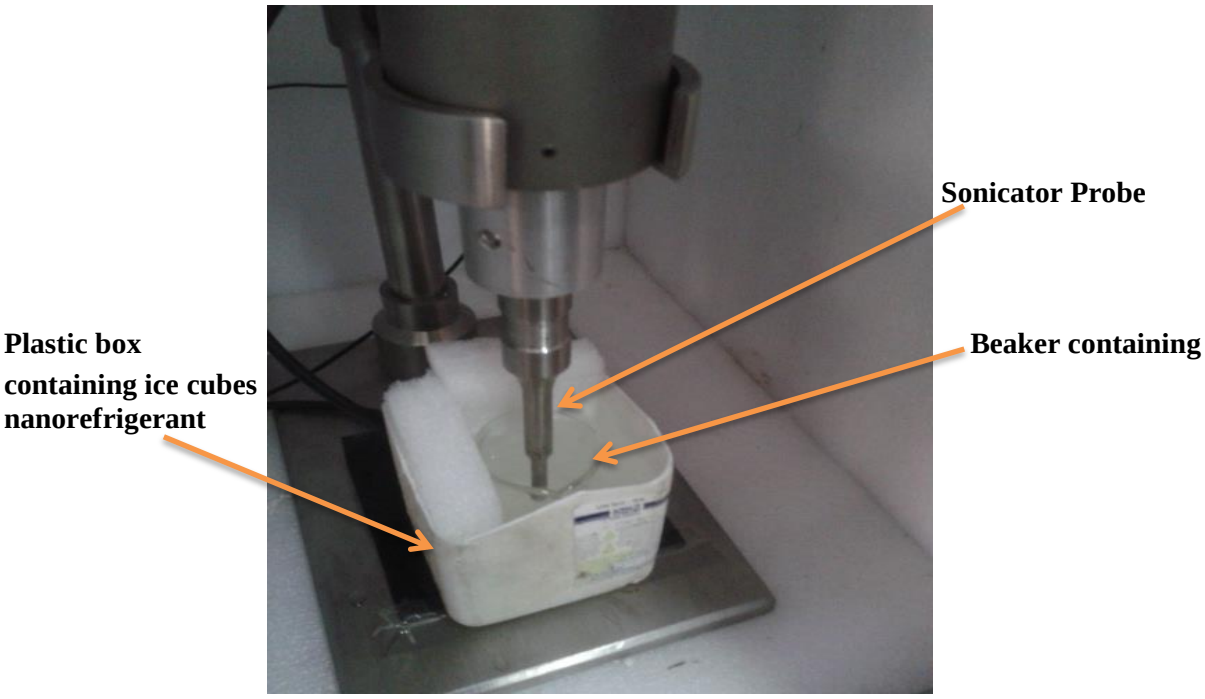


**Figure 5.10** Sonication of $Al_2O_3$/R-11 nanorefrigerant

After dispersing $Al_2O_3$ nanoparticles in R-11 refrigerant at particular weight concentration, the sonication is done for uniform suspension of nanoparticles. Ultra Sonicator (SONOPROS

PR-250 MP) was used to sonicate the $Al_2O_3$/R-11 nanorefrigerant for about 4 hours. The temperature around beaker is maintained below 20°C to avoid evaporation of refrigerant. It is done by keeping beaker inside a larger size plastic cup and ice cubes are kept between plastic box and beaker as shown in Figure 5.10.

**Figure 5.11** $Al_2O_3$/R-11 nanorefrigerant after sonication

Figure 5.11 shows $Al_2O_3$/R-11 nanorefrigerant after sonication in beaker and test tube for measurement of thermal conductivity and viscosity.

## 5.4 Measurement of thermal conductivity

Thermal conductivity of nanorefrigerant is measured by using KD2 Pro instrument. The sample of $Al_2O_3$/R-11 nanorefrigerant is taken into test tube which is covered with rubber cork. The temperature of nanorefrigerant is maintained by keeping chilled water inside a beaker as shown in Figure 5.12. The following steps are taken for measurement of thermal conductivity of nanorefrigerant:

1. Attach KS-1 needle sensor then turn on the KD2 Pro.
2. Properly insert the KS-1 needle sensor into the nanorefrigerant test tube and the needle should be kept parallel to side walls of test tube for accurate measurements.
3. When the KD2 Pro turns on, press the Menu key and then press Enter to begin the measurement.


**Figure 5.12** Measurement of thermal conductivity using KD2 Pro

4. An icon will appear on the left and right side of the screen. The icon at left indicates the type of sensor connected. The circular icon indicates that a reading is underway. It will change to a thermometer icon to indicate whether the measurement is currently in heating or cooling mode; when the thermometer is rising, heat is applied to the needle, and when it is falling, heat is off. A progress bar shows the elapsed time.
5. When the progress bar has fully darkened, the results are displayed on screen. The time gap between two successive readings should be at least 10 minutes to avoid convectional effect inside nanorefrigerant solution.

## 5.5 Measurement of viscosity

The viscosity of the nanorefrigerants was measured using a Brookfield Rheometer (LV DV-IIICP) with a small sample adaptor. The adaptor consists of a cylindrical sample holder, a water jacket, and spindle. The viscometer drives the spindle immersed into the sample holder containing the test fluid sample. The viscometer provides a rotational speed that can be controlled to vary from 0.01 to 250 rpm yielding the shear rate ($sec^{-1}$) 3.84 N. It measures viscosity by measuring the viscous drag of the fluid against the spindle when it rotates. The spindle CPE-42 is used in these measurements. The sample holder can hold a

small sample volume of 1 mL and the temperature of the test sample is monitored by a temperature sensor embedded into the water bath. Figure 5.13 below shows the Brookfield Rheometer.


**Figure 5.13** Measurement of viscosity by Brookfield Rheometer (LV DV-IIICP)

The following procedure is adapted to measure viscosity of nanorefrigerant as discussed in detail in chapter 4:

1. Autozero the rheometer by keeping cup attached without cone plate.
2. With the motor off, thread the cone spindle by using the spindle wrench to secure the viscometer coupling nut.
3. Attach the cup, taking care not to hit the cone with the cup
4. Follow the gap setting procedure.
5. Remove the cap and take 1 ml solution of nanorefrigerant inside cap.
6. Replace cap and lock it.
7. Set the water circulating temperature (4-16 °C).
8. Enter the speed of rotation using the number pad and ENTER key.
9. Record % torque, shear rate, shears stress and viscosity.
10. Change speed of rotation and temperature to take more readings under different temperature and r.p.m.

# CHAPTER-6

# RESULTS AND DISCUSSION

## 6.1 Introduction

In this chapter a detailed discussion on the experiment results of $Al_2O_3$/R-11 nanorefrigerant has been presented. The thermal conductivity and viscosity is measured and plotted at different weight concentrations (0.02-0.10%), temperature (4-16°C), size of nanoparticles (20 & 40 nm) and shape of nanoparticles (spherical & elongated). Also, experimental results are compared with theoretical models of thermal conductivity and viscosity.

## 6.2 Thermal conductivity of $Al_2O_3$/R-11 nanorefrigerant

### 6.2.1 Effect of weight concentration on thermal conductivity

Concentration of particles would be regarded as one of the most significant features affecting thermal conductivity of nanorefrigerants. Basically, it is expected that adding nanoparticles would improve heat transfer performance of nanorefrigerants and also would increase thermal conductivity of them. The results of thermal conductivity v/s weight concentration % at different temperatures are shown below in the Figure 6.1, 6.2 & 6.3.

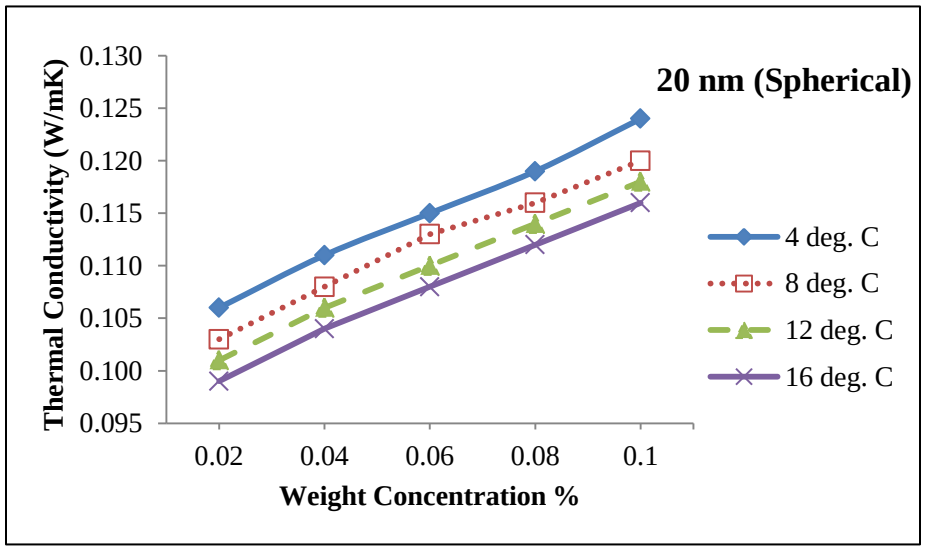


**Figure 6.1** Thermal conductivity v/s weight concentration % of 20 nm (spherical) $Al_2O_3$ nanoparticles at different temperatures

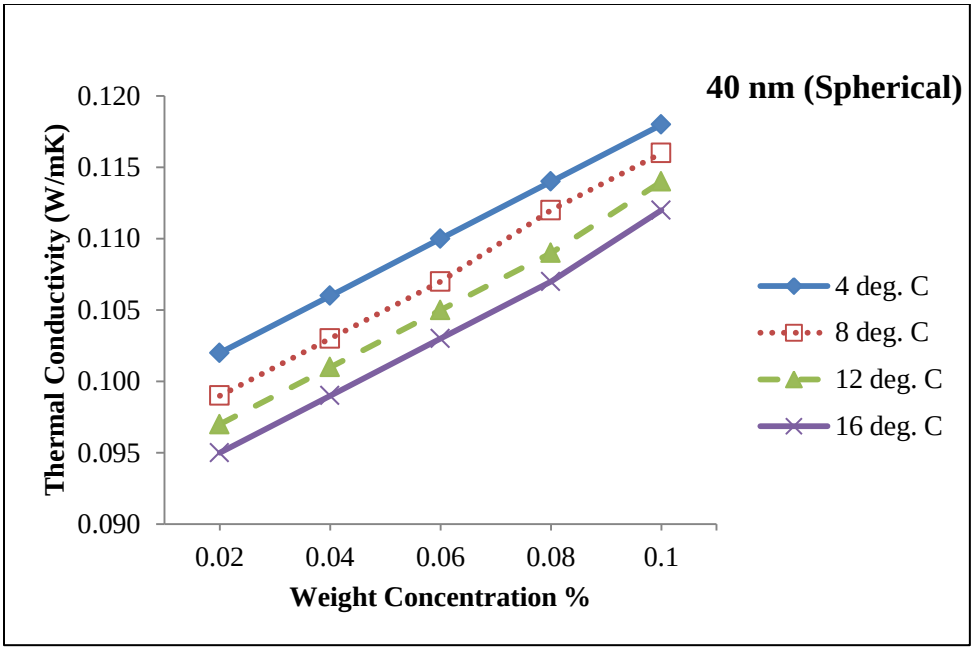


**Figure 6.2** Thermal conductivity v/s weight concentration % of 40 nm (spherical) $Al_2O_3$ nanoparticles at different temperatures

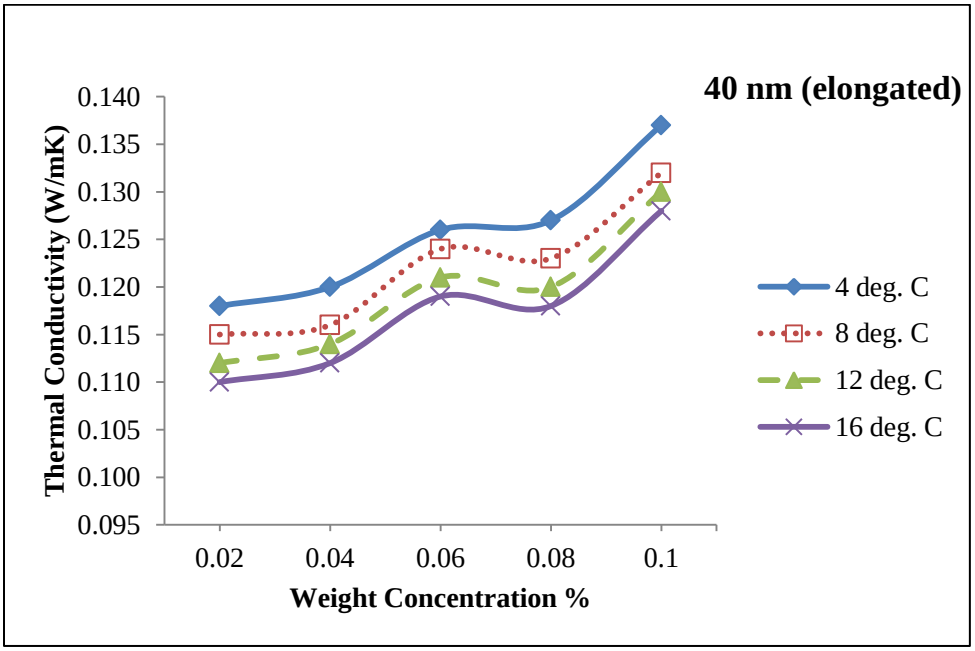


**Figure 6.3** Thermal conductivity v/s weight concentration % of 40 nm (elongated) $Al_2O_3$ nanoparticles at different temperatures

It has been observed that the thermal conductivity of $Al_2O_3$/R-11 nanorefrigerant is increasing with the weight concentration (0.02- 0.10%) of nanoparticles. The enhancement in thermal conductivity is mainly due to micro convection caused by the Brownian motion of the nanoparticles and aggregation of nanoparticles causing a local percolation and clustering to the nanoparticle occurs more actively in fluid with higher concentration. The use of $Al_2O_3$ 20nm in diameter at 0.1 wt. % concentration and at 4°C temperature increased the thermal conductivity of refrigerant R-11 under stationary conditions by 29 %. The highest enhancement of thermal conductivity observed is 42% at 0.1% wt. concentration of 40 nm (elongated) $Al_2O_3$ nanoparticles.

The behavior of increase in thermal conductivity is almost linear for 20 nm (spherical) & 40 nm (spherical) nanoparticles. A nonlinear relationship is observed between thermal conductivity and particle weight concentrations for 40 nm (elongated) nanoparticles. The nonlinearity is attributed to the rapid clustering of elongated nanoparticles which is an indication of interactions between particles due to high nanoparticle concentrations.

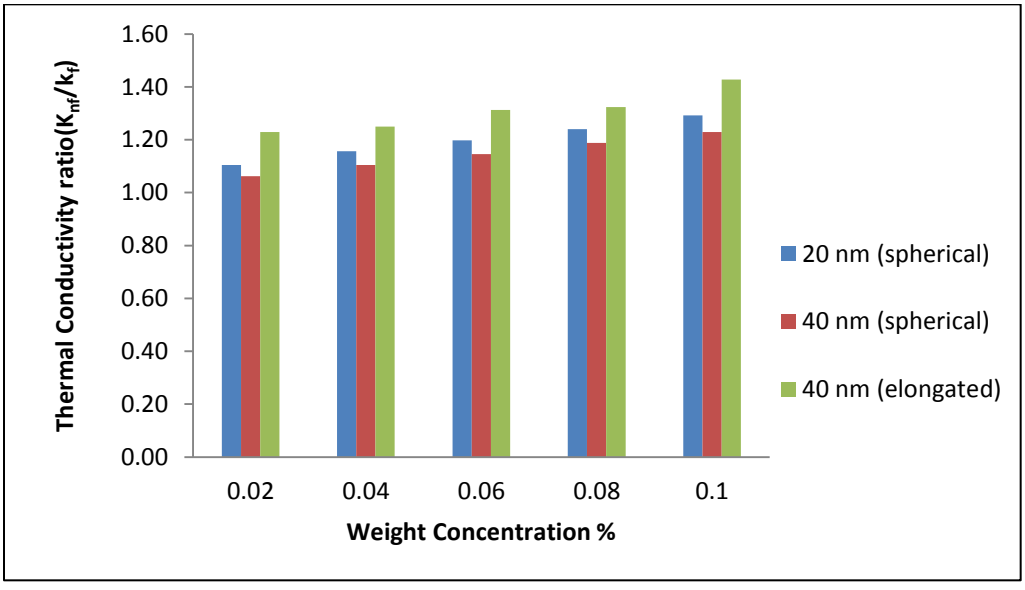


**Figure 6.4** Thermal conductivity ratio v/s wt. concentration % for 20 nm (spherical) & 40 nm (spherical & elongated) $Al_2O_3$ nanoparticles

In Figure 6.4 thermal conductivity enhancement of nanorefrigerant can be observed. Among them nanorefrigerant with 0.1 % weight percentage of $Al_2O_3$ nanoparticles shows maximum

increase in thermal conductivity. There are three types of $Al_2O_3$ (20 nm-spherical, 40 nm-spherical, 40 nm- elongated) nanoparticles with same concentration of nanoparticles showing different values of enhancement. It might be due to the variety in size and shape of nanoparticles which will be discussed in section 6.2.3 & 6.2.4 respectively.

### 6.2.2 Effect of temperature on thermal conductivity

In conventional suspensions of solid particles (with sizes on the order of millimeters or micrometers) in liquids, thermal conductivity of the mixture depends on temperature only due to the dependence of thermal conductivity of base liquid and solid particles on temperature. However, in case of nanorefrigerants the change of temperature affects the Brownian motion of nanoparticles. The results of thermal conductivity v/s temperatures at different weight concentrations are shown below in the Figure 6.5, 6.6 & 6.7.

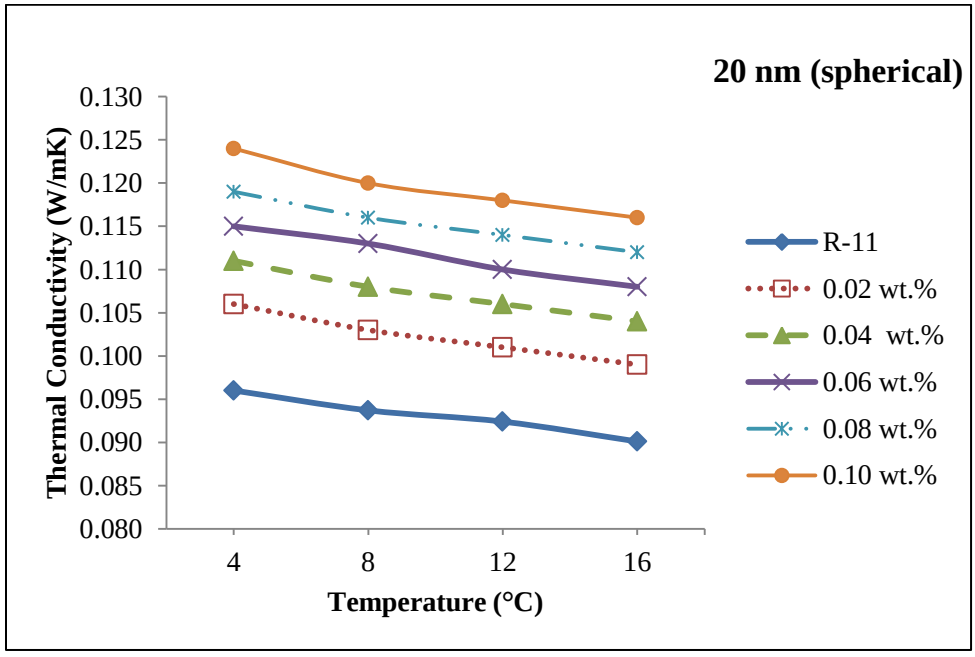


**Figure 6.5** Thermal conductivity v/s temperature at different weight concentrations % of 20 nm (spherical) $Al_2O_3$ nanoparticles

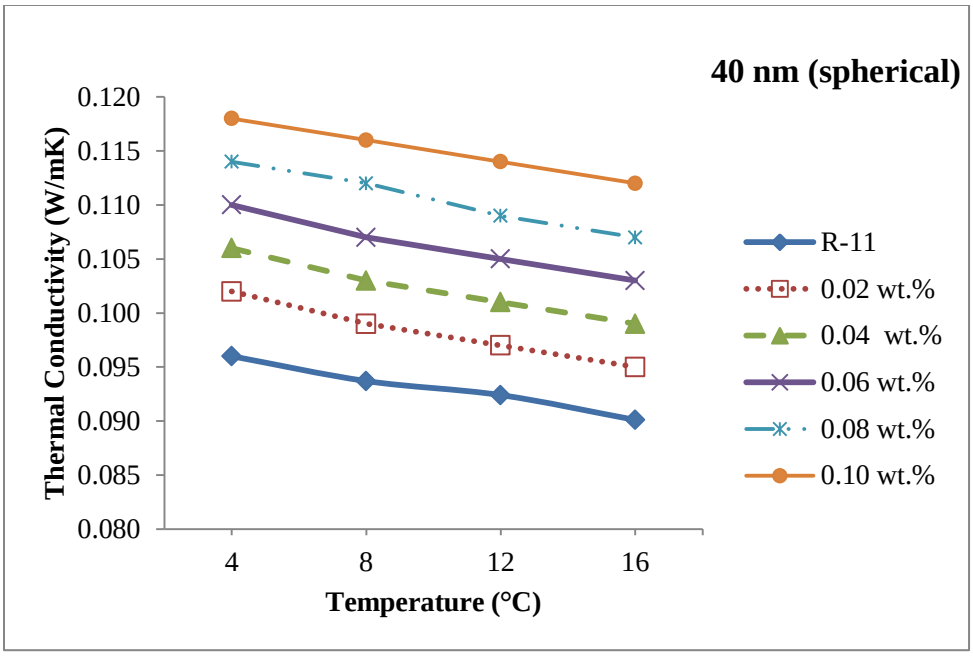


**Figure 6.6** Thermal conductivity v/s temperature at different weight concentrations % of 40 nm (spherical) $Al_2O_3$ nanoparticles

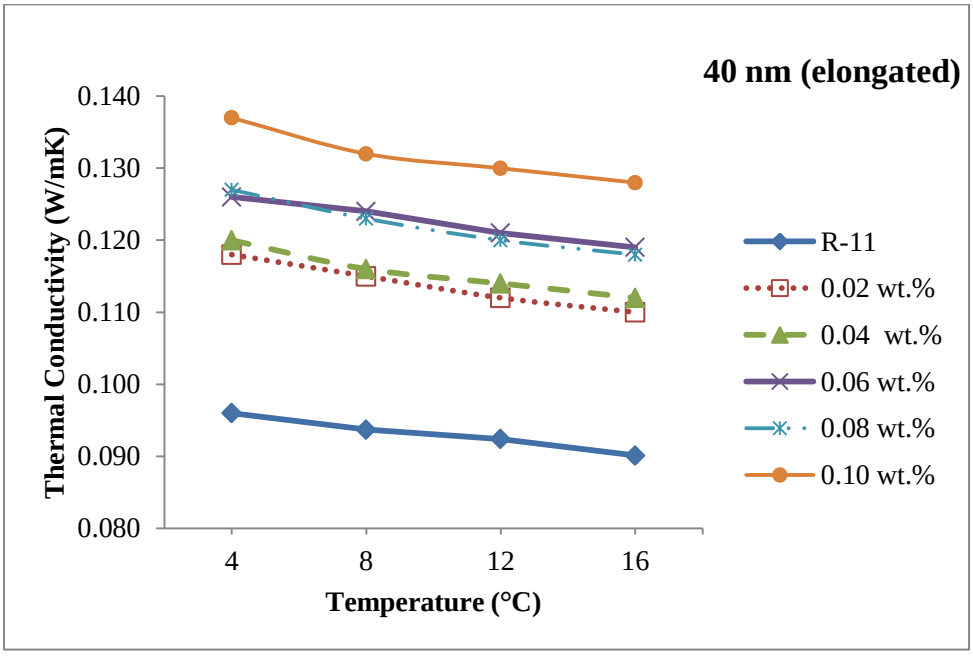


**Figure 6.7** Thermal conductivity v/s temperature at different weight concentrations % of 40 nm (elongated) $Al_2O_3$ nanoparticles

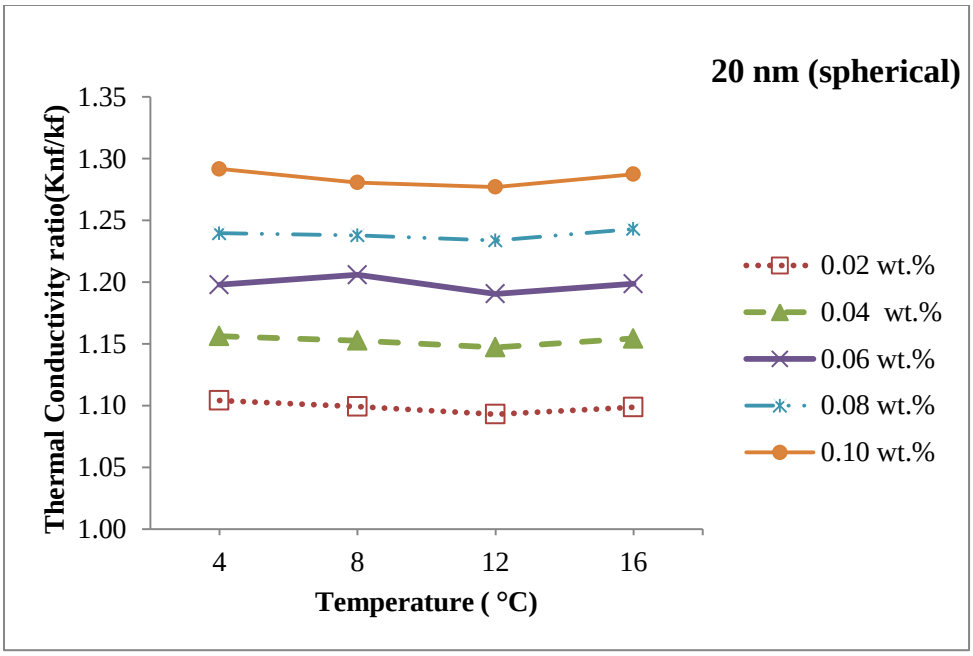


**Figure 6.8** Thermal conductivity ratio v/s temperature at different weight concentrations % of 20 nm (spherical) $Al_2O_3$ nanoparticles

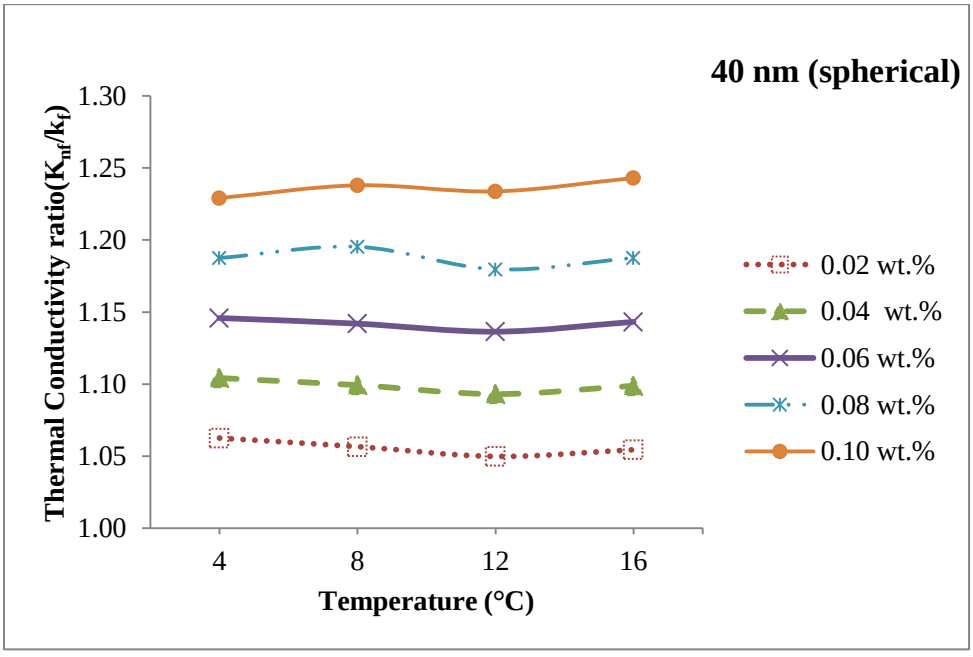


**Figure 6.9** Thermal conductivity ratio v/s temperature at different weight concentrations % of 40 nm (spherical) $Al_2O_3$ nanoparticles

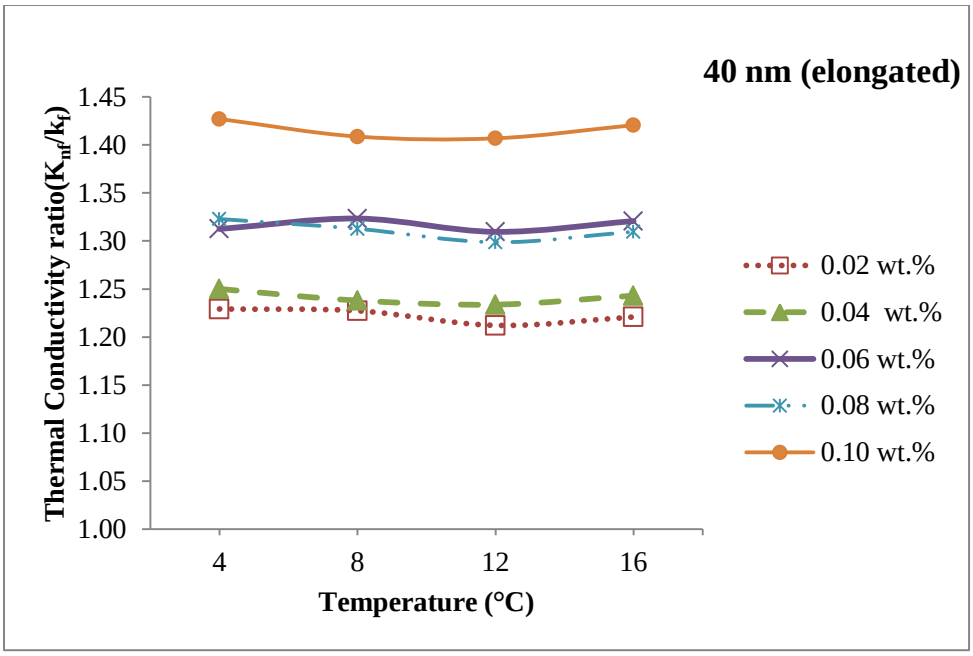


**Figure 6.10** Thermal conductivity ratio v/s temperature at different weight concentrations % of 40 nm (elongated) $Al_2O_3$ nanoparticles

Measurements has been done at four different temperatures; 4, 8, 12 and 16°C. Particle weight concentration was varied between 0.02 and 0.1%. It is found that thermal conductivity decreases with the temperature. For the nanorefrigerant, the mean distance of separation of the centers of the molecules decrease with rising temperature, so that thermal conductivity is expected to decrease with rising temperature. A maximum drop of thermal conductivity is achieved from 4 to 8°C for 0.1 wt% concentration of 40 nm (elongated) $Al_2O_3$ nanoparticle i.e. from 0.137 to 0.132 W/mK. The behavior of decrease in thermal conductivity is almost linear for 20 nm & 40 nm (spherical) $Al_2O_3$ nanoparticles as shown in Figure 6.5 & 6.6. But, the elongated 40 nm $Al_2O_3$ nanoparticles shows nonlinear behavior because of more particles interaction between them. It is observed from Figure 6.8, 6.9 & 6.10 that thermal conductivity ratio remains almost invariant (1% variation) with increase in temperature.

### 6.2.3 Effect of size of $Al_2O_3$ nanoparticles on thermal conductivity

The results of thermal conductivity v/s temperature for different size of $Al_2O_3$ nanoparticles at different weight concentrations are shown in the Figure 6.11, 6.12, 6.13, 6.14 & 6.15.

Also, the results of thermal conductivity ratio v/s weight concentration % are shown in Figure 6.16. The thermal conductivity ratio is the ratio of thermal conductivity of nanorefrigerant to thermal conductivity of fluid i.e. R-11 refrigerant ($K_{nf}/K_f$). Here, $K_{nf}$ is thermal conductivity of $Al_2O_3$/R-11 nanorefrigerant and $K_f$ is thermal conductivity of R-11 refrigerant.

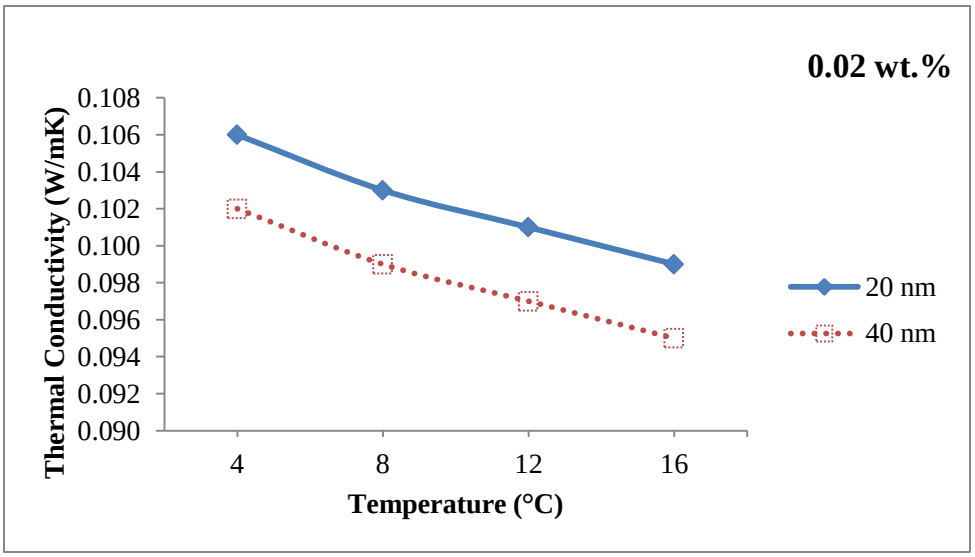


**Figure 6.11** Thermal conductivity v/s temperature for different size of $Al_2O_3$ nanoparticles at 0.02 wt. % concentration

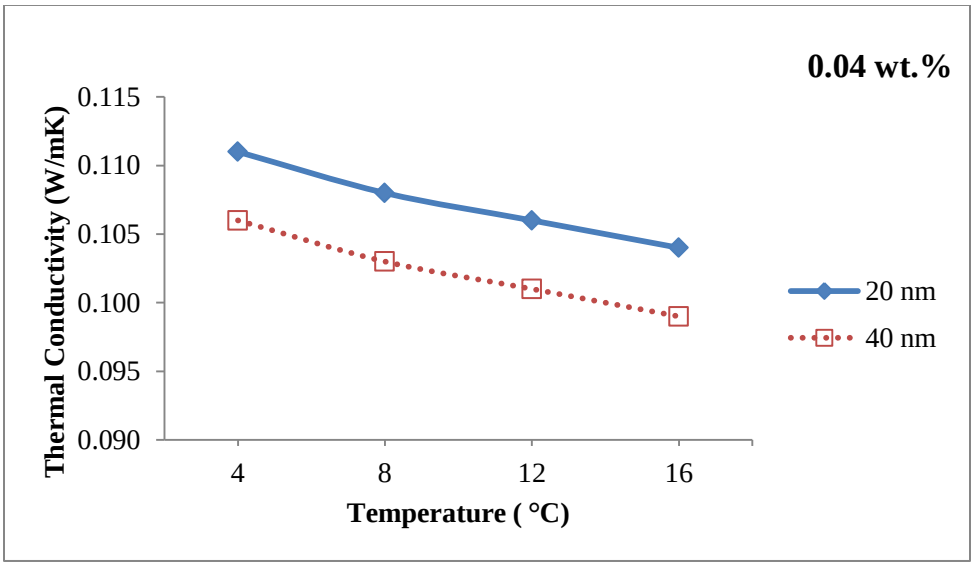


**Figure 6.12** Thermal conductivity v/s temperature for different size of $Al_2O_3$ nanoparticles at 0.04 wt. % concentration

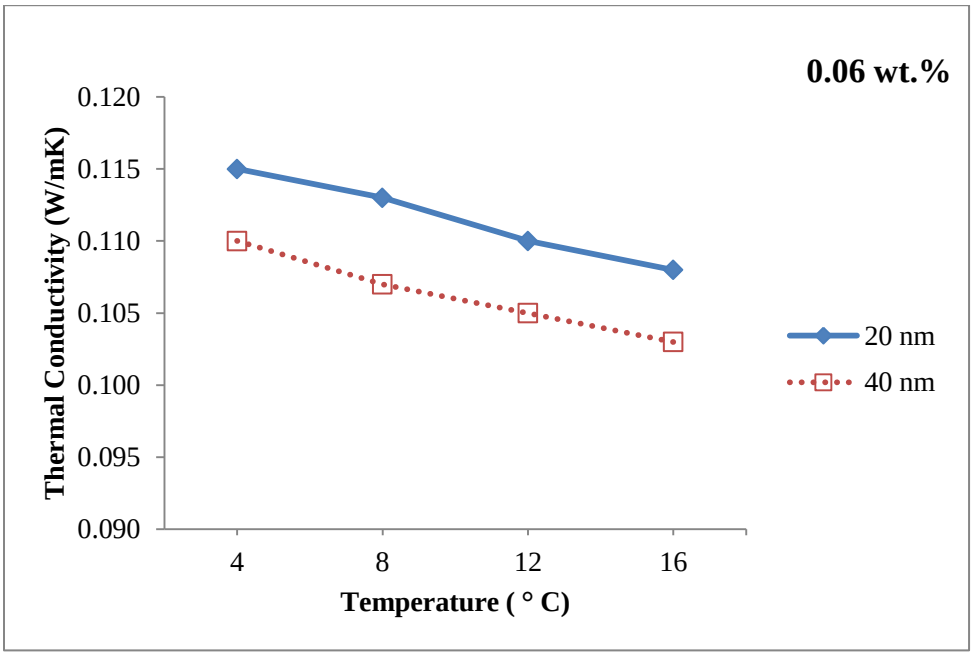


**Figure 6.13** Thermal conductivity v/s temperature for different size of $Al_2O_3$ nanoparticles at 0.06 wt. % concentration

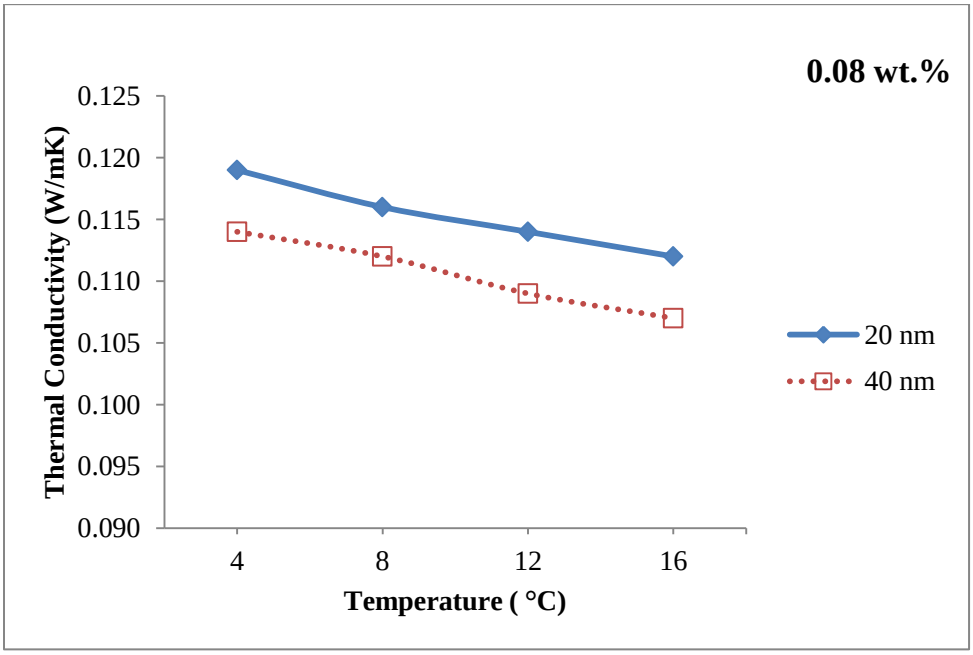


**Figure 6.14** Thermal conductivity v/s temperature for different size of $Al_2O_3$ nanoparticles at 0.08 wt. % concentration

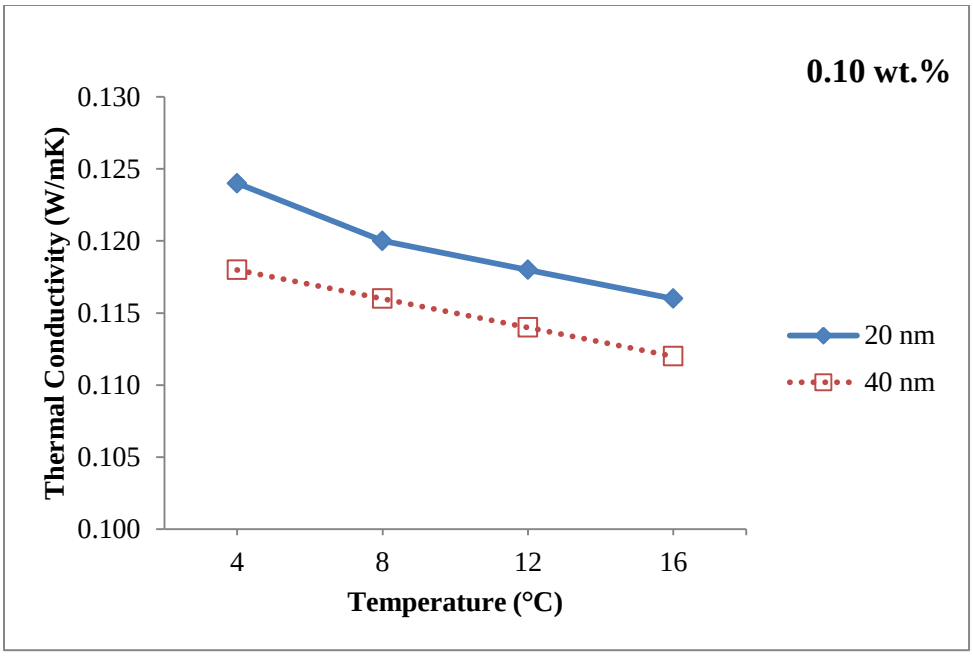


**Figure 6.15** Thermal conductivity v/s temperature for different size of $Al_2O_3$ nanoparticles at 0.10 wt. % concentration

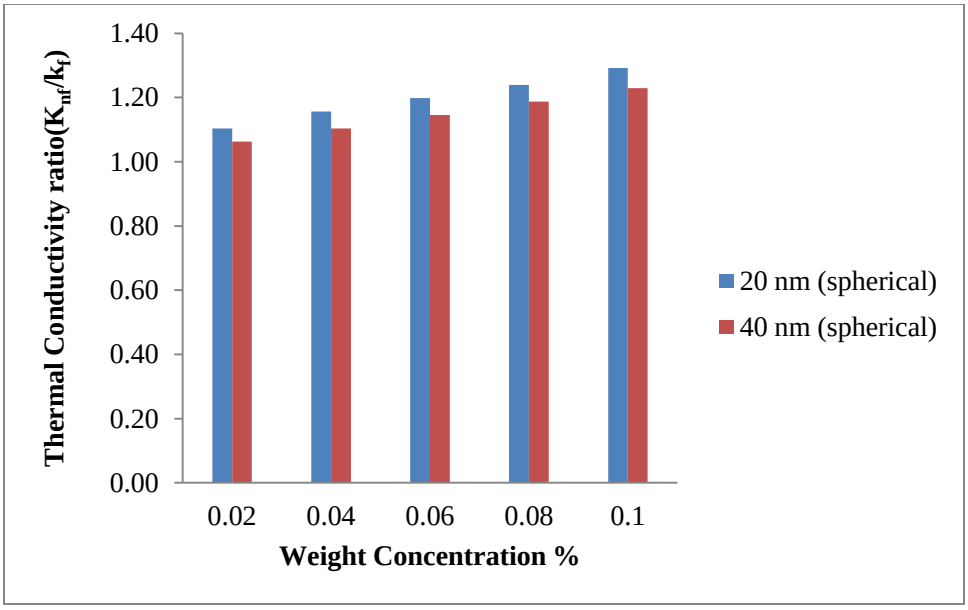


**Figure 6.16** Thermal conductivity ratio v/s wt. concentration % for different size of $Al_2O_3$ nanoparticles

It is observed that for the same particle weight concentration, thermal conductivity decreases with increasing particle size. The results are with the effect of Brownian motion, since the effect of Brownian motion decreases with increasing particle size, which decreases the associated thermal conductivity enhancement. $Al_2O_3$ nanoparticles of size 20 nm have higher value of thermal conductivity than 40 nm particles within measured temperature range (4-16 °C). Figure 6.16 shows thermal conductivity ratio v/s wt. concentration % for 20 & 40 nm size of $Al_2O_3$ nanoparticles. It has been observed that for 0.1 wt. % nanorefrigerant, thermal conductivity enhancement decreased from 29 to 23% by increasing the particle size from 20 to 40 nm.

The general trend in the experimental data is that the thermal conductivity of nanorefrigerants increases with decreasing particle size. The trend is theoretically supported by two mechanisms of thermal conductivity enhancement; Brownian motion of nanoparticles and liquid layering around nanoparticles.

### 6.2.4 Effect of shape of $Al_2O_3$ nanoparticles on thermal conductivity

The results of thermal conductivity v/s temperature for different shape of $Al_2O_3$ nanoparticles are shown in the Figure 6.17, 6.18, 6.19, 6.20 & 6.21. Also, results of thermal conductivity ratio v/s weight concentration % for different shapes $Al_2O_3$ nanoparticles are shown in Figure 6.22.

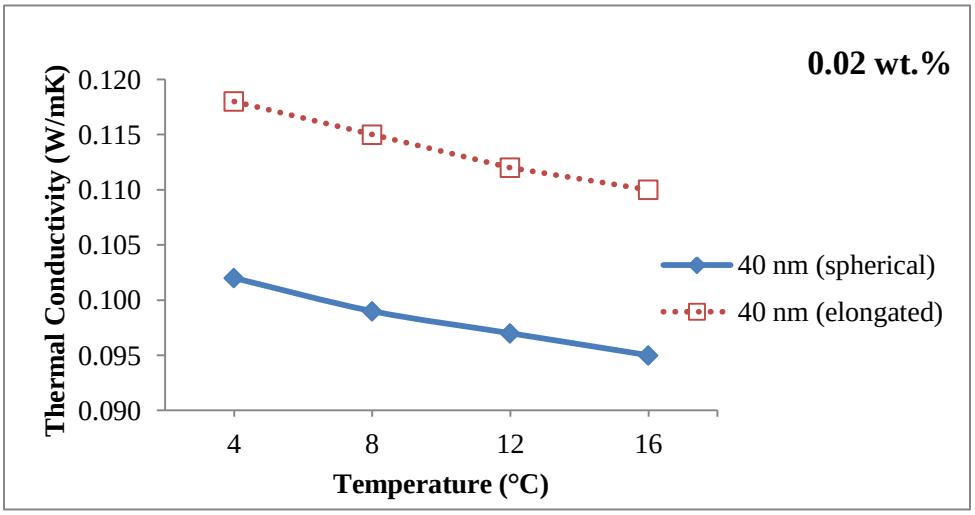


**Figure 6.17** Thermal conductivity v/s temperature for different shape of $Al_2O_3$ nanoparticles at 0.02 wt. % concentration

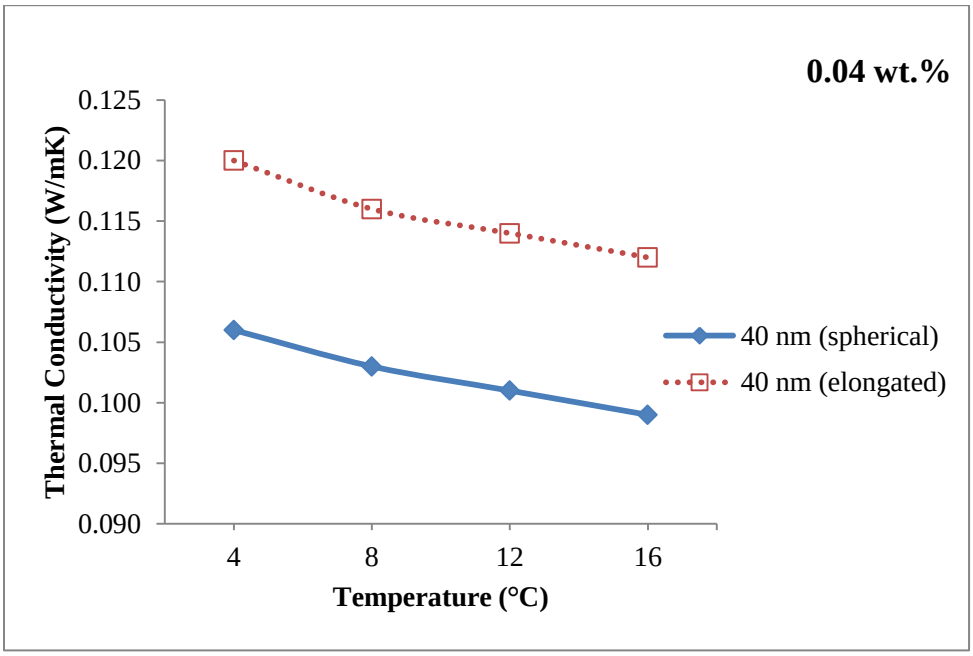


**Figure 6.18** Thermal conductivity v/s temperature for different shape of $Al_2O_3$ nanoparticles at 0.04 wt. % concentration

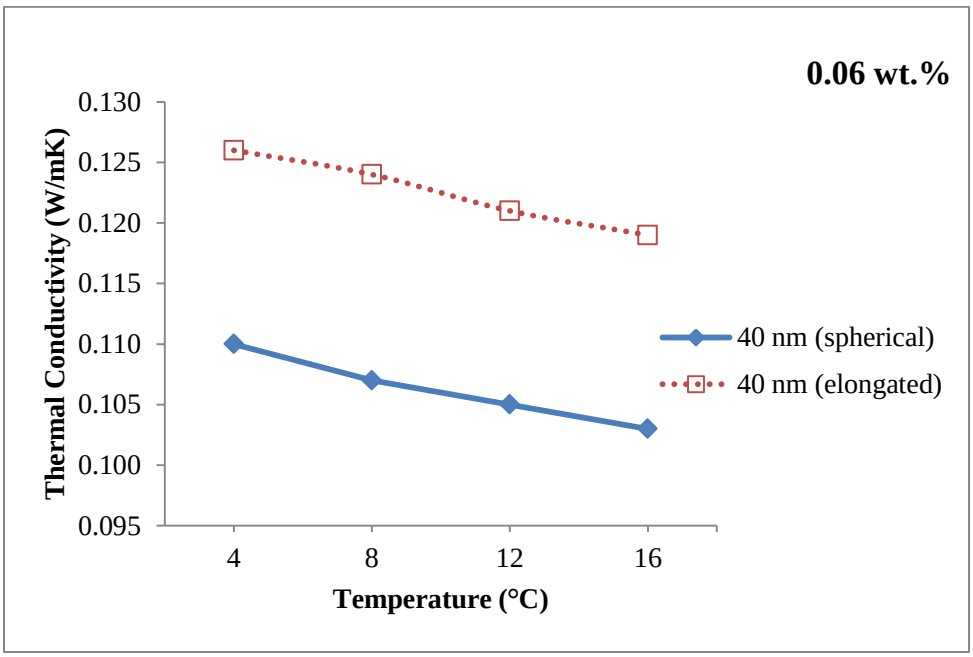


**Figure 6.19** Thermal conductivity v/s temperature for different shape of $Al_2O_3$ nanoparticles at 0.06 wt. % concentration

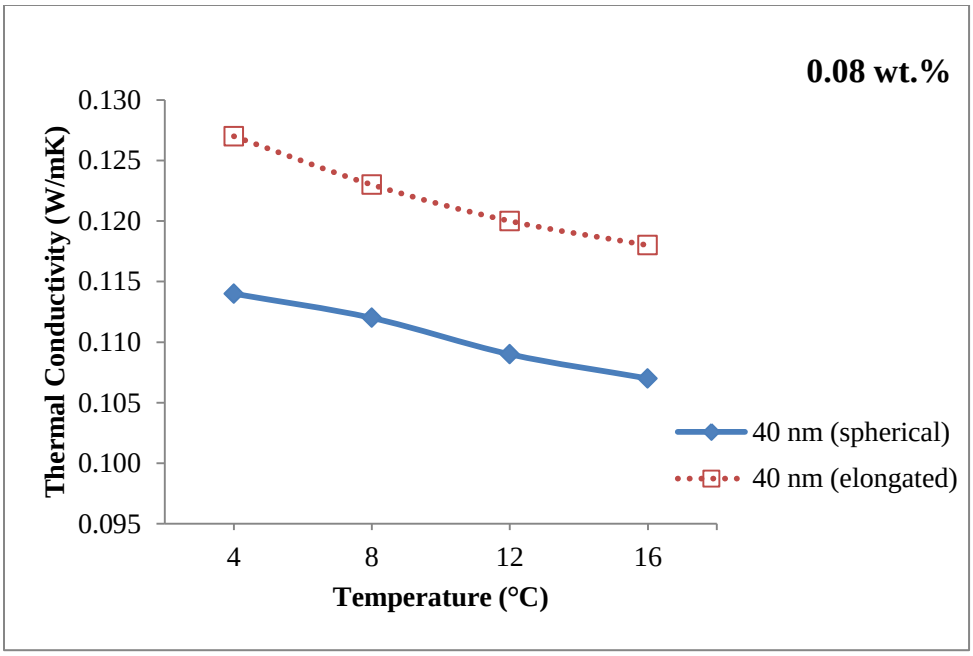


**Figure 6.20** Thermal conductivity v/s temperature for different shape of $Al_2O_3$ nanoparticles at 0.08 wt. % concentration

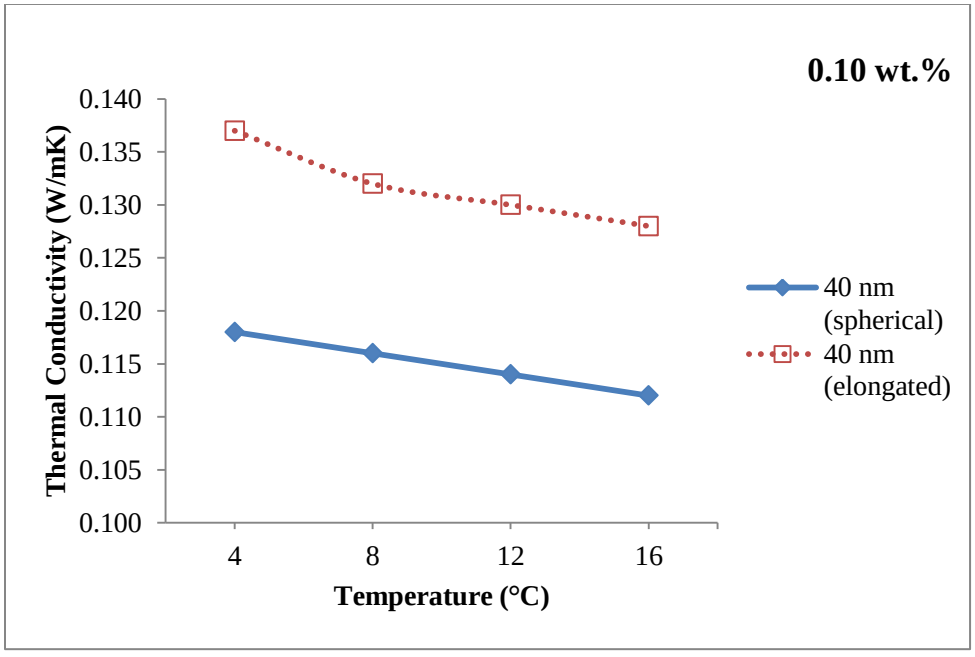


**Figure 6.21** Thermal conductivity v/s temperature for different shape of $Al_2O_3$ nanoparticles at 0.10 wt.% concentration

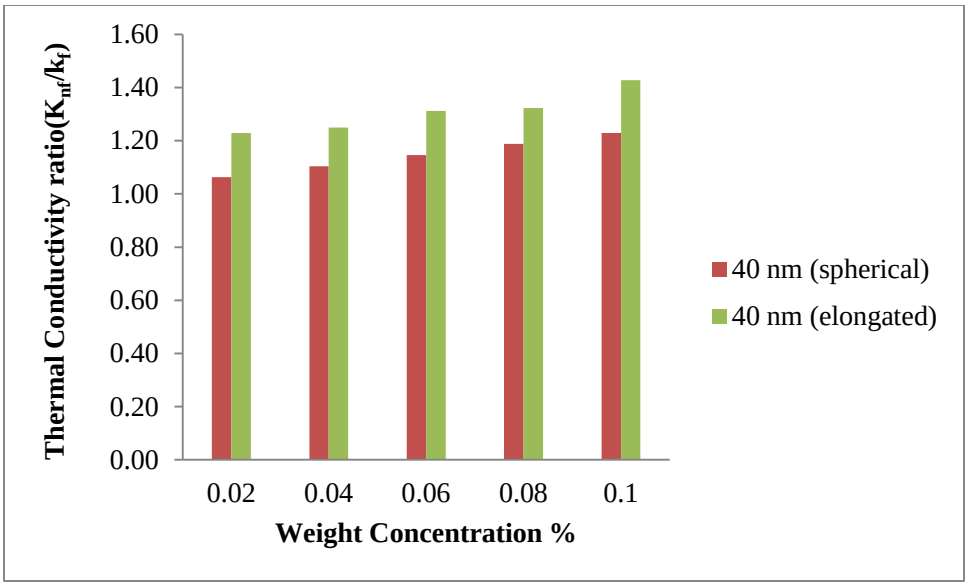


**Figure 6.22** Thermal conductivity ratio v/s wt. concentration % for different shape of $Al_2O_3$ nanoparticles

Two types of nanoparticles shapes are used for the preparation of nanorefrigerant; spherical particles with 40 nm average diameter and elongated particles with 40 nm average diameter. It is found that 0.1 wt.% $Al_2O_3$/R-11 nanorefrigerant with spherical particles had a thermal conductivity enhancement of 24%, whereas 0.1 wt. % nanofluid with elongated particles had a thermal conductivity enhancement of 43%.

In addition to these experimental results, the fact that thermal conductivity enhancement of nanorefrigerants with elongated shaped $Al_2O_3$ nanoparticles (40 nm) is more than spherical shaped (40 nm) $Al_2O_3$ nanoparticles within measured temperature range (4-16°C). As a result, one can conclude that elongated nanoparticles provide higher thermal conductivity enhancement than spherical particles. Among the possible reasons of this is the rapid heat transport along relatively larger distances in elongated particles since elongated particles usually have larger lengths as compare to its diameter.

### 6.2.5 Comparison of experimental data of thermal conductivity with theoretical models

The values for the effective thermal conductivities were calculated for Hamilton Crosser (1962), Jeffrey (1973), Lu & Lin (1996) models. The experimental data along with theoretical models is plotted as a function of the weight concentration (0.02, 0.04, 0.06, 0.08 & 0.10 %) for 20 nm (spherical), 40 nm (spherical) $Al_2O_3$ nanoparticles in Figure 6.23.

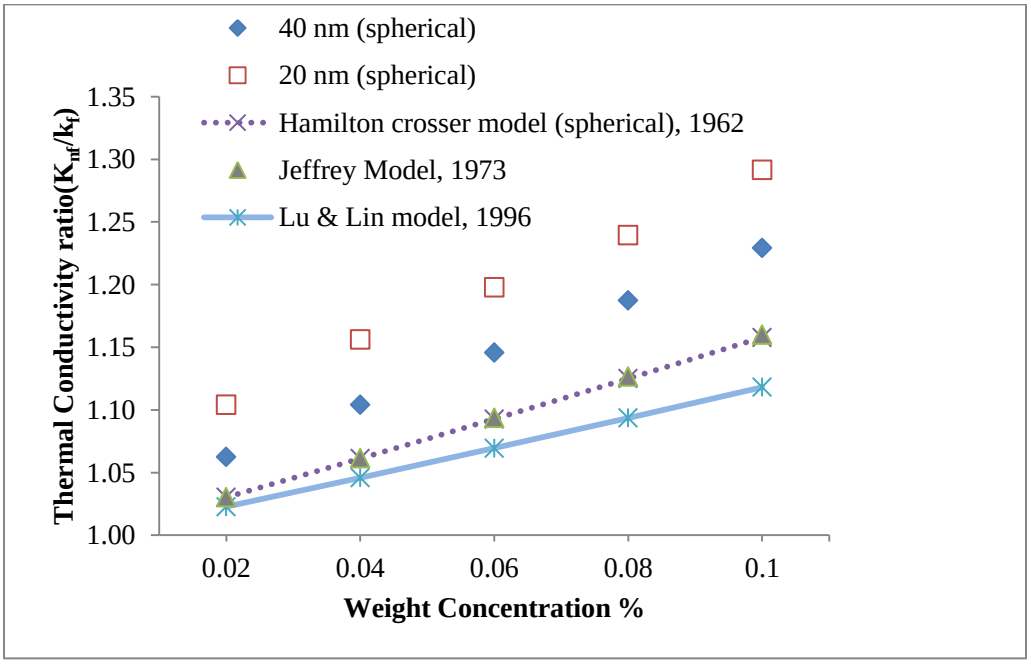


**Figure 6.23** Measured thermal conductivities of $Al_2O_3$/R-11 nanorefrigerant v/s effective thermal conductivities calculated from theories for spherical nanoparticles

When the predictions of the models are compared (Figure 6.23), it is seen that Hamilton Crosser & Jeffrey models provide very close results. The data shown in Figure 6.23 shows some degree of under prediction by theoretical models than the experimental values of thermal conductivity. The Hamilton and Crosser model may be under predicting since it does not incorporate the Brownian motion and the resulting heat transfer by convection. At such low particle sizes (20 nm & 40 nm), Brownian motion should not be neglected. Also, the Hamilton and Crosser model does not take the effect of particle size on thermal conductivity into account. At this point, it should be noted that thermal conductivity increases with decreasing particle size when Brownian motion is considered as the main

mechanism of thermal conductivity enhancement, because the effect of Brownian motion increases with decreasing particle size, which improves micro-convection around nanoparticles.

When the experimental results are observed, it is seen that the discrepancy in the data is somewhat larger for the 0.01 wt. % case. This might be due to the fact that at higher particle weight concentrations, clustering of particles is more pronounced, which affects the thermal conductivity of nanorefrigerants. It should be noted that clustering may increase or decrease the thermal conductivity enhancement. If a network of nanoparticles is formed as a result of clustering, this may enable fast heat transport along nanoparticles. On the other hand, excessive clustering may result in sedimentation, which decreases the effective particle weight concentration of nanorefrigerant.

The maximum thermal conductivity deviation from Hamilton & Crosser model for 20 & 40 nm (spherical) $Al_2O_3$ nanoparticles is 13% and 10% respectively at 0.10 % weight concentration. But the minimum deviation of thermal conductivity for 20 & 40 nm (spherical) $Al_2O_3$ nanoparticles is 7% and 3% respectively at 0.02 % weight concentration. Also, the mean deviation of thermal conductivity for 20 & 40 nm (spherical) $Al_2O_3$ nanoparticles is 11% and 6% respectively for Hamilton & Crosser model.

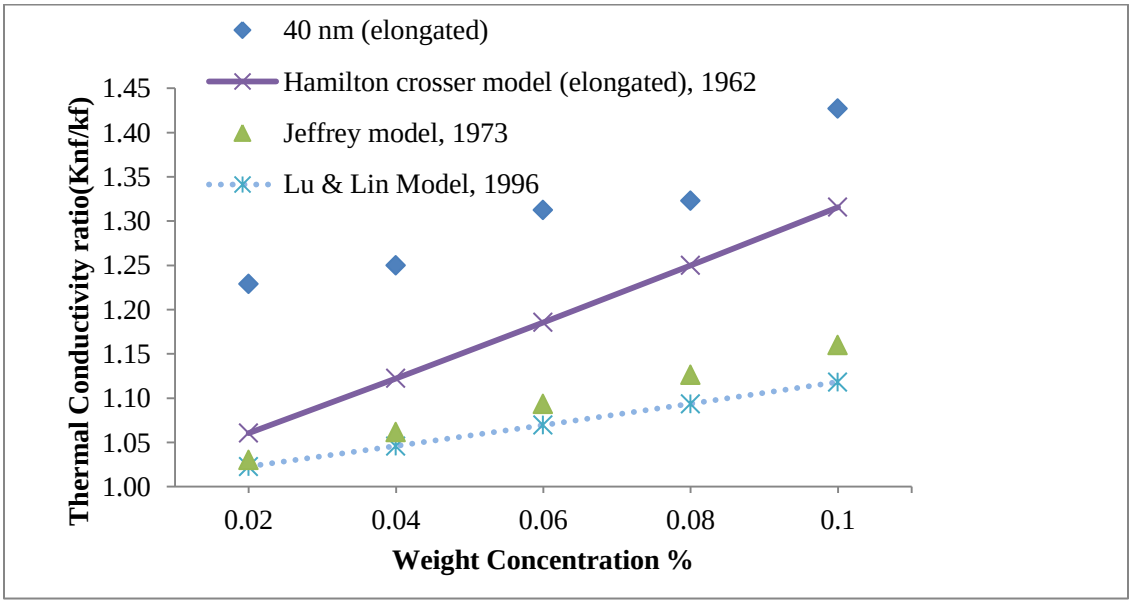


**Figure 6.24** Measured thermal conductivities of $Al_2O_3$ /R-11 nanorefrigerant v/s effective thermal conductivities calculated from theories for elongated nanoparticles

It is observed from Figure 6.24 that the thermal conductivity prediction from Hamilton & Crosser model is close to experimental data of 40 nm (elongated) $Al_2O_3$ nanoparticles. The minimum deviation of thermal conductivity observed is & 7% at 0.08 % weight concentration and maximum is 17% at 0.02 % weight concentration. Also, the mean deviation of thermal conductivity for 40 nm (elongated) $Al_2O_3$ nanoparticles is 13% for Hamilton & Crosser model.

It is also observed that the experimental values of 40 nm elongated shaped Al2O3 nanoparticles are nonlinear function of the weight concentration. On the other hand, all the models evaluated showed a linear relationship. A close observation of the models shows that at low concentrations, a linear relationship is expected. This deviation may be a result of three causes. The first could simply be an experimental error. The second reason may be due to the assumptions. For example, the Hamilton crosser assumes a single particle with no nanolayer and no Brownian motion and such an assumption may be validate these weight concentrations for the current nanorefrigerants systems. Also, with an increase in the weight concentration, clustering may become more evident and as a result, the experiment shows better correlation. The final cause may be that the mean particle diameter shown is not sufficient to accurately predict the nanorefrigerants behavior since the particles/cluster may have a size distribution which is not very narrow. Thus care needs to be taken in understanding the size distribution and the aggregation phenomena for accurate predictions.

### 6.3 Viscosity of $Al_2O_3$/R-11 nanorefrigerant

#### 6.3.1 Effect of weight concentration on viscosity

The results of viscosity v/s weight concentration % at different temperatures are shown below in the Figure 6.25, 6.26 & 6.27.

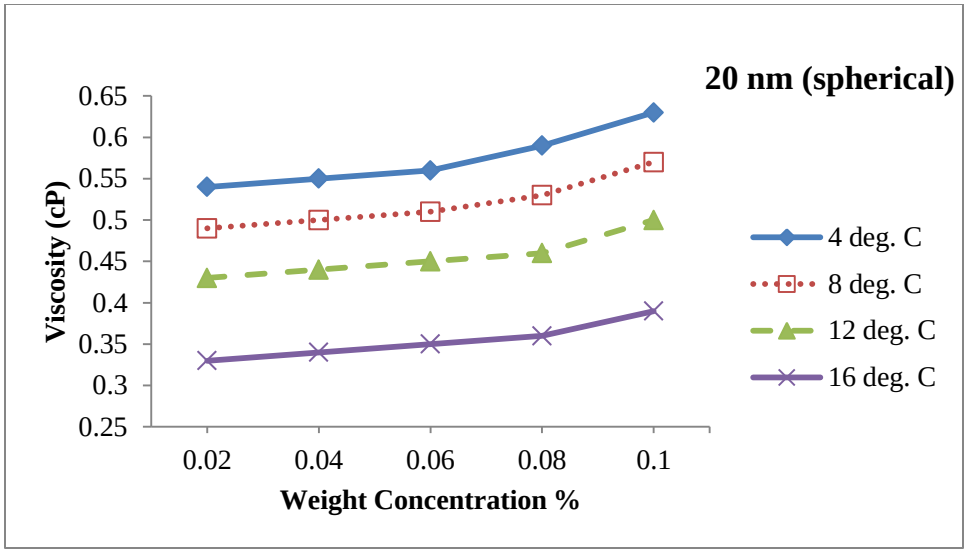


**Figure 6.25** Viscosity v/s weight concentration % at different temperatures for 20 nm (spherical) $Al_2O_3$ nanoparticles

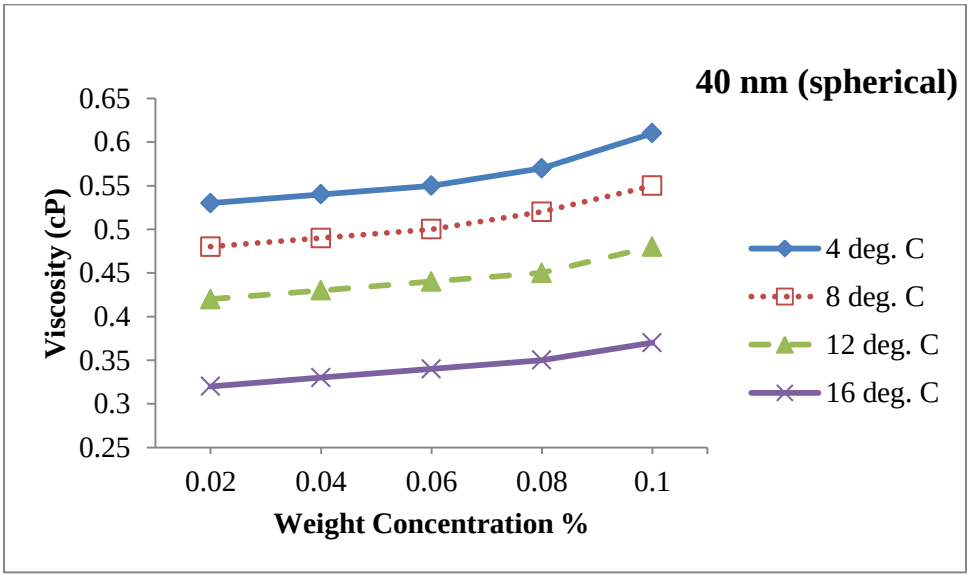


**Figure 6.26** Viscosity v/s weight concentration % at different temperatures for 40 nm (spherical) $Al_2O_3$ nanoparticles

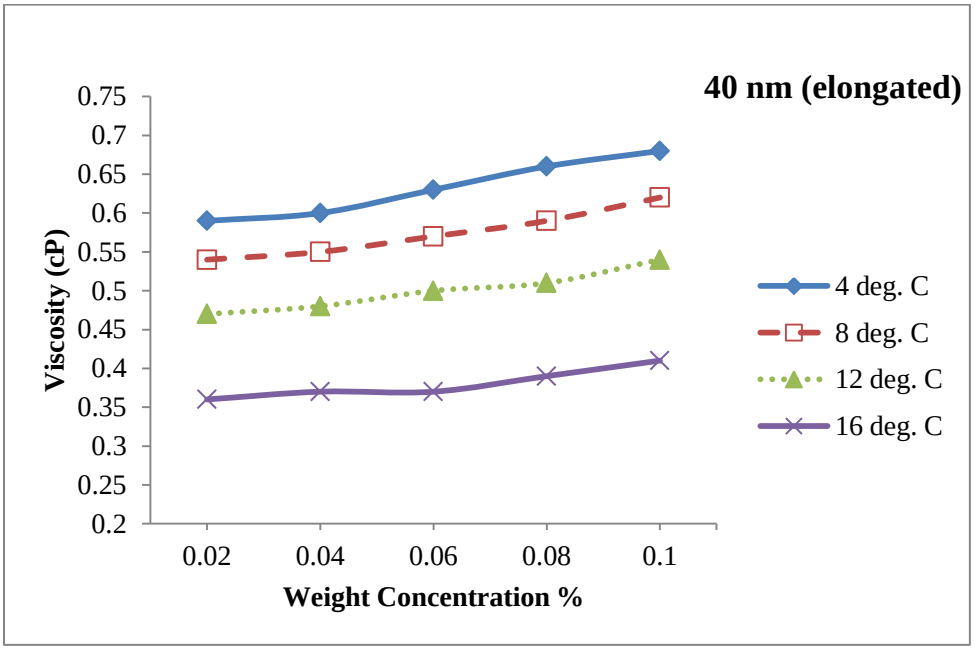


**Figure 6.27** Viscosity v/s weight concentration % at different temperatures for 40 nm (elongated) $Al_2O_3$ nanoparticles

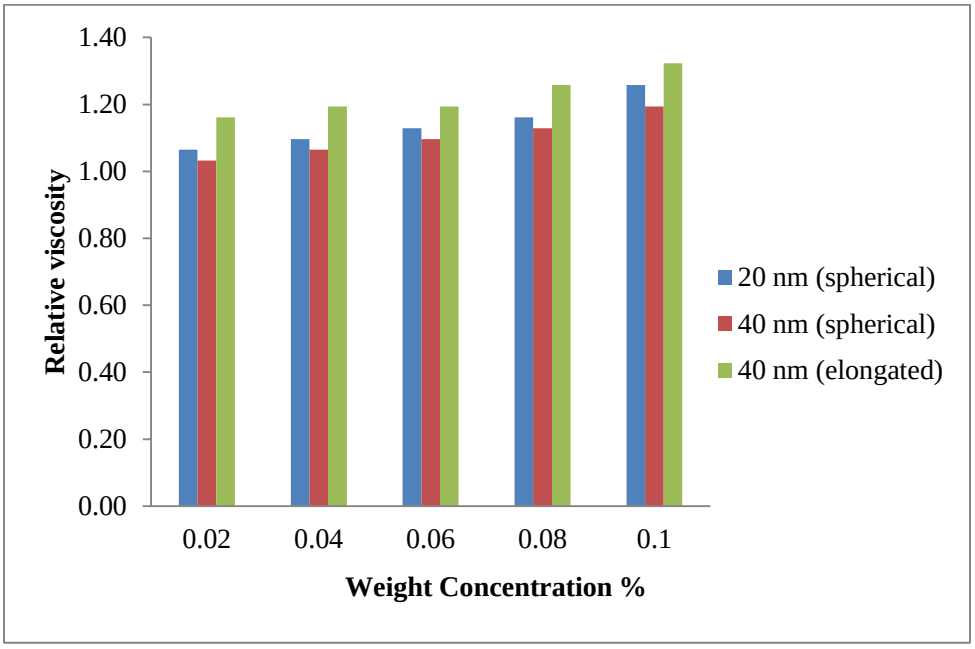


**Figure 6.28** Relative viscosity v/s wt. concentration % for 20 nm (spherical) & 40 nm (spherical & elongated) $Al_2O_3$ nanoparticles

The viscosity of $Al_2O_3$/R-11 nanorefrigerant is increased with the weight concentration of nanoparticles. The increase of viscosity is more at higher weight concentration i.e. from 0.08 to 0.10% and behavior of increase in viscosity is almost linear upto 0.08 wt. % concentration for 20 & 40 nm nanoparticles. A nonlinear relationship is observed between viscosity and particle weight concentrations for 40 nm (elongated) nanoparticles. The nonlinearity is attributed to the rapid clustering of elongated nanoparticles which is an indication of interactions between particles due to high particle concentrations. The use of $Al_2O_3$ 20 nm in diameter at 0.1 wt. % concentration and at 4°C temperature increased the viscosity of refrigerant R-11 by 21 %. The highest enhancement of viscosity observed is 31% at 0.1% wt. concentration and 4°C of 40 nm (elongated) $Al_2O_3$ nanoparticles.

### 6.3.2 Effect of temperature on viscosity

The results of viscosity v/s temperatures at different weight concentrations are shown below in the Figure 6.29, 6.30 & 6.31.

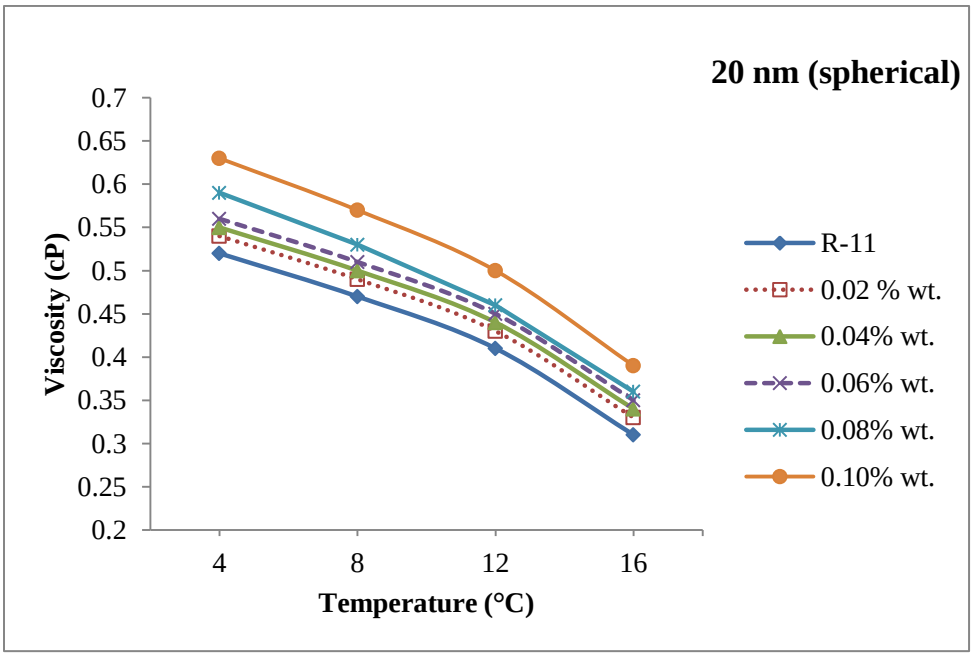


**Figure 6.29** Viscosity v/s temperature at different weight concentrations % for 20 nm (spherical) $Al_2O_3$ nanoparticles

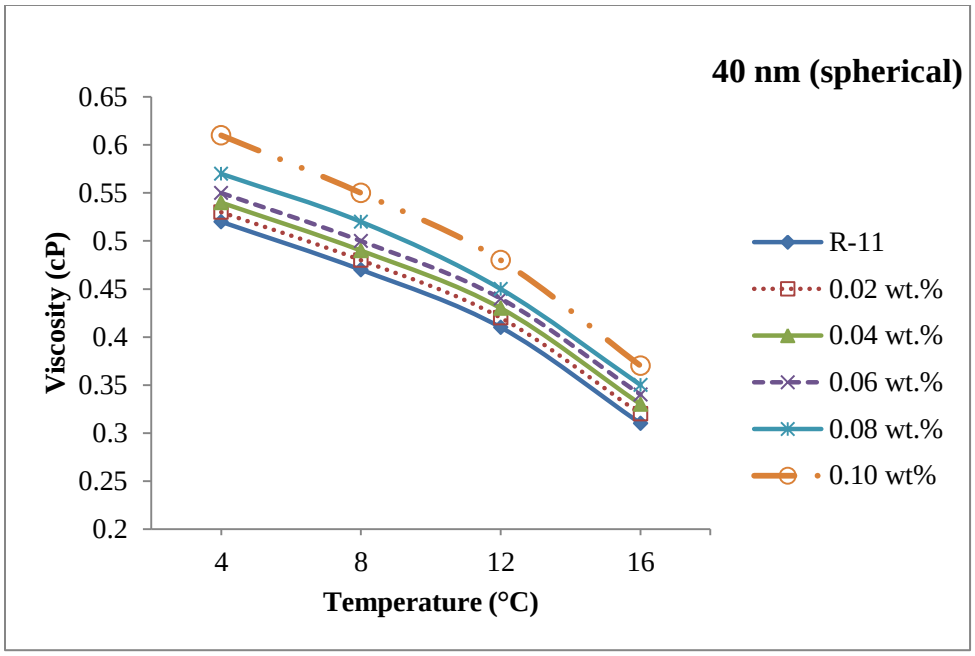


**Figure 6.30** Viscosity v/s temperature at different weight concentrations % for 40 nm (spherical) $Al_2O_3$ nanoparticles

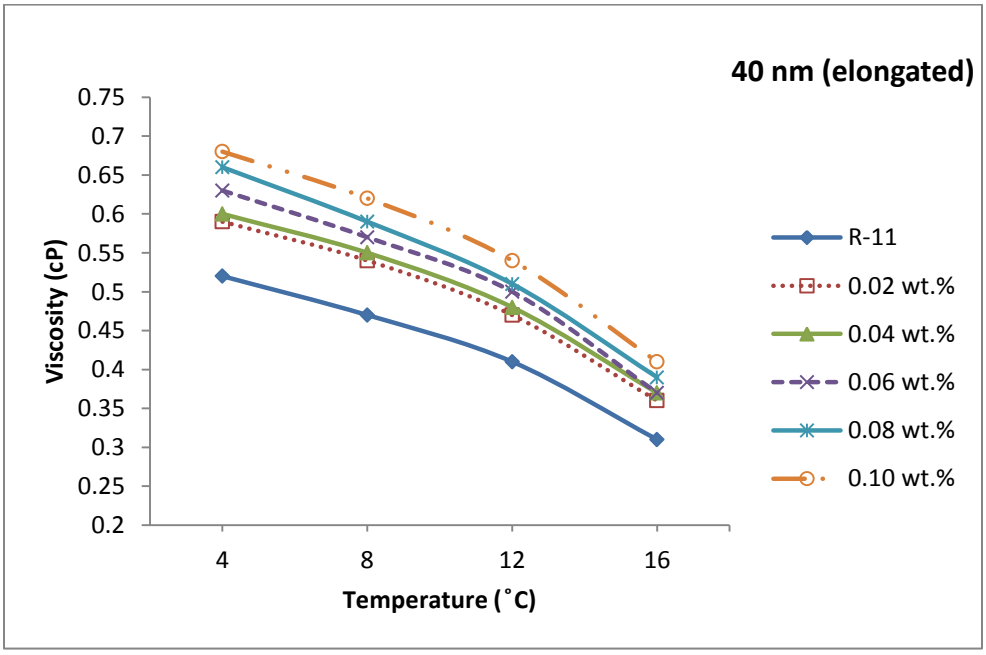


**Figure 6.31** Viscosity v/s temperature at different weight concentrations % for 40 nm (elongated) $Al_2O_3$ nanoparticles

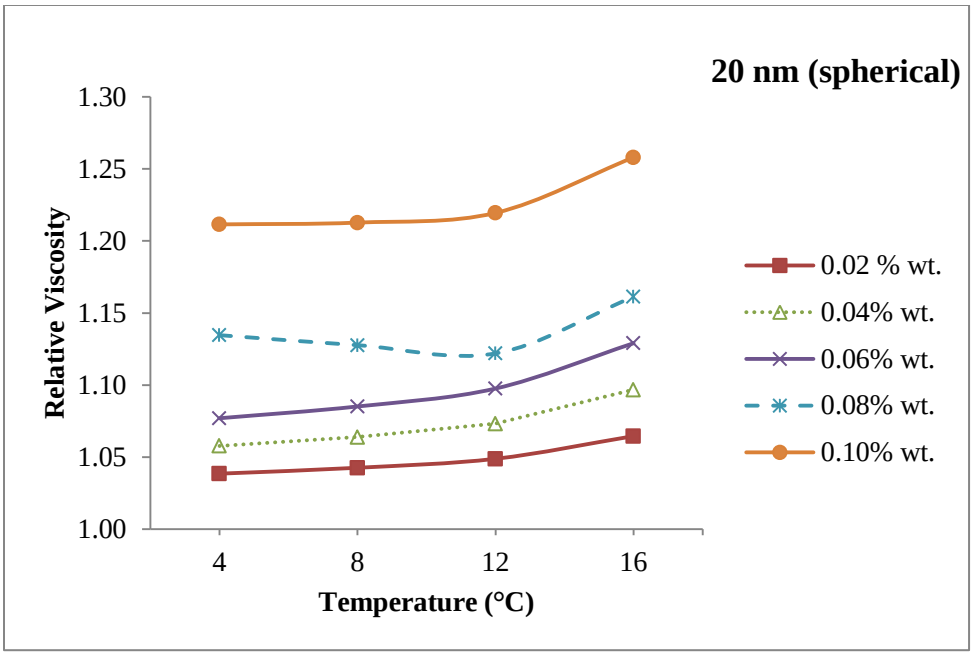


**Figure 6.32** Relative viscosity v/s temperature at different wt. concentrations for 20 nm (spherical) $Al_2O_3$ nanoparticles

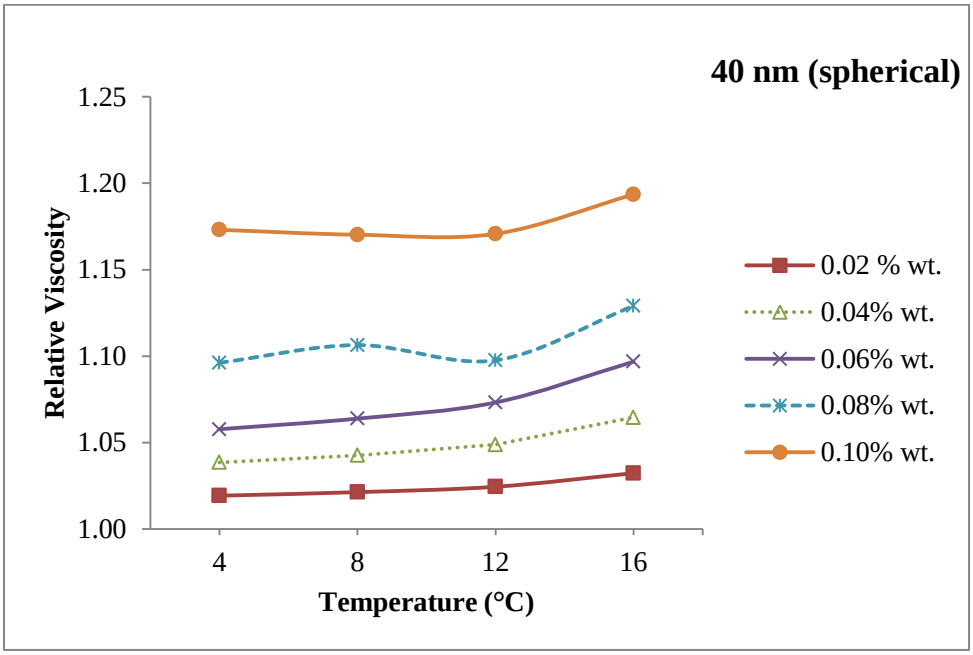


**Figure 6.33** Relative viscosity v/s temperature at different wt. concentrations for 40 nm (spherical) $Al_2O_3$ nanoparticles

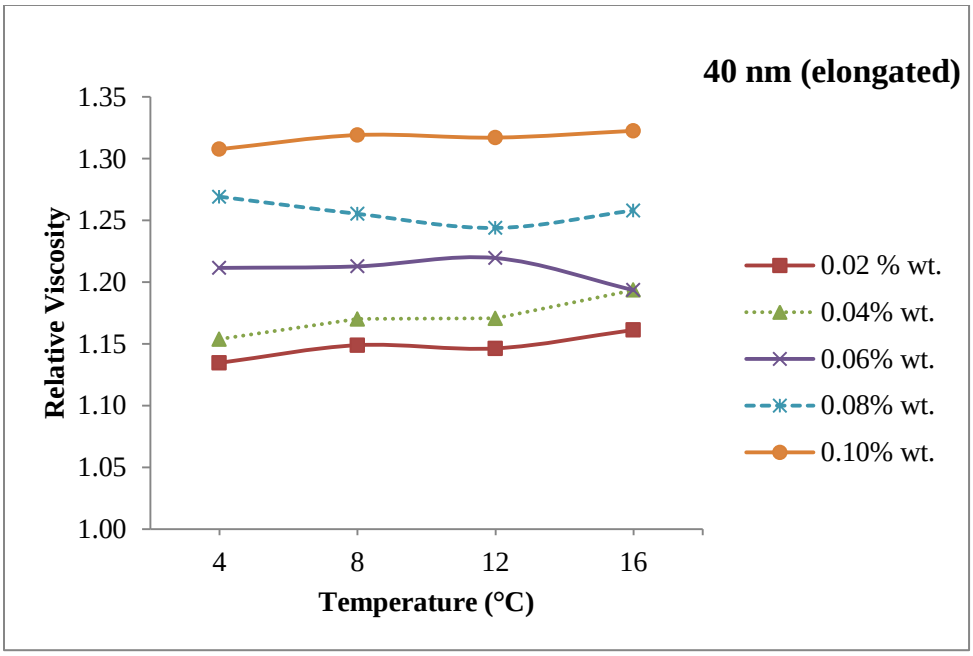


**Figure 6.34** Relative viscosity v/s temperature at different wt. concentrations for 40 nm (elongated) $Al_2O_3$ nanoparticles

Figure 6.29, 6.30 & 6.31 shows the variation in viscosity of $Al_2O_3$ based nanorefrigerant for five different weight concentrations (0.02, 0.04, 0.06, 0.08, 0.10 %) of nanoparticles with the rise in temperature (4-12°C). Although the absolute viscosity decreases with increase in temperature in both the base fluids and the nanorefrigerant, the relative viscosity remains almost constant with increase in temperature, which is a clear indication for the absence of aggregation with temperature. The viscosity of $Al_2O_3$/R-11 nanorefrigerant is decreasing with the rise of temperature of nanoparticles. The increasing temperature would weaken the inter-particle and inter-molecular adhesion forces. The behavior of viscosity decreasing is linear up to 12°C, but from 12 to 16°C there is sharp decline in slope. Figure 6.32, 6.33 & 6.34 show that relative viscosity is almost invariant with variation of 1-2 % with the increase in temperature of nanorefrigerant. In the experiments, it has been attempted to measure viscosity at the temperature lower than boiling point of R-11 refrigerant i.e. 23°C. The particles have a tendency to form aggregation, resulting in the observed unpredictable increase of the nanorefrigerant viscosity.

### 6.3.3 Effect of size of $Al_2O_3$ nanoparticles on viscosity

The results of viscosity v/s weight concentration % for different size of $Al_2O_3$ nanoparticles are shown in the Figure 6.35, 6.36, 6.37, 6.38 & 6.39. Also, the results of relative viscosity v/s weight concentrations % for different size of nanoparticles is shown in Figure 6.40. The relative viscosity is the ratio of viscosity of nanorefrigerant to viscosity of fluid i.e. R-11 refrigerant ($\mu_{nf}/\mu_f$). Here, $\mu_{nf}$ is viscosity of $Al_2O_3$/R-11 nanorefrigerant and $\mu_f$ is viscosity of R-11 refrigerant.

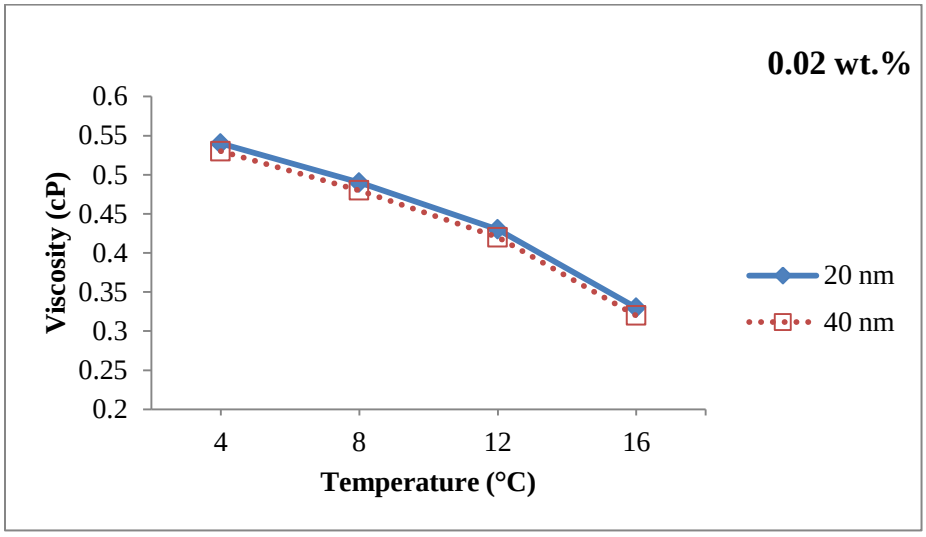


**Figure 6.35** Viscosity v/s temperature for different size of $Al_2O_3$ nanoparticles at 0.02 wt. % concentration

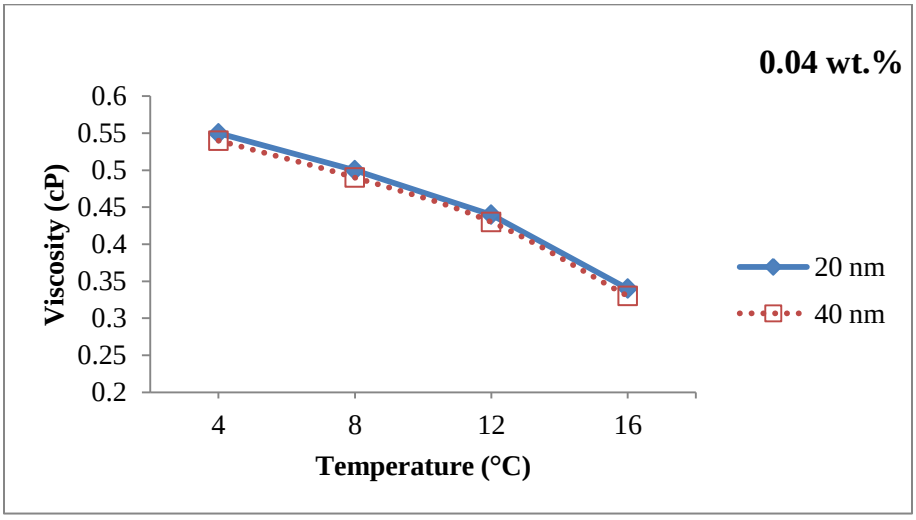


**Figure 6.36** Viscosity v/s temperature for different size of $Al_2O_3$ nanoparticles at 0.04 wt. % concentration

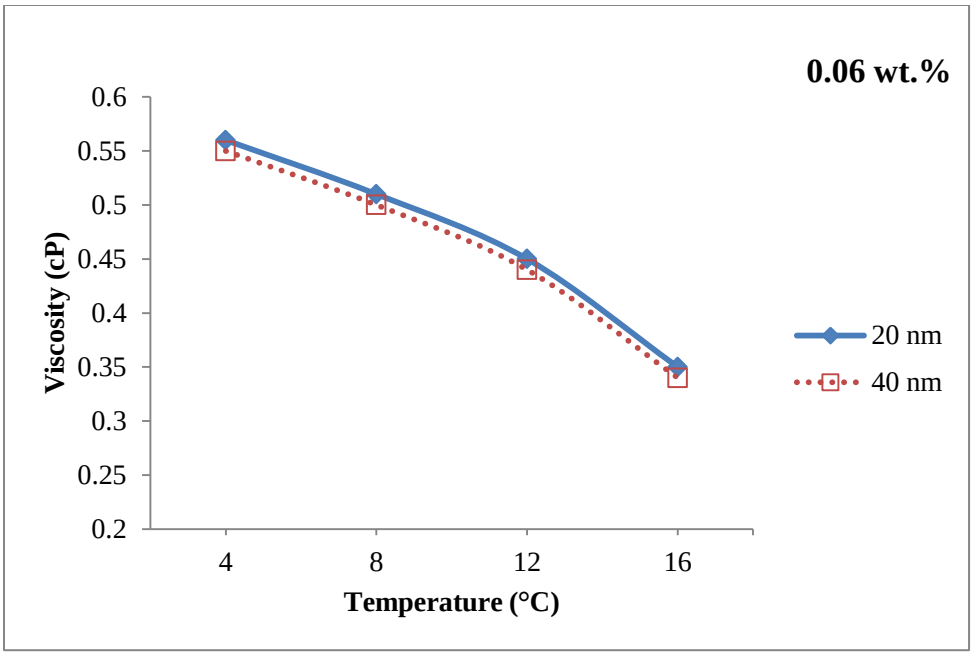


**Figure 6.37** Viscosity v/s temperature for different size of $Al_2O_3$ nanoparticles at 0.06 wt. % concentration

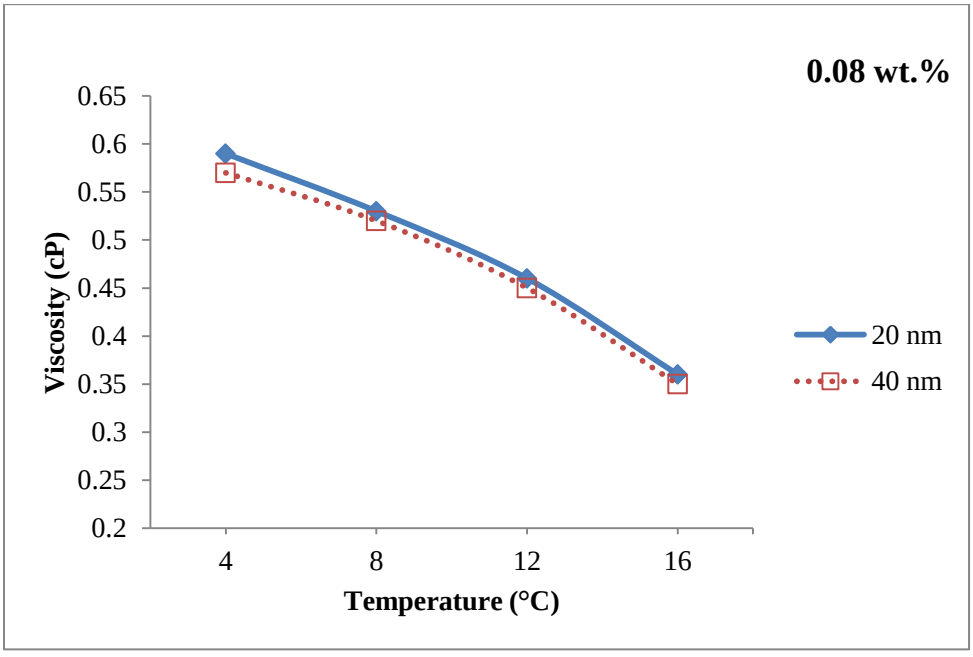


**Figure 6.38** Viscosity v/s temperature for different size of $Al_2O_3$ nanoparticles at 0.08 wt. % concentration

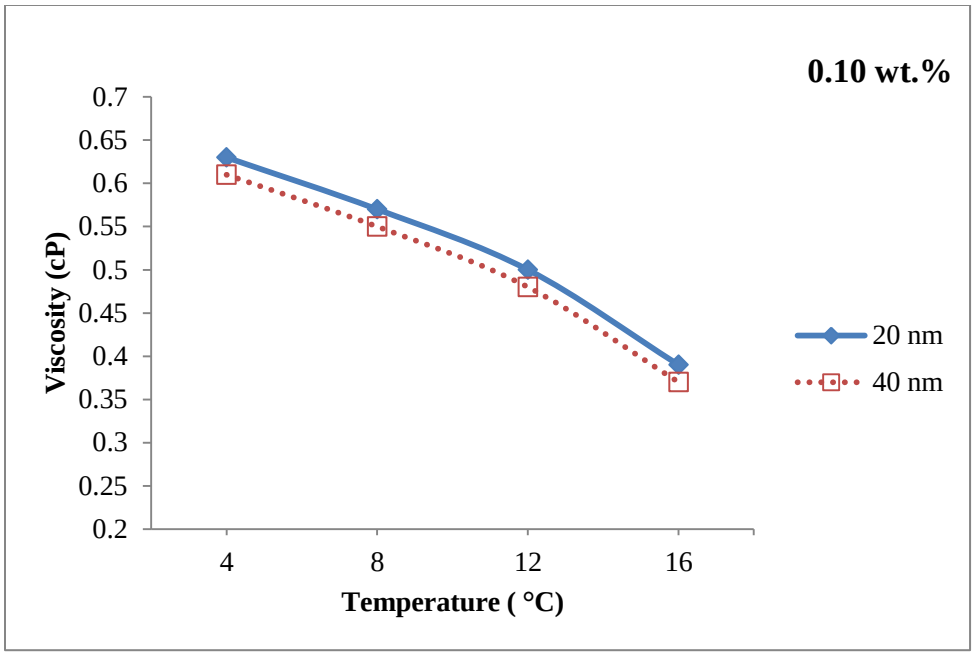


**Figure 6.39** Viscosity v/s temperature for different size of $Al_2O_3$ nanoparticles at 0.10 wt. % concentration

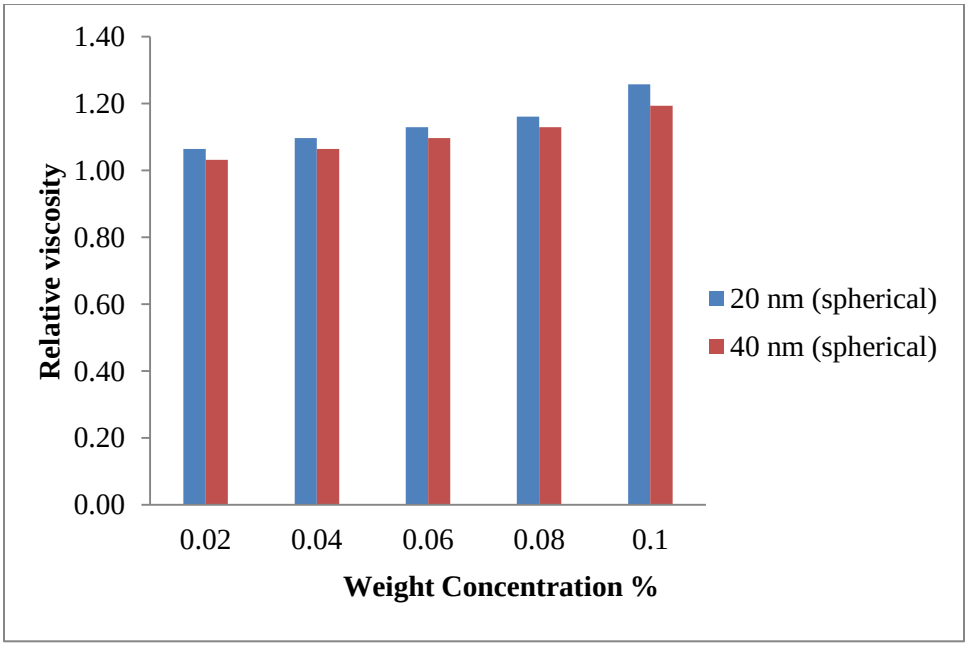


**Figure 6.40** Relative viscosity v/s wt. concentration % for different size of $Al_2O_3$ nanoparticles

It has been predicted that the viscosity of a nanorefrigerant increase with decrease in particle size. $Al_2O_3$ nanoparticles of size 20 nm have more viscosity than 40 nm within measured

temperature range (4-16°C). The viscosity drop is 2% from 0.02 to 0.06 wt. % concentration, when we replace 20 nm with 40 nm $Al_2O_3$ nanoparticles. At 0.08 wt. % concentration, the viscosity drop increased to 3 % and the maximum viscosity drop 4 % is observed at 0.10 wt. % concentrations between 20 nm and 40 nm nanoparticles. When nanoparticle size increases, the magnitude of interspatial distance between particles increase, thus the weight fraction of the aggregates decreases and relative viscosity ratio decreases. The interaction between the particles is also important because it determines particle agglomeration and degrees of freedom of motion in nanorefrigerants. As particle size decreases, the total area of the solid/liquid interface and the number of particles at the same particle weight concentration increases. In addition, due to aggregation, the shape of the aggregate is no longer spherical as the aggregate shape becomes disordered. It can also account for the increase of viscosity ratio as the particle diameter decreases.

### 6.3.4 Effect of shape of $Al_2O_3$ nanoparticles on viscosity

The results of viscosity v/s weight concentration % for different shape of $Al_2O_3$ nanoparticles are shown in the Figure 6.41, 6.42, 6.43, 6.44 & 6.45. Also, results of relative viscosity v/s weight concentrations for different shapes of nanoparticles are shown in Figure 6.46.

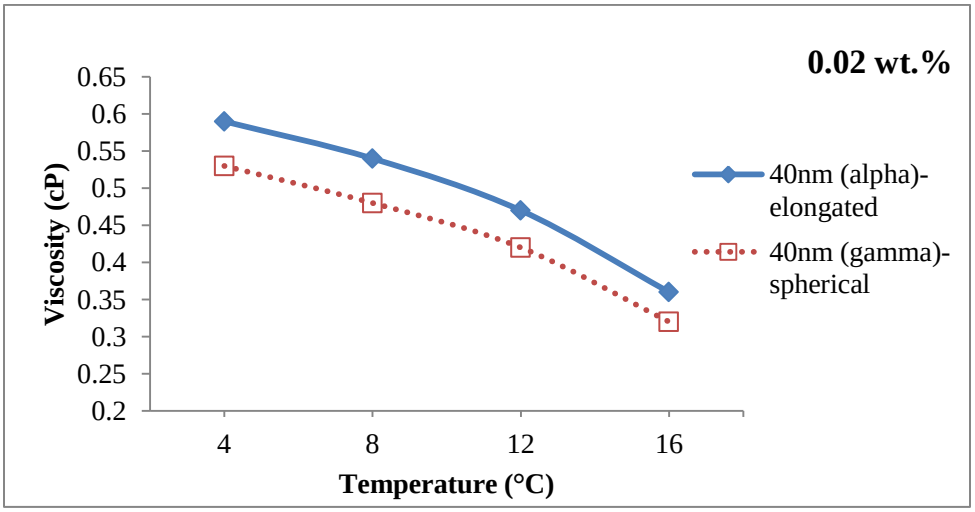


**Figure 6.41** Viscosity v/s temperature for different shape of $Al_2O_3$ nanoparticles at 0.02 wt. % concentration

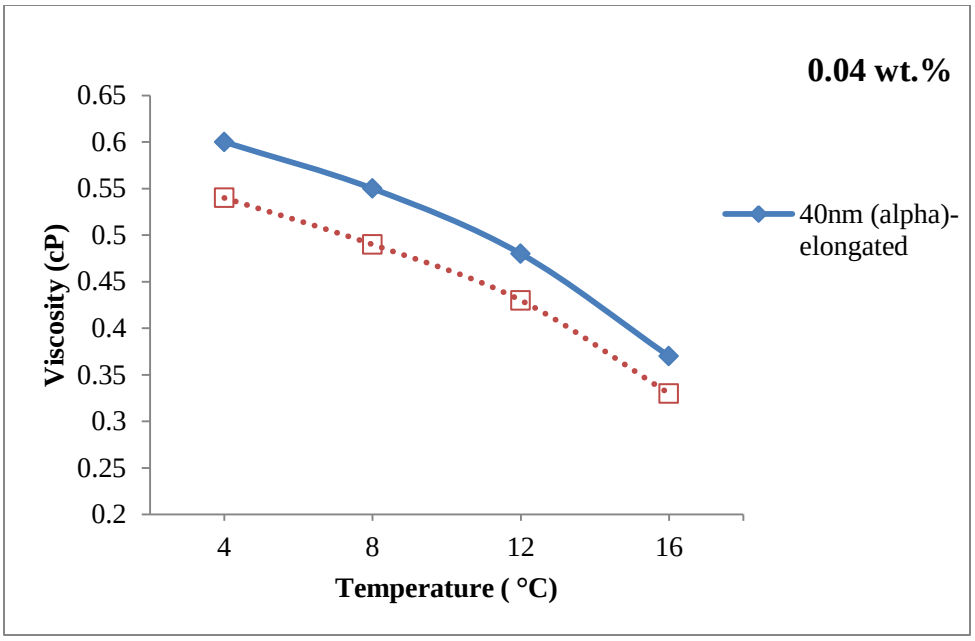


**Figure 6.42** Viscosity v/s temperature for different shape of $Al_2O_3$ nanoparticles at 0.04 wt. % concentration

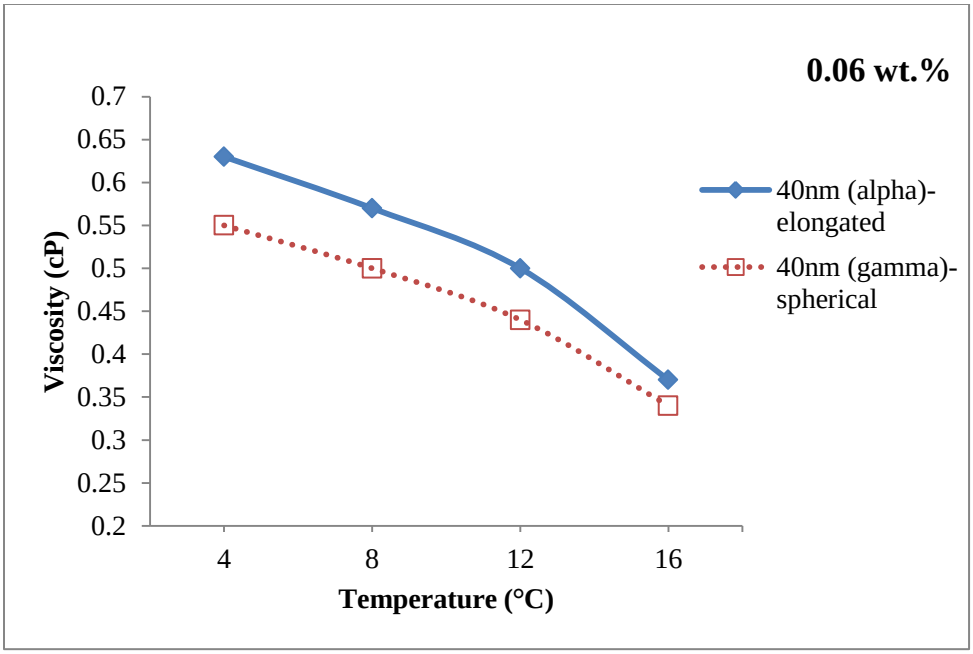


**Figure 6.43** Viscosity v/s temperature for different shape of $Al_2O_3$ nanoparticles at 0.06 wt. % concentration

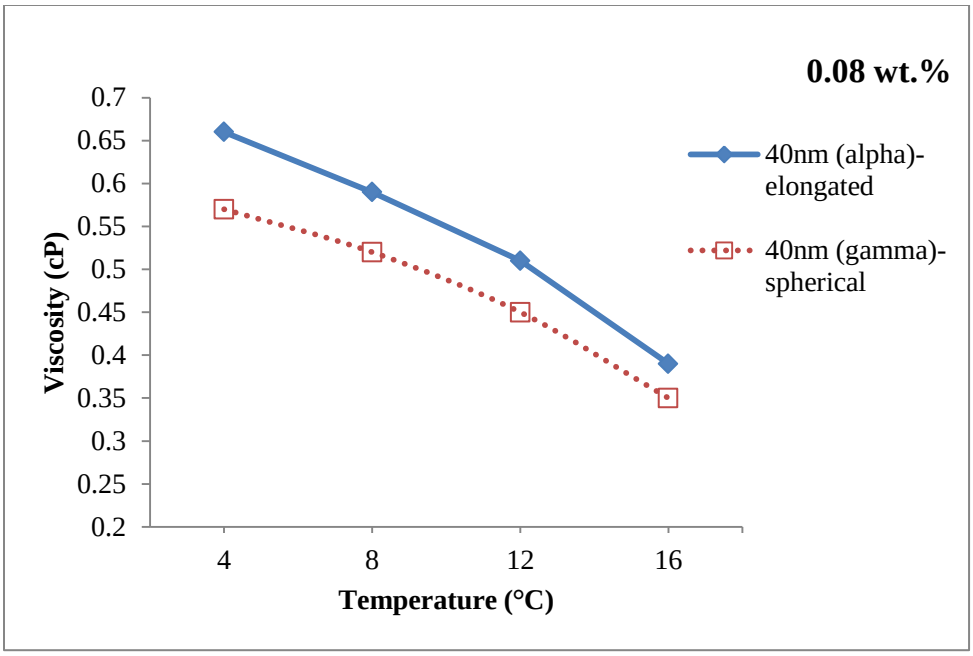


**Figure 6.44** Viscosity v/s temperature for different shape of $Al_2O_3$ nanoparticles at 0.06 wt. % concentration

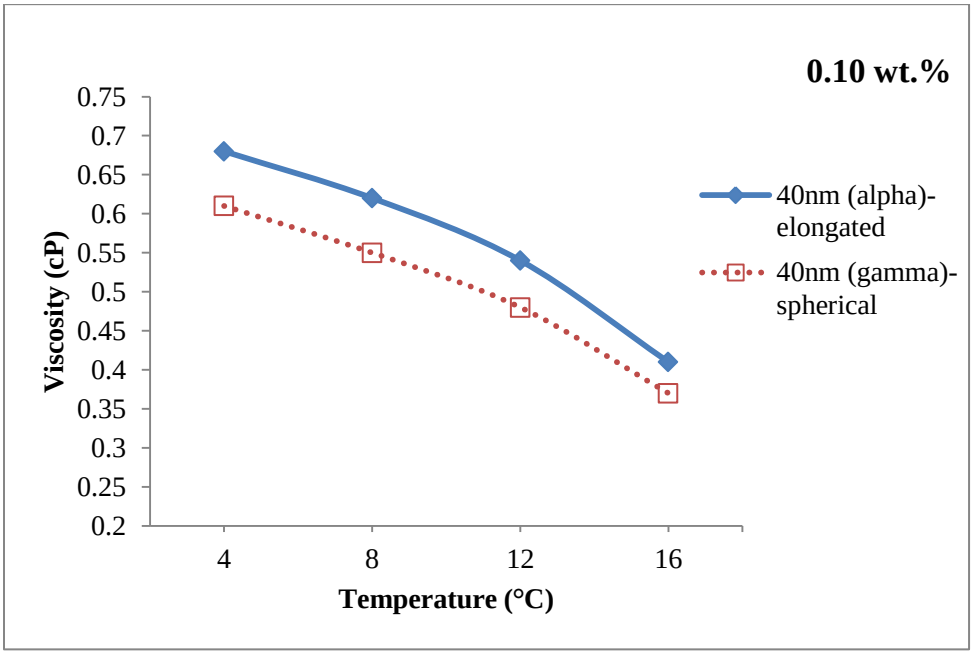


**Figure 6.45** Viscosity v/s temperature for different shape of $Al_2O_3$ nanoparticles at 0.08 wt. % concentration

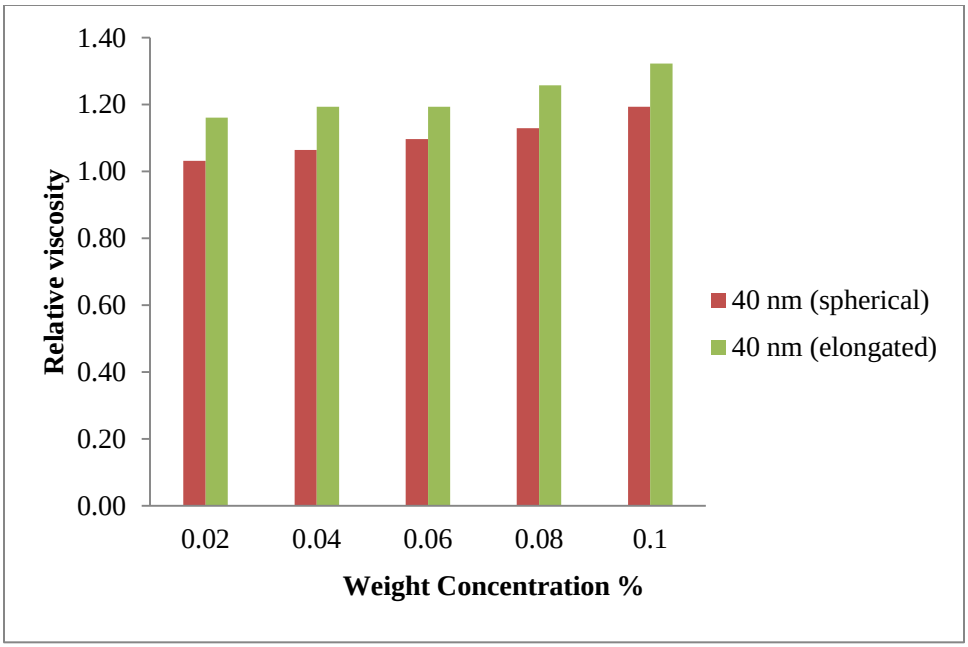


**Figure 6.46** Relative viscosity v/s wt. concentration % for different shape of $Al_2O_3$ nanoparticles

The viscosity of a nanorefrigerant with elongated shaped $Al_2O_3$ nanoparticles (40 nm) has higher value than spherical shaped (40 nm) $Al_2O_3$ nanoparticles within measured temperature range (4-16°C). One of the possible reasons of this is that elongated particles have less number of degree of freedom of motion due to its larger length, while spherical particles have more access of movement in the refrigerant. Thus elongated nanoparticles produce more interlayer resistance as compare to spherical and cause more viscosity increment. It is found that 0.1 wt.% $Al_2O_3$ based nanorefrigerants with spherical particles had a viscosity enhancement of 17 %, whereas 0.1 wt. % nanorefrigerant with elongated particles had a viscosity enhancement of 31%. The viscosity of nanorefrigerant containing spherical shape 40 nm $Al_2O_3$ nanoparticles changes from almost 5 to 1.5% in temperature range of 4 to 16 °C.

However, it should be noted that nanorefrigerants with elongated particles usually have much larger viscosities than those with spherical nanoparticles. As a result, the associated increase in pumping power is large and this reduces the feasibility of usage of nanorefrigerants with elongated nanoparticles.

### 6.3.5 Comparison of experimental data of viscosity with theoretical models

The values for relative viscosity of $Al_2O_3$/R-11 nanorefrigerant calculated for Vand, Batchelor and Brinkman models. The experimental data of relative viscosity along with theoretical models is plotted as a function of the weight concentration (0.02, 0.04, 0.06, 0.08 & 0.10 %) for 20 nm (spherical), 40 nm (spherical) $Al_2O_3$ nanoparticles in Figure 6.47. The result shows that the enhancement in viscosity ratio of 20 nm (spherical) $Al_2O_3$ nanoparticles is almost same from 0.02 to 0.06 % weight concentrations as predicted by Vand, Batchelor and Brinkman models. But from 0.06 % to 0.1 % wt. concentration, the viscosity rise sharply to 21% of R-11 viscosity. While for 40 nm (spherical) $Al_2O_3$ nanoparticles, the viscosity enhancement is less than theoretical models up to 0.08% wt. concentration. This deviation may be due to assumptions and number of parameters considered for experimentation. Also, Vand, Batchelor and Brinkman models are not based on nanoparticle size. So size effect is not predicted by theoretical models and agglomeration may also appear which may causes sharp rise in viscosity of nanorefrigerant. Thus care needs to be taken in understanding the size distribution and the aggregation phenomena for accurate predictions. The deviation of 40 nm (elongated) $Al_2O_3$ nanoparticles is more than theoretical models and behavior is nonlinear.

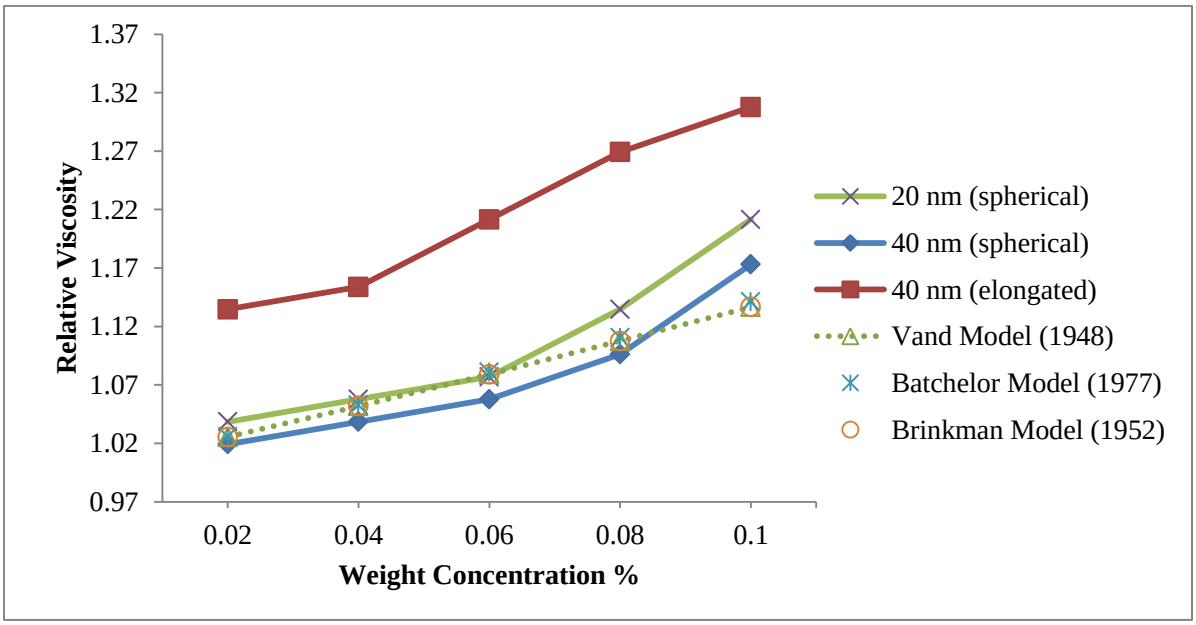


**Figure 6.47** Measured relative viscosity of $Al_2O_3$/R-11 nanorefrigerant v/s relative viscosity calculated from theories for nanoparticles

The maximum viscosity deviation from theoretical models for 20 nm, 40 nm (spherical) and 40 nm (elongated) $Al_2O_3$ nanoparticles is 7%, 3% and 17 % respectively at 0.10 % weight concentration. And the mean deviation of thermal conductivity for 20 nm, 40 nm (spherical) and 40 nm (elongated) $Al_2O_3$ nanoparticles is 2%, 0 % and 14 % respectively for Vand, Batchelor and Brinkman models. Moreover, Figure 6.47 shows that the measured viscosity of the $Al_2O_3$/R-11 nanorefrigerant is nonlinear with the 40 nm (elongated) $Al_2O_3$ nanoparticles weight concentration, while the described models predict a linear relationship. The Vand, Batchelor and Brinkman models viscosity equations are known to for spherical particles which are not applicable for elongated nanoparticles. What's unexpected is that, for the $Al_2O_3$/R-11 nanorefrigerants, the nonlinear viscosity behavior occurs at very low particle concentrations far below 0.1 wt.%. Nonlinear behavior implies that there is particle–particle interactions which invalidate the Vand equation developed for dilute suspensions. It can be argued that this nonlinear behavior could be related to the increased surface of well-dispersed nanoparticles in the nanorefrigerant sonicated for 4 hour and used in the measurement of the viscosities because the flow behavior of a solid–liquid suspension depends on the hydrodynamic force acting on the surface of solid particles. However, presently it is challenging to understand the physical mechanisms for the discrepancy in the magnitude and concentration-dependency of the viscosity of the $Al_2O_3$/R-11 nanorefrigerants at very low concentrations below 0.1%. Therefore, this nonlinear viscosity behavior of the nanorefrigerants needs further experimental and theoretical studies.

# CHAPTER-7

# CONCLUSION AND FUTURE SCOPE

The present chapter summarizes the results on thermal conductivity and viscosity of $Al_2O_3$ /R-11 nanorefrigerant at different temperature, weight concentration, shape and size of nanoparticles. Mostly researchers used volume concentration for experimentation, but weight concentration gives more accurate results because density of refrigerant changes with change in temperature. So, its volume changes with temperature which results change in volume concentration. The weight concentration remains same at any temperature and helpful to minimize measurement errors.

## 7.1 Thermal conductivity of $Al_2O_3$ /R-11 nanorefrigerant

1. The present studies show a prominent role of weight concentration on enhancements of the thermal conductivity of nanorefrigerant. It increases with rise in weight concentration. The enhancement in thermal conductivity is mainly due to micro convection caused by the Brownian motion of the nanoparticles and aggregation of nanoparticles causing a local percolation and clustering to the nanoparticle occurs more actively in fluid with higher concentration.

2. The highest enhancement of thermal conductivity observed is 42% at 0.1% wt. concentration of 40 nm (elongated) $Al_2O_3$ nanoparticles.

3. The behavior of increase in thermal conductivity is almost linear for 20 nm (spherical) & 40 nm (spherical) nanoparticles. A nonlinear relationship is observed between thermal conductivity and particle weight concentrations for 40 nm (elongated) nanoparticles. The nonlinearity is attributed to the rapid clustering of elongated nanoparticles which is an indication of interactions between particles due to high nanoparticle concentrations.

4. The thermal conductivity of nanorefrigerant decrease with temperature (4-16°C) because the mean distance of separation of the centers of the molecules decrease with rising temperature while it shows increase in aqueous nanofluids. The thermal conductivity ratio remains constant with an increase in temperature. These results suggest that the thermal conductivity of the nanorefrigerant simply track the thermal conductivity of the base fluid i.e. R-11 refrigerant and the enhancement in nanorefrigerant relative to base fluids is essentially temperature independent.

5. A maximum drop of thermal conductivity was achieved from 4°C to 8°C for 0.1 wt.% concentration of 40 nm (elongated) $Al_2O_3$ nanoparticle i.e. from 0.137 to 0.132 W/mK. The behavior of decrease in thermal conductivity with the temperature is almost linear for 20 nm & 40 nm (spherical) $Al_2O_3$ nanoparticles. But, the elongated 40 nm $Al_2O_3$ nanoparticles shows nonlinear behavior because of more particles interaction between them.

6. $Al_2O_3$ nanoparticles of size 20 nm have more thermal conductivity than 40 nm particles within measured temperature range (4-16°C). It has been observed that for 0.1 wt. % nanorefrigerant, thermal conductivity enhancement decreased from 29 to 23% by increasing the particle size from 20 to 40 nm. The general trend in the experimental data is that the thermal conductivity of nanorefrigerant increases with decreasing particle size. Since the effect of Brownian motion decreases with increasing particle size, which decreases the associated thermal conductivity enhancement.

7. The thermal conductivity enhancement of nanorefrigerant with elongated shaped $Al_2O_3$ nanoparticles (40 nm) is more than spherical shaped (40 nm) $Al_2O_3$ nanoparticles within measured temperature range (4-16°C). It is because of rapid heat transport along relatively larger distances in elongated particles since elongated particles usually have larger lengths as compare to its diameter.

8. It is found that 0.1 wt.% $Al_2O_3$/R-11 nanorefrigerant with spherical particles had a thermal conductivity enhancement of 24%, whereas 0.1 wt.% nanorefrigerant with elongated particles had a thermal conductivity enhancement of 43%.

9. When the experimental results are observed, it is seen that the discrepancy in the data is somewhat larger for the 0.1 wt.% case. The maximum thermal conductivity deviation from Hamilton & Crosser model for 20 & 40 nm (spherical) $Al_2O_3$ nanoparticles is 13% and 10% respectively at 0.10 % weight concentration. Also the mean deviation of thermal conductivity for 20 & 40 nm (spherical) $Al_2O_3$ nanoparticles is 11% and 6% respectively for Hamilton & Crosser model.

10. It was noted that Hamilton and Crosser model was successful in predicting the enhancement in elongated particles.

## 7.2 Viscosity of $Al_2O_3$/R-11 nanorefrigerant

1) The viscosity of $Al_2O_3$/R-11 nanorefrigerant is increasing with the weight concentration of nanoparticles. The increase of viscosity is more at higher weight concentration i.e. from 0.08 to 0.10% and behavior of increase in viscosity is almost linear up to 0.08 wt. % concentration for 20 & 40 nm nanoparticles.

2) A nonlinear relationship is observed between viscosity and particle weight concentrations for 40 nm (elongated) nanoparticles. The highest enhancement of viscosity observed is 31% at 0.1% wt. concentration and 4°C of 40 nm (elongated) $Al_2O_3$ nanoparticles.

3) The viscosity of $Al_2O_3$/R-11 nanorefrigerant is decreasing for different weight concentrations (0.02, 0.04, 0.06, 0.08, 0.10 %) of nanoparticles with the rise in temperature (4-12°C). It is because of increasing temperature would weaken the inter-particle and inter-molecular adhesion forces.

4) The behavior of viscosity decreasing is linear up to 12°C, but from 12 to 16°C there is sharp decline in slope with the increase in temperature. Although the absolute viscosity decreases with increase in temperature in both the base fluids (R-11) and the nanorefrigerant ($Al_2O_3$/R-11), the relative viscosity remains almost invariant with variation of 1-2% with increase in temperature, which is a clear indication for the absence of aggregation with temperature.

5) The viscosity of $Al_2O_3$/R-11 nanorefrigerant increase with decrease in particle size. $Al_2O_3$ nanoparticles of size 20 nm have more viscosity than 40 nm within measured temperature range (4-16°C). When nanoparticle size increases, the magnitude of interspatial distance between particles increase, thus the weight fraction of the aggregates decreases and relative viscosity ratio decreases.

6) The viscosity drop is 2% from 0.02 to 0.06 wt. % concentration, when we replace 20 nm with 40 nm $Al_2O_3$ nanoparticles. At 0.08 wt. % concentration, viscosity drop increased to 3 % and the maximum viscosity drop 4 % is observed at 0.10 wt. % concentrations between 20 nm and 40 nm nanoparticles.

7) The viscosity of $Al_2O_3$/R-11 nanorefrigerant with elongated shaped $Al_2O_3$ nanoparticles (40 nm) is more than spherical shaped (40 nm) $Al_2O_3$ nanoparticles within measured temperature range (4-16°C).One of the possible reasons of this is that elongated particles have less number of degree of freedom of motion due to its larger length, while spherical particles have more access of movement in the refrigerant. Thus elongated nanoparticles produce more interlayer resistance as compare to spherical and cause more viscosity increment.

8) It is found that 0.1 wt.% $Al_2O_3$ based nanorefrigerants with spherical particles had a viscosity enhancement of 17 %, whereas 0.1 wt. % nanorefrigerant with elongated particles had a viscosity enhancement of 31%. The viscosity of nanorefrigerant containing spherical shape 40 nm $Al_2O_3$ nanoparticles changes from almost 5 to 1.5% in temperature range of 4 to 16°C.

9) However, it should be noted that nanorefrigerants with elongated particles usually have much larger viscosities than those with spherical nanoparticles. As a result, the associated increase in pumping power is large and this reduces the feasibility of usage of nanorefrigerants with elongated nanoparticles.

10) The maximum viscosity deviation from Vand, Batchelor and Brinkman models for 20 nm, 40 nm (spherical) and 40 nm (elongated) $Al_2O_3$ nanoparticles is 7%, 3% and 17 % respectively at 0.10 % weight concentration. And the mean deviation of thermal conductivity for 20 nm, 40 nm (spherical) and 40 nm (elongated) $Al_2O_3$ nanoparticles is 2%, 0% and 14% respectively for Vand, Batchelor and Brinkman models. This deviation may be due to assumptions and number of parameters considered for experimentation. Vand, Batchelor and Brinkman models are not based on nanoparticle size. So size effect is not predicted by theoretical models and agglomeration may also appear which may causes sharp rise in viscosity of nanorefrigerant.

## 7.3 Suggestions for future work

At present, there is significant discrepancy in thermal conductivity data of nanorefrigerants. For the practical application of nanorefrigerants in refrigeration devices, these discrepancies should be eliminated by systematically investigating the effects of some parameters on thermal conductivity of nanorefrigerants. In the literature, the research about the effects of clustering, pH value and ultrasonic vibration on thermal conductivity is very limited and further research is required regarding the effects of these parameters. When it comes to the theoretical studies about the thermal conductivity of refrigerants, it is seen that the relative significance of the proposed enhancement mechanisms of thermal conductivity are not known. Development of new mechanisms and comparison of these models predictions with systematically obtained experimental data will provide insight to the theoretical explanation of anomalous thermal conductivity enhancement with nanorefrigerants.

In the literature, there are different theoretical approaches for the analysis of viscosity of nanorefrigerants. In order to understand the validity of the proposed approaches, numerical analyses that are based on those approaches are useful. At present, numerical studies in the literature about this issue are not sufficient to reach a conclusion about the accuracy of the approaches. On the other hand, there is very limited experimental data about viscosity of nanorefrigerants and this prevents the systematic comparison of numerical results with experimental findings.

Similar to the case of thermal conductivity, viscosity of nanorefrigerants is also dependent on many parameters such as particle weight fraction, sonication time, particle material, temperature and refrigerant type. Detailed experimental investigation of the effects of most of these parameters on heat transfer has not been performed yet.

However, presently it is challenging to understand the physical mechanisms for the discrepancy in the magnitude and concentration dependency of the viscosity of the nanorefrigerants at very low concentrations below 0.1%. Therefore, this nonlinear viscosity behavior of the nanorefrigerants needs further experimental and theoretical studies.

# REFERENCES


Akbari, B, Pirhadi Tavandashti, M and Zandrahimi, M 2011, 'Particle size characterization of nanoparticles-A Practical approach', *Iranian Journal of Materials Science & Engineering*, vol. 8, no. 2, pp. 48-56.

Bachelor, GK 1977, 'The effect of Brownian motion on the bulk stress in a suspension of spherical particles', *J. Fluidmech*, vol. 83, pp. 97-117.

Bi, S, Guo, K and Liu, Z 2011, 'Performance of a domestic refrigerator using $TiO_2$-R600a nanorefrigerant as working fluid', *Energy Conversion and Management*, vol. 52, pp. 733-737.

Bi, S, Shi, L and Zhang, L 2007, 'Performance study of a domestic refrigerator using 134a/ mineral oil/nano-$TiO_2$ as working fluid', *ICR07-B2-346*.

Bi, S, Shi, L, Zhang, L 2008, 'Application of nanoparticles in domestic refrigerators', *Applied Thermal Engineering*, vol. 28, pp.1834-1843.

Bobbo, S, Fedele, L, Fabrizio, M, Barison, S, Battiston, S and Pagura, C 2010, 'Influence of nanoparticles dispersion in POE oils on lubricity and R134a solubility', *International Journal of Refrigeration*, vol. 33, no. 6, pp. 1180-1186.

Bridgman, PW 1923, 'The thermal conductivity of liquids', *Proc. Natl. Acad. Sci.*, vol. 9, no. 10, pp. 341-345.

Brinkman, HC 1952, 'The viscosity of concentrated suspensions and solutions', *J. Chemistry Phy.*, vol. 20, pp. 571-581.

Brooks, RF, Dinsdale, AT and Quested, PN 2005, 'The Measurement of Viscosity of Alloys -A Review of Methods, Data and Model', *Measurement Science and Technology*, vol.16, pp. 354-362.

Chen, H, Ding, Y and Tan, C 2007, 'Rheological behavior of nanofuids', *New J. Phys*., vol. 9, no. 10, pp.267.

Chen, L, Xie, H, Li, Y and Yu, W 2008, 'Nanofuids containing carbon nanotubes treated by mechanochemical reaction', *Thermochim. Acta*, vol. 477, no. 12, pp. 21–24.

Choi, SUS, Zhang, ZG, Yu, W, Lockwood, FE and Grulke, EA, 2001, 'Anomalous Thermal Conductivity Enhancement in Nanotube Suspensions', *Appl. Phys. Lett.*, vol. 79, no. 14, pp. 2252-2254.

Chopkar, M, Sudarshan, S, Das, P and Manna, I, 2008, 'Effect of Particle Size on Thermal Conductivity of Nanofluid', Metall. *Mater. Trans. A*, vol. 39, no. 7, pp. 1535-1542.

Das, SK, Putra, N and Roetzel, W 2003, 'Pool boiling characteristics of nanofluids', *International Journal of Heat and Mass Transfer*, vol. 46, no. 5, pp. 851-862.

Ding, Y, Alias, H, Wen, D and Williams, RA 2006, 'Heat transfer of aqueous suspensions of carbon nanotubes (CNT nanofluids)', *Int. J. Heat Mass Transfer*, vol. 49, pp. 240–250.

Eastman, JA, Choi, SUS, Li, S, Yu, W and Thompson, LJ 2001, 'Anomalously Increased Effective Thermal Conductivities of Ethylene Glycol-Based Nanofluids Containing Copper Nanoparticles', *Appl. Phys. Lett.*, vol. 78, no. 6, pp. 718-720.

Einstein, A 1906, 'Eine neue Bestimmung der Molekuldimensionen', *Annalen der Physik*, vol. 19, pp. 289-306.

Hamilton, RL and Crosser, OK 1962, 'Thermal Conductivity of Heterogeneous Two-Component Systems', *Ind. Eng. Chem. Fund.*, vol. 1, no. 3, pp. 187-191.

Henderson, K, Park,Y, Liu, L and Jacobi**,** M 2010, 'Flow boiling heat transfer of R134a based nanofluids in a horizontal tube', *IJHMT*, vol.53, no. 5, pp. 944- 951.

Incropera, FP, Dewitt, DP 2009, 'Fundamentals of Heat and Mass Transfer', Sixth edition, *John Wiley and Sons*, USA.

Jeffrey, DJ, 1973, 'Conduction through a random suspension of spheres', *Proceedings of the Royal Society of London*, Series A, Vol. 335, no. 1602, pp. 355-367.

Jiang, W, Ding, G and Peng, H 2009, 'Measurement and model on thermal conductivities of carbon nanotube nanorefrigerants', *International Journal of Thermal Sciences*, vol. 48, pp. 1108-1115.

Jwo, CS, Jeng, LY, Chang, H and Teng, TP 2008, 'Experimental Study on thermal conductivity of lubricant containing nanoparticles', *Rev. Adv. Material Sci.*, vol. 18, pp. 660-666.

Jwo, CS, Jeng, LY, Teng, TP and Chang, H 2009, 'Effect of nanolubricant on the performance of Hydrocarbon refrigerant system', *J. Vac. Sci. Technology B*, vol.27, no. 3, pp. 1473-1477.

Kittel, C 2004, 'Introduction to Solid State Physics', Seventh edition, *John Wiley & Sons*, U.K.

Koo, J and Kleinstreuer, C 2004, 'A New Thermal Conductivity Model for Nanofluids', *J. Nanopart. Res*., vol. 6, no. 6, pp. 577-588.

Kumar, P, Kumar, J, Suresh, S 2012, 'Review on nanofluid theoretical viscosity models', *International Journal of Engineering Innovation and Research*, vol. 1, pp. 2277-5668.

Lee, D 2007, 'Thermophysical Properties of Interfacial Layer in Nanofluids', *Langmuir*, vol. 23, no. 11, pp. 6011-6018.

Lee, S, Choi, SUS, Li, S and Eastman, JA 1999, 'Measuring Thermal Conductivity of Fluids Containing Oxide Nanoparticles', *J. Heat Transfer*, vol. 121, no. 2, pp. 280-289.

Lee, SW, Park, SD, Kang, S, Bang, C and Kim, H 2011, 'Investigation of viscosity and thermal conductivity of SiC nanofluids for heat transfer applications', *International Journal of Heat and Mass Transfer*, vol. 1, pp. 433-438.

Li, JM, Li, ZL and Wang, BX 2002, 'Experimental viscosity measurements for copper oxide nanoparticle suspensions', *Tsing hua Sci. Technology*, vol. 7, pp. 198- 201.

Li, Q, and Xuan, Y 2000, 'Experimental Investigation on Transport Properties of Nanofluids', *Heat Transfer Science and Technology*, B. Wang, ed., Higher Education Press, Beijing, pp. 757–762.

Li, Y, Zhou, J, Tung, S, Schneider E and Xi, S 2009, 'A review on development of nanofluid preparation and characterization', *Powder Technology*, vol. 196, pp. 89–101.

Liu, M, Lin, MC, Huang, I, and Wang, C 2005, 'Enhancement of Thermal Conductivity with Carbon Nanotube for Nanofluids', *Int. Comm. Heat Mass*, vol. 32, no. 9, pp. 1202-1210.

Lu, S and Lin, S 1996, 'Effective thermal conductivity of composites containing aligned inclusions of finite conductivity', *Journal of Applied Physics*, vol. 79, no. 9, pp. 6761-6769.

Mahbubul, IM, Fadhilah, SA, Saidur, R, Leong, KY and Amalina, MA 2013, 'Thermophysical properties and heat transfer performance of $Al_2O_3$/R-134a nanorefrigerants', *International Journal of Heat and Mass Transfer*, vol. 57, pp.100–108.

Mahbul, IM, Saidur, R and Amalina, MA 2012, 'Investigation of Viscosity of R123- $TiO_2$ nanoregerigerant', *IJMME*, vol. 7, pp. 146-151.

Murshed, S, Leong, K and Yang, C 2005, 'Enhanced Thermal Conductivity of $TiO_2$-Water Based Nanofluids', *Int. J. Therm. Sci*., vol. 44, no. 4, pp. 367-373.

Nguyen, F, Desgranges, Roy, G 2007, 'Temperature and particle size dependent viscosity data for water based nanofluids- Hysteresis phenomenon', *Int. J. Heat and Fluid flow*, vol. 28, pp. 1492-1506.

Özerinç, S, Kakaç, S, and Yazıcıoğlu, AG 2010, 'Enhanced Thermal Conductivity of Nanofluids: A State-of-the-Art Review', *Microfluid Nanofluid*, vol. 8, no. 2, pp. 145-170.

Paul, G, Chopkar, M, Manna, I and Das, PK 2010, 'Techniques for measuring the thermal conductivity of nanofluids: A review', *Renewable and Sustainable Energy Reviews*, vol. 14, pp.1913–1924.

Prasher, P, Song, D and Wang, J 2006, 'Measurements of nanofluid viscosity and its implications for thermal applications', *Appl. Phys. Lett.*, vol. 89, pp.1– 3.

Schartl, W 2007, 'Light Scattering from Polymer Solutions and Nanoparticle Dispersions', *Springer*,Germany.

Suzuki, E 2002, 'High-resolution scanning electron microscopy of immunogold-labelled cells by the use of thin plasma coating of osmium', *Journal of Microscopy*, vol. 208, no. 3, pp. 153–157.

Turgut, A, Tavman, I, Chirtoc, M, Schuchmann, H, Sauter, C, and Tavman, S 2009, 'Thermal Conductivity and Viscosity Measurements of Water-Based $TiO_2$ Nanofluids', *Int. J. Thermophys*, vol. 30, no.4, pp. 1213-1226.

Vand, V 1948, 'Viscosity of solutions and suspensions theory', *J. Phys. and Colloid Chemistry*, vol. 52, pp. 277-299.

Wang, X, Xu, X and Choi, SUS 1999, 'Thermal conductivity of nanoparticle–fluid mixture', *J. Thermophys Heat Transfer*, vol.13, pp. 474–480.

White, F 2005, 'Viscous fluid flow', Third edition, *TMH*, New York.

Williams, DB and Carter, CB 1996, 'Transmission Electron Microscopy', *A Textbook for Materials Science*, Springer, New York.

Xie, H, Wang, J, Xi, T, and Liu, Y 2002, 'Thermal Conductivity of Suspensions Containing Nanosized SiC Particles', *Int. J. Thermophys.*, vol. 23, no. 2, pp. 571-580.

Xie, H, Wang, J, Xi, T, Liu Y, Ai, F and Wu, Q 2002, 'Thermal Conductivity Enhancement of Suspensions Containing Nanosized Alumina Particles', *J. Appl. Phys.*, vol. 91, no. 7, pp. 4568-4572.

Xuan, Y, Li, Q, and Hu, W 2003, 'Aggregation Structure and Thermal Conductivity of Nanofluids', *AICHE Journal*, vol. 49, no. 4, pp. 1038-1043.

Yu, W, and Choi, SUS 2003, 'The Role of Interfacial Layers in the Enhanced Thermal Conductivity of Nanofluids: A Renovated Maxwell Model', *J. Nanopart. Res.*, vol. 5, no. 1, pp. 167-171.

Zhu, H, Zhang, C, Liu, S, Tang, Y, and Yin, Y 2006, 'Effects of Nanoparticle Clustering and Alignment on Thermal Conductivities of $Fe_3O_4$ Aqueous Nanofluids', *Appl. Phys. Lett*., vol. 89, no. 2, 023123-3.

# BIBLIOGRAPHY

ASHRAE Fundamentals Handbook, 2001.

Das, SK, Nanofluids Science and Technology.

Manual of KD2 Pro thermal properties analyser.

Manual of probe type Oscar Sonicator.

Manual of Wells- Brookfield cone/plate viscometers.